

Development of a Simplified Analytical Method to Estimate the Seismic
Response of Reinforced Concrete Frames
with Solid Masonry Infills

by

AUSTIN REESE

Presented to the Faculty of the Graduate School of
The University of Texas at Arlington in Partial Fulfillment
of the Requirements
for the Degree of

MASTER OF SCIENCE IN CIVIL ENGINEERING

THE UNIVERSITY OF TEXAS AT ARLINGTON

May 2014

Copyright © by Austin Reese 2014

All Rights Reserved



*To my Mom and Dad,
Who made me the engineer I am*

Acknowledgements

I am thankful to Dr. Andreas Stavridis for his insight and patient guidance through my graduate school journey, both in my courses and research. I am also gracious for the help of my peers who contributed to my research project. This includes Alireza Sayah, who gave his help when he had little time and gave priceless advice about anything I asked. My gratitude also goes to Margarita Takou who worked countless hours running and re-running computer models, without which the study in this thesis could not have been conducted. Two undergraduate research assistants, Martin Ramirez and Ramin Faroozi, helped make the study complete by performing additional finite element analyses and producing figures that would be essential in this thesis. Lastly I am thankful for the untrammled love and support of my family and friends, this journey would not have been the same without them.

April 4, 2014

Abstract

Development of a Simplified Analytical Method to Estimate the Seismic Response of Reinforced Concrete Frames with Solid Masonry Infills

Austin Reese, MS

The University of Texas at Arlington, 2014

Supervising Professor: Andreas Stavridis

This thesis discusses the analysis of the lateral force-vs-drift relation of reinforced concrete (RC) frames with masonry infill panels under in-plane lateral loads. Such structures have been the topic of several studies due to their recurring catastrophic failures during seismic events. Due to the large number of variables that can affect their seismic performance and lead to various possible failure mechanisms there is no widely accepted method for the assessment of the structural behavior of infilled frames under seismic loads. A parametric study was performed here using detailed analytical models which provided insight to the influence of the various design parameters and material properties. The observations from the parametric study and selected experimental studies were taken into account in the development of a simplified procedure that is proposed here for the estimation of the force-vs-drift behavior of infilled frames. With the proposed method, the force-vs-drift curve for an infilled RC frame can be estimated based on the frame geometry, reinforcing details, and basic material properties. The simplified method is based upon the prediction of the expected failure pattern for an infilled frame which can be achieved using some simple to apply criteria based on the relative shear and flexural strengths of the frame and infill. Four classes have been proposed ranging from strong infill- strong frame cases to weak infill- weak frame. Each class tends to develop a different failure pattern that may include plastic hinges and/or shear failures in the columns as well as diagonal sliding and/or cracking of the infill.

The framework has been validated with data from experimental and analytical studies on single-bay, single-story specimens with a wide range of geometries, design details, and material properties. The comparison of the analytical and experimental results indicates that the proposed methodology, although simplified, it can successfully capture the main features of the seismic response of infilled frames, including the initial stiffness as well as the strength and drift at the apparent yield point, peak load and onset of residual capacity.

Table of Contents

Acknowledgements	iv
Abstract.....	v
List of Illustrations	x
List of Tables	xiv
Chapter 1 Introduction	1
Thesis Overview.....	2
Chapter 2 Outline: Review of Previously Proposed Analytical Methods	2
Chapter 3 Outline: Review of Available Experimental Studies	2
Chapter 4 Outline: Parametric Study	2
Chapter 5 Outline: Analysis of Parametric Study Results	3
Chapter 6 Outline: Simplified Method Overview	3
Chapter 7 Outline: Validation of Proposed Method	3
Chapter 8 Outline: Summary and Conclusions.....	3
Chapter 2 Review of Previously Proposed Analytical Methods	4
Finite Element Methods	4
Equivalent Strut Methods	6
Polyakov 1956.....	6
Stafford-Smith & Carter 1961.....	7
Liauw & Kwan 1984	7
Limit State Methods	8
Mainstone 1971.....	8
Wood 1978.....	9
Rosenblueth 1980.....	9
Liauw & Kwan 1983	10
Stafford-Smith & Coull 1991	10
Mehrabi, Shing, Schuller, and Noland 1994	11

Galanti, Scarpas and Vrouwenvleder, 1998	12
FEMA 306 1999	13
ASCE 41 2006	13
Stavridis 2009	14
Chapter 3 Review of Available Experimental Studies	16
Leuchars and Scrivener 1979	16
Haider 1995	18
Kakaletsis and Karayannis 2009	18
Mehrabi et al. 1994	19
Blackard et al. 2009	22
Chapter 4 Parametric Study	24
Finite Element Model	25
Parametric Study Base Models	26
Parametric Study Models	29
Parametric Study Set 1	29
Parametric Study Set 2	30
Parametric Study Set 3	31
Parametric Study Results	32
Effect of Vertical Load	32
Effect of Aspect Ratio	36
Effect of Shear Reinforcement	40
Effect of Longitudinal Reinforcement	45
Effect of Column Width	48
Chapter 5 Analysis of Parametric Study Results	50
Strong & Weak Definition	50
Strong Infill- Weak Frame Cases	53
Strong Infill- Strong Frame Cases	54

Weak Infill- Weak Frame Cases	55
Weak Infill- Strong Frame Cases	55
Chapter 6 Simplified Method Overview	58
Initial Stiffness	58
Apparent Yield Point	59
Point at Peak Load	59
Point at Onset of Residual Load	63
Chapter 7 Validation of the Proposed Method	68
Validation with Results from Mehrabi et al. (1994)	68
Weak Infill Cases	69
Strong Infill Cases	69
Comparison of Simplified Method with Other Experiments	73
Leuchars and Scrivener 1979	73
Haider 1995	73
Comparison of Simplified Method with Analytical Models	74
Models with Vertical Load Changed	74
Models with Aspect Ratio Changed	79
Models with Stirrup Area Changed	84
Models with Stirrup Spacing Changed	89
Models with Longitudinal Steel Area Changed	90
Models with Column Width Changed	93
Comparison with Other Methods from Literature	94
Chapter 8 Summary	97
Conclusions	98
Recommended Future Research	101
References	103
Biographical Information	106

List of Illustrations

Figure 1.1 Examples of damaged buildings with RC frames and masonry infill panels.....	1
Figure 2.1 Provisions of ASCE 41 (2006).	14
Figure 3.1 Test results from Leuchars and Scrivener (1979).....	17
Figure 3.2 Test results for specimen A-1 from Haider (1995).	18
Figure 3.3 Test results from Kakaletsis and Karayannis (2009)..	19
Figure 3.4 Force-vs-drift curves for Mehrabi et al. specimens with solid brick infill..	21
Figure 3.5 Design of RC frame for Specimen CU1 of Blackard et al. (2009).....	23
Figure 3.6 Force-vs-drift curve for specimen CU1 Blackard et al. (2009).....	23
Figure 4.1 Finite element discretization scheme of infilled frame elements Stavridis (2009).	25
Figure 4.2 Validation of finite element modeling scheme Stavridis and Shing (2010).....	25
Figure 4.3 Specimen CU1, base model for first set of parametric study models.	27
Figure 4.4 Specimen CU1M8, base model for second set of parametric study models.	28
Figure 4.5 Specimen CU1S, base model for third set of parametric study models.	29
Figure 4.6 Parametric study results of first set models with different vertical loads.....	34
Figure 4.7 Cracking patterns at 1.0% drift for frames with different vertical load.....	34
Figure 4.8 Force distribution along five cross sections at the instant of peak strength for cases of the first set with different vertical loads.	34
Figure 4.9 Parametric study results of second set models with different vertical loads.....	35
Figure 4.10 Cracking patterns at 1.0% drift for frames with different vertical load.....	35
Figure 4.11 Force distribution along three cross sections at the instant of peak strength for cases of the second set with different vertical loads.....	35
Figure 4.12 Parametric study results of third set models with different vertical load	36
Figure 4.13 Cracking patterns at 1.0% drift for third set specimens with different vertical load.	36

Figure 4.14 Parametric study results of first set models with different aspect ratios.	38
Figure 4.15 Cracking patterns at 1.0% drift for frames with different aspect ratio.	38
Figure 4.16 Force distribution along five cross sections at the instant of peak strength for cases of the first set with different aspect ratio.	38
Figure 4.17 Parametric study results of second set models with different aspect ratio	39
Figure 4.18 Cracking patterns at 1.0% drift for frames of second set with different aspect ratio..	39
Figure 4.19 Force distribution along three cross sections at the instant of peak strength for cases of the second set with different aspect ratio.	39
Figure 4.20 Parametric study results of third set specimens with different aspect ratio	39
Figure 4.21 Cracking patterns at 1.0% drift for frames with different aspect ratio.	40
Figure 4.22 Parametric study results of first set specimens with different column transverse steel area.....	41
Figure 4.23 Cracking patterns at 1.0% drift for first set specimens with different transverse steel area.....	41
Figure 4.24 Force distribution along three cross sections at 1% drift for cases of the first set with different area of transverse steel.	42
Figure 4.25 Parametric study results of second set specimens with different transverse steel area	42
Figure 4.26 Cracking patterns at 1.0% drift for second set specimens with different transverse steel area.	42
Figure 4.27 Force distribution along three cross sections at 1% drift for cases of the second set with different area of transverse steel.	43
Figure 4.28 Parametric study results of third set specimens with different transverse steel area	43
Figure 4.29 Cracking patterns at 1.0% drift for third set specimens with different transverse steel area.....	43
Figure 4.30 Parametric study results of first set specimens with different transverse steel spacing	44

Figure 4.31 Cracking patterns at 1.0% drift for first set specimens with different transverse steel spacing	44
Figure 4.32 Force distribution along three cross sections at the instant of peak load for cases of the first set with different spacing of transverse steel.	44
Figure 4.33 Parametric study results of second set specimens with different transverse steel spacing	44
Figure 4.34 Cracking patterns at 1.0% drift for second set specimens with different transverse steel spacing.....	45
Figure 4.35 Force distribution along three cross sections at the instant of peak load for cases of the second set with different spacing of transverse steel.....	45
Figure 4.36 Parametric study results of first set specimens with different longitudinal steel area	46
Figure 4.37 Cracking patterns at 1.0% drift for second set specimens with different longitudinal steel area.....	47
Figure 4.38 Force distribution along three cross sections at instant of peak load for cases of the first set with different area of longitudinal steel.	47
Figure 4.39 Parametric study results of second set specimens with different longitudinal steel area.....	47
Figure 4.40 Cracking patterns at 1.0% drift for second set specimens with different longitudinal steel area.....	48
Figure 4.41 Force distribution along three cross sections at the instant of peak load for cases of the second set with different area of longitudinal steel.	48
Figure 4.42 Parametric study results of third set specimens with different column width.....	49
Figure 4.43 Cracking patterns at 1.0% drift for third set specimens with different column width..	49
Figure 5.1 Typical failure pattern of Strong infill- weak frame specimens.....	53
Figure 5.2 Typical failure pattern of Strong infill- strong frame specimens	54
Figure 5.3 Typical failure pattern of weak infill- weak frame specimens.....	55
Figure 5.4 Typical failure pattern of weak infill- strong frame specimens	56

Figure 5.5 Ratio of V_m/V_n for the first set of models in parametric study	57
Figure 5.6 Ratio of V_m/V_n for the second set of models in parametric study	57
Figure 5.7 Ratio of V_m/V_n for the third set of models in parametric study	57
Figure 6.1 Lateral drift at peak load vs aspect ratio of infill for weak infill specimens.....	60
Figure 6.2 Lateral drift at peak load vs aspect ratio of infill for strong infill specimens	60
Figure 6.3 Shear displace-normal displacement relation results from Mehrabi et al. (1994).....	62
Figure 6.4 Drift at residual load/ drift at peak for first set of models.....	64
Figure 6.5 Drift at residual load/ drift at peak for second set of models	64
Figure 6.6 Drift at residual load/ drift at peak for third set of models.....	65
Figure 6.7 Drift at peak and residual load for first set of models.....	65
Figure 6.8 Drift at peak and residual load for second set of models	65
Figure 6.9 Drift at residual load for third set of models.....	66
Figure 7.1 Comparison of simplified method with other methods from literature.....	95
Figure 7.2 Comparison of simplified method with other methods from literature with models from set 1	95
Figure 7.3 Comparison of simplified method with other methods from literature with models from set 2.....	96
Figure 7.4 Comparison of simplified method with other methods from literature with models from set 3.....	96

List of Tables

Table 3.1. Properties of specimen tested by Leuchars and Scrivener (1979)	17
Table 3.2 Properties of specimens tested by Haider (1995)	18
Table 3.3 Properties of specimens tested by Kakaletsis and Karayannis (2009)	19
Table 3.4 Properties of solid brick specimens tested by Mehrabi et al. (1994).....	20
Table 3.5 Properties of hollow brick infilled specimens tested by Mehrabi et al. (1994).....	21
Table 3.6 Properties of specimen CU1 from Blackard et al. (2009).....	23
Table 4.1 Properties of base models in parametric study	24
Table 4.2 Properties of first set of models in parametric study	30
Table 4.3 Properties of second set of models in parametric study	31
Table 4.4 Properties of third set of models in parametric study	32
Table 5.1 Classification of infilled frames	52
Table 6.1 Equations of simplified method for peak and residual load points	67
Table 7.1 Results from Mehrabi et al. (1994)	68
Table 7.2 Comparison of simplified method results with Mehrabi et al. (1994)	70
Table 7.4 Comparison of simplified method results from selected experiments	74
Table 7.5 Results from parametric study of cases with different vertical load	75
Table 7.6 Comparison of simplified method results from cases with varied vertical load	75
Table 7.7 Comparison of simplified method results from cases with varied vertical load	77
Table 7.8 Comparison of simplified method results from cases with varied vertical load	78
Table 7.9 Results from parametric study of cases with different aspect ratio	79
Table 7.10 Comparison of simplified method results from cases with varied aspect ratio.....	81
Table 7.11 Comparison of simplified method results from cases with varied Aspect ratio	82
Table 7.12 Comparison of simplified method results from cases with varied Aspect ratio	83
Table 7.13 Results from parametric study of cases with different transverse steel area.....	84
Table 7.14 Comparison of simplified method results from cases with varied area of steel	85

Table 7.15 Comparison of simplified method results from cases with varied area of steel	87
Table 7.16 Comparison of simplified method results from cases with varied area of steel	88
Table 7.17 Comparison of simplified method results from cases with varied steel spacing	89
Table 7.18 Results from parametric study of cases with different longitudinal steel area	90
Table 7.19 Comparison of simplified method results from cases with varied longitudinal steel area	91
Table 7.20 Comparison of simplified method results from cases with varied longitudinal steel area	92
Table 7.21 Results from parametric study of cases with different column width	93
Table 7.22 Comparison of simplified method results from cases with varied column width	94
Table 8.1 Failure patterns of each class of infilled frames	99

Chapter 1

Introduction

Buildings with reinforced concrete (RC) frames infilled with unreinforced masonry panels exist worldwide. Masonry infilled frames, shown in Figure 1.1, utilize the strength of the concrete frame to uphold the structure, and the area of masonry for creating a building exterior. Generally, the masonry panels in these structures are considered in the design as partitions used for creating the exterior walls. When used for exterior walls masonry is efficient in maintaining a sound and temperature barrier, thus leading to its wide use in areas where materials are readily available.



Figure 1.1 Examples of damaged buildings with RC frames and masonry infill panels. (a) Izmit, Turkey and (b) California, US.

While overlooked in the early design of these buildings, the addition of a masonry infill to a bare RC frame generally increases the lateral capacity of the system. The benefit of added capacity provided by infilling an RC frame with masonry is often negated by the negative impact the infill can have on the overall structural behavior. In areas with high seismicity this oversight in the design has led to catastrophic brittle failures of structures with masonry infill panels. Modern design and analysis of masonry infilled frames is made difficult by the unpredictability of the structural behavior at failure.

Thesis Overview

Chapter 2 Outline: Review of Previously Proposed Analytical Methods

This chapter describes the various analytic techniques developed for infilled frames over the last 60 years. These methods include those aimed at defining the stiffness of the structure, either through principles of mechanics or an equivalent strut, and methods aimed at defining the capacity of an infilled frame. The methods are described in chronological order and are divided into a group of equivalent strut methods and a group of limit state methods. Finally, the use of finite element analysis for infilled frames is introduced.

Chapter 3 Outline: Review of Available Experimental Studies

Chapter 3 introduces the tests that were helpful in the creation of the simplified method proposed in this thesis. The most important test is that conducted by Mehrabi et al. (1994), in which a series of 12 infilled frames were tested while varying parameters of interest. This testing sequence is crucial as it is used in this study to validate both the FEM model and simplified method results. Other tests presented in this chapter are the tests by Leuchers and Scrivener (1979), Kakaletsis et al. (2009) and Haider (1995).

Chapter 4 Outline: Parametric Study

A finite element modeling scheme described in Stavridis (2009) is used in a parametric study on the properties of the infill and frame. The parametric study consists of three sets of models, each set is based on a base model with selected properties to have a certain behavior. The models of the first set have a very strong infill and fail in brittle manner. The second set of models have a hollow brick infill and are therefore much more ductile than the first set. The third set of models vary from brittle to ductile as the infill and frame are of comparable strength. Design parameters changed include vertical load, infill length, column reinforcement and column width.

Chapter 5 Outline: Analysis of Parametric Study Results

The analysis of the results from the parametric study is presented in Chapter 5 to provide insight as to how the steps of the simplified method were determined. First a discussion of the weak or strong nature of the specimens is given. This is followed by the analysis of the drift at peak or onset of residual capacity of the specimens.

Chapter 6 Outline: Simplified Method Overview

The steps of the simplified method for analyzing masonry infilled RC frames are presented in Chapter 6. The procedure allows the estimation of the strength and drift at the yield, peak and onset of residual load for single bay, single story infilled frames. The proposed methodology also provide guidance as to determining if a case is weak or strong, as well as the expected failure pattern of the specimen. By following the steps of the simplified method a backbone curve can be derived to capture the behavior of an infilled frame without the need for an elaborate finite element modeling analysis.

Chapter 7 Outline: Validation of Proposed Method

The simplified method described in Chapter 6 is validated with the results of experiments as well as the results of the parametric study. The results from the experiments discussed in Chapter 3 are first used to evaluate the simplified method when applied to experimental results. Then, the results of the parametric study are used to assess the proposed simplified method. The experimental and parametric study results show the simplified method is accurate for a wide range of cases.

Chapter 8 Outline: Summary and Conclusions

A brief summary of the previous chapters is presented in chapter 8. Following the summary the important conclusions from the parametric study are reviewed. The chapter concludes with a number of suggestions for future research in the topic of simplified methods for the analysis of infilled RC frames.

Chapter 2

Review of Previously Proposed Analytical Methods

The seismic performance of infilled RC frames has been the subject of many experimental and analytical studies for the last fifty years. The result of this research is a plethora of suggestions for the analysis of infilled frames. The finite element method has become the most reliable means of analyzing all types of structures, and many case studies have been devoted to the development of finite element methods applicable to infilled RC frames. The use of finite element analysis for infilled frames is introduced below through a discussion of the history and significant steps to developing a reliable finite element procedure for infilled frames. Many of the proposed 'simplified' methods aim at estimating the strength and stiffness of the structure by using an equivalent compressive strut which is used to simulate the effect of the infill and analyzing the structure as a simple braced frame. These methods are discussed in the section of this chapter reviewing various equivalent strut methods. Finally, numerous methods have been proposed for finding the strength of an infilled frame by defining the strength associated with the expected failure. The limit state methods are often the quickest means of analysis, but often the least accurate. These methods will be discussed below in the section reviewing limit state methods.

Finite Element Methods

Finite element analysis of masonry infilled frames is the most refined and accurate means for analyzing infilled frames. Beginning with Mallick and Severn (1967) the development of a finite element method that captures the behavior of infilled frames has been a long process. The earliest finite element techniques as proposed by Mallick and Severn accounted for the varying contact length between the infill and masonry as

well as friction in the infill. Klingner and Bertero (1978) produced a numerical analysis for several tested specimens using elastic-hardening elements in the frame and diagonal strut elements in the infill. The method by Klingner and Bertero involved more elements that had been calibrated for each model and was thus more effective than the method introduced by Mallick and Severn (1976). The smeared crack approach was shown to be effective in modeling RC members but Lotfi and Shing (1991) argued the method alone is ineffective for masonry infilled frames. To overcome the shortcomings of the smeared crack approach Mehrabi and Shing (1997) as well as Shing and Spencer (2001) introduced the combination of discrete crack elements with the smeared crack elements. Finally the use of interface elements in the columns introduced by Shing and Spencer (2001) allowed modeling of shear cracks in the column. The smeared crack and discrete crack elements of these methods required constitutive models that govern the behavior of the frame properties.

Constitutive models allow the finite element analysis to capture the nonlinear behavior of the infill and frame. However, a majority of the constitutive models are only applicable to the models it has been developed for and thus many constitutive models have been proposed including Cervenka and Gerstle (1971), Lotfi and Shing (1991), and Oliveira and Lourenco (2004) to name only a few. Stavridis and Shing (2010) present a finite element modeling and calibration scheme which is discussed in depth in Chapter 4. The method by Stavridis and Shing (2010) combines the use of smeared crack and interface elements to reproduce the different types of cracking in infilled frames.

As opposed to the limit state and equivalent strut methods the finite element methods are a collective effort by many studies that is growing more accurate with time. With the combined elements and proper calibration the finite element analysis is capable of accurately reproducing experimental results. The details of finite element modeling of

infilled frames are described further in Chapter 4 when the finite element method used in this case study is introduced.

Equivalent Strut Methods

Much of the focus given to estimating the stiffness of infilled frames has been toward finding the properties of an equivalent compressive strut. The goal is to find the properties of the strut that when placed as a brace along the diagonal of the frame of interest, the braced frame structure behaves in a way similar to the real infilled frame. The main variable of interest when defining the equivalent strut is the strut width; therefore many of the methods described have the objective of developing an equation for the strut width. While methods by Stafford-Smith and Carter (1961), Liauw and Kwan (1984) and others provide lengthy, empirical equations for the strut width, many researchers proposed the strut width be a fraction of an infill dimension. For example: Holmes (1961) suggested the width be 1/3rd of the infill diagonal length, Moghaddam and Dowling (1988) suggested the width be 1/6th of the infill diagonal length, Paulay and Priestley (1992) suggested the strut width be 1/4th of the infill diagonal length. In this section some of the studies using diagonal strut methods that provided new insight or became widely embraced in the proposed methods of others are discussed briefly. The list is not exhaustive by any means as there were contributions made by Holmes (1961), Decanni et al. (1986), Durrani et al. (1994), Bennet et al. (1996), and many others that further aimed to accurately quantify the equivalent strut width.

Polyakov 1956

Polyakov (1956) was the first to report the relation between infilled frames and braced frames through the use of an equivalent strut. By studying four-hinge steel frames with masonry infills Polyakov (1956) provided the first equations to calculate the strut

properties. An equivalent strut having the material properties and thickness of the masonry, was suggested along with a suggestion for the equivalent strut width. Much of the following research expanded upon Polyakov's method with more realistic specimens having fixed bases and RC frames.

Stafford-Smith & Carter 1961

The equivalent strut method was expanded upon by Stafford-Smith and Carter (1961) who provided an equation to directly estimate the width of the equivalent strut of a masonry infilled RC frame. The equation takes into account the dimensions and material properties of the frame and infill through the use of a 'characteristic stiffness parameter' λ . Stafford-Smith and Carter (1961) provide curves correlating the equivalent strut width to the stiffness parameter λ .

The equation for the equivalent strut width is given as:

$$a = \frac{\pi}{2\lambda} \quad (2.1)$$

$$\lambda = \sqrt[4]{\frac{E_m t \sin 2\theta}{4E_c I h}} \quad (2.2)$$

Where a is the length of contact between frame and infill, E_i is the modulus of elasticity of the infill, t is the thickness of the infill, θ is the angle of diagonal of infill, E_m is the modulus of elasticity of frame, I is the moment of inertia of column, and h is the height of the infill.

Liauw & Kwan 1984

Liauw and Kwan further expanded on the equivalent strut method with the use of finite element analysis and experimental results from Barau and Mallick (1977). The line of best fit from the experimental data and the finite element analysis results yields the equations for the equivalent strut width in equation (2.3) .

$$w = \min \left\{ \begin{array}{l} 0.45h \cos \theta \\ w = \frac{0.86h \cos \theta}{\sqrt{\lambda h}} \end{array} \right. \quad (2.3)$$

Where w is the equivalent strut width in mm , h is the story height in mm , θ is the angle of diagonal of the infill, and λ is the characteristic stiffness parameter as in Eq. 2.2.

Limit State Methods

The strength of infilled frames is not easy to predict due to the many possible failure mechanisms. To address this, many researchers have provided equations to find the capacity for various limit states of an infilled frame. Many methods for calculating the strength still use the equivalent strut method, while others aim to predict the force required to initiate failure in the specimen such as sliding or crushing in the infill, or plastic failure of the frame. Studies that identified the mechanics behind the prominent failure mechanisms are listed in this section. The studies have been listed here as they yield equations that influenced or are ultimately used in the proposed simplified analytical procedure. A number of studies that produced important findings for defining the limit states of infilled frames are not discussed here for conciseness as they are not directly applicable or are redundant to the other studies described.

Mainstone 1971

Mainstone (1971) suggested the ultimate strength of an infilled frame be given by the summation of the lateral strengths of the frame and infill as given below:

$$H = H_f + H_i \quad (2.4)$$

$$H_i = R_c \cos \theta \quad (2.5)$$

$$R_c = f'_m w_i t \quad (2.6)$$

Where H is the lateral strength of an infilled frame, H_f is the lateral strength of a bare frame, H_i is the lateral strength of an infill, R_c is the maximum diagonal load on the infill, θ is the maximum diagonal load on the infill, f'_m is the crushing strength of the infill, w_i is the equivalent strut width of the infill and t is the infill thickness.

The equivalent strut width used in Equation 2.6 is found in Mainstone (1971) and is dependent on infill type and the value of the characteristic stiffness parameter.

Wood 1978

The first study towards the plastic strength contribution of the frame was conducted by Wood (1978). Two modes of failure are considered, the first mode is the shear failure of the infill with plastic hinges in the frame, and the second involves shear rotation of the infill with plastic hinges in the frame. The equations for finding the capacity associated with these failures are given below as:

$$F_s = \frac{4M_p}{h} + \frac{1}{2} \sigma_c Bt \quad (2.7)$$

$$F_r = \frac{2(M_p + M_e)}{h} + \sqrt{(C - C^2)} \sigma_c Bt \quad (2.8)$$

Where F_s is the ultimate capacity of a shear sliding/plastic hinge failure, F_r is the ultimate capacity of shear rotation/plastic hinge failure, M_p is the plastic moment of columns, M_e is the end plastic moment of the frame beam, h is the infill height, C is the ratio of horizontal wall stress to crushing stress, σ_c is the compressive principle stress in infill, B is the infill length, and t is the infill width.

Rosenblueth 1980

Rosenblueth (1980) suggested that rather than plastic strength of the frame influencing the capacity, the resistance is instead controlled by the failure of the infill, either in shear or compression. Rosenblueth presents two equations, the first for estimating the strength of a panel when infill sliding is expected, the second for the case when infill crushing is expected.

$$R_s = (0.9 + 0.3 \frac{l}{h}) f_b h t \quad (2.9)$$

$$R_c = 2/3 a t f'_m \sec \theta \quad (2.10)$$

Where R_s is the diagonal strut force at the onset of sliding, R_c is the diagonal strut force at onset of crushing, l is the infill length, h is the infill height, f_b is the cohesive bond strength of infill, t is the infill thickness, a is the contact length between column and infill, f'_m is the compressive strength of masonry and θ is the angle of diagonal of infill.

Liauw & Kwan 1983

Liauw and Kwan (1983) tried to find the strength capacity in situations with infill crushing and frame plastic failure. Liauw and Kwan (1983) propose equations that estimate the capacity of four modes of failure: Mode-I involves crushing of the infill corner and column plastic failure, Mode-II involves crushing of the infill corner and beam plastic failure, Mode-III involves crushing of the infill diagonal and beam plastic failure, Mode-IV involves crushing of the infill diagonal and column plastic failure. The equations below can be used to estimate the capacity of the four modes of failure.

$$H_1 = \sigma_c t h \sqrt{\frac{2(M_{pj} + M_{pb})}{\sigma_c t h^2}} \quad (2.11)$$

$$H_2 = \frac{\sigma_c t h}{\tan \theta} \sqrt{\frac{2(M_{pj} + M_{pb})}{\sigma_c t h^2}} \quad (2.12)$$

$$H_3 = \frac{4M_{pj}}{h} + \frac{\sigma_c t h}{6} \quad (2.13)$$

$$H_4 = \frac{4M_{pj}}{h} + \frac{\sigma_c t h}{6 \tan^2 \theta} \quad (2.14)$$

Where H_i is the collapse shear of failure mode i , σ_c is the compressive strength of infill, t is the infill thickness, h is the story height, M_{pj} is the plastic moment capacity of joint, M_{pb} is the plastic moment capacity of beam and θ is the angle of the diagonal of the infill.

Stafford-Smith & Coull 1991

Stafford-Smith and Coull (1991) expanded upon the work of Stafford-Smith and Carter (1966) to provide equations that capture the limit state of infill crushing and sliding, as well as corner crushing and tensile splitting. Equation 2.15 estimates the shear

capacity, F , of the infill. Equation 2.16 is given for cases where corner crushing is expected and Equation 2.17 applies for the tensile splitting failure mode.

$$F_s = 0.7Lt f_{s,max} \quad (2.15)$$

$$F_c = 1.12 \left(\frac{4EI}{E_m t h^3} \right)^{0.22} f'_m h t \cos^2 \theta \quad (2.16)$$

$$F_t = 1.7L t f'_t \quad (2.17)$$

Where F_s is the shear sliding strength in KN , F_c is the force initiate infill crushing in KN , F_t is the force to cause tensile splitting in KN , L is the infill length in mm , t is the infill thickness in mm , $f_{s,max}$ is the maximum allowable shear stress in the infill in KN/mm^2 , E in KN/mm^2 and I in mm^4 are the Young's modulus and moment of inertia of the columns respectively, E_m is the Young's modulus of the masonry in KN/mm^2 , h is the infill height in mm , f'_m is the masonry strength in KN/mm^2 , θ is the angle of the diagonal of the infill and f'_t is the allowable tensile stress in the infill in KN/mm^2 .

Mehrabi, Shing, Schuller, and Noland 1994

Mehrabi et al. (1994) tested 13 structures in an experimental study that will be discussed in depth in the next chapter. An entire procedure for the analysis of infilled frames stiffness and strength is proposed. Several equations were adopted and from other studies and modified to match the observations of the study by Mehrabi et al. (1994). Mehrabi et al. (1994) proposed two possible failures, infill sliding and crushing, and the corresponding capacities are shown in the equations below.

$$V_{wc} = \frac{C + \frac{\mu P}{A_w + 2A_c}}{1 - \frac{\mu h}{L}} A_w \quad (2.18)$$

$$V_{crush} = w t f'_m \cos \theta \quad (2.19)$$

Where V_{wc} is the horizontal sliding strength of infill, V_{wc} is the crushing strength of infill, A_w is the cross sectional area of infill, A_c is the cross sectional area of the columns, P is the

total vertical load, μ is the coefficient of sliding friction, L is the infill length, h is the infill height, w is the equivalent strut width, t is the infill thickness and θ is the angle of the infill diagonal.

These capacities are modified and combined with the column capacities to define 5 possible failure mechanisms including sliding failure of the infill and shear or flexural failure of one or both columns. Mechanism 1 applies to the case of ductile infills in which flexural failures of both columns is expected. Mechanism 2 applies to cases with flexural failure at one column and shear failure in the other. Mechanism 3 applies to cases where infill crushing is expected along with plastic hinge failures of the columns. Mechanism 4 is another case where plastic hinges are expected to form, but closer to the columns and with infill crushing localized at the corners. Lastly, mechanism 5 applies to cases with poor bonding between the frame and infill and estimates the strength as the sum of the frame flexural strength and the infill sliding strength.

Galanti, Scarpas and Vrouwenvelder, 1998

Galanti et al (1998) analyzed sliding of the infill along with sliding along the bed joint. The sliding strength of the infill is given by Equation 2.20. The equation assumes sliding is possible along any bed joint of the infill and thus it is difficult to provide reinforcement that would stop this kind of failure. Galanti et al. (1998) proposed that the strength found in Equation 2.20 serve as a conservative maximum allowable strength of the infill.

$$F = \tau lt \tag{2.20}$$

Where τ is the shear strength of the infill mortar, l is the infill length and t is the infill thickness.

FEMA 306 1999

FEMA 306 (1999) provides capacity estimates for four expected failures for infilled frames. The failures considered include sliding failure, compressive failure of the infill, tension failure of the infill or shear failure of the infill. The equations for determining the strength associated with these four failures are given below

$$V = \mu N \quad (2.21)$$

Where V is the sliding strength of the infill, μ is the coefficient of sliding friction in the infill, and N is the vertical force on the infill.

$$V = atf'_m \cos \theta \quad (2.22)$$

Where V is the shear force to start crushing of the infill, a is the equivalent strut width as in Mainstone (1970), f'_m is the strength of masonry in horizontal direction, and θ is the angle of diagonal of infill.

$$V = \frac{2\sqrt{2}t\sigma}{\left(\frac{L}{h} + \frac{h}{L}\right)} \quad (2.23)$$

Where V is the shear force to start tension splitting in infill, t is the infill thickness, σ is the masonry cracking capacity, l is the length of infill and h is the height of infill, all units in SI.

$$V_i = 2\sqrt{f'_m}A_w \quad (2.24)$$

$$V_f = 0.3V_i \quad (2.25)$$

Where V_i is the initial shear failure capacity, V_f is the final shear failure capacity, A_w is the area of the infill and f'_m is the compressive strength of masonry.

ASCE 41 2006

ASCE 41(2006) provides recommendations for assessing the need of seismic rehabilitation of infilled frames. ASCE 41 (2006) provides guidelines for estimating the strength and possible drift of infilled frames and recommends the use of a backbone curve as shown in Figure 2.1 as the shape of this backbone can be used to idealize the

behavior of infilled frames. ASCE 41-06 provides acceptance criteria for the points on the backbone curve but is limited in the subject infilled frames as shown in Table 1.1. The table shows that of the four definable points only the length 'd', the drift at peak capacity, is included in ASCE 41 (2006). Unfortunately the ASCE 41 (2006) does not suggest acceptance criteria for the strength of the infilled frame or the drift at the yield and point at the onset of residual load plateau.

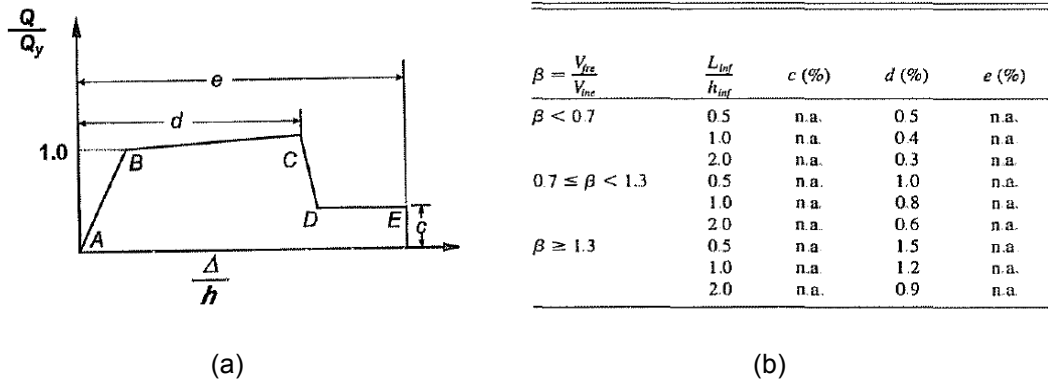


Figure 2.1 Provisions of ASCE 41 (2006). (a) Backbone curve of force-vs-drift for RC elements ASCE 41 (2006) and (b) Acceptance criteria for backbone curve from ASCE 41 (2006).

Stavridis 2009

The study by Stavridis (2009) serves as the basis for the final method proposed in this study. Stavridis (2009) performed a parametric study on infilled frames with a strong infill using finite element analysis. Using the results of the parametric study and provisions from previous research, Stavridis (2009) presents a set of steps for estimating both the strength and stiffness of an infilled frame. The initial stiffness is calculated as that proposed by Mehrabi et al. (1994) based on the shear beam concept proposed by Fiorato (1970). The peak strength equation assumes a shear failure in each of the RC columns and shear/sliding failure of the infill and is given by Equation 2.26.

$$V_{max} = \Psi(V_{c1} + V_{c2}) + P_w\mu + A_wC \quad (2.26)$$

Where V_{max} is the peak capacity of the infilled frame, Ψ is a reduction factor from 0 – 1, V_c is the shear strength of the column from ACI 318, P_w is the vertical load on the infill, μ is the coefficient of sliding friction, A_w is the area of infill and C is the cohesive bond strength of the infill.

Stavridis (2009) built upon the recommendations of ASCE 41-06 which suggests the relation between infill aspect ratio and lateral drift at peak load. From the linear trend found through a parametric study the following equation for drift at peak load, Δ_{peak} , is given:

$$\text{For } l/h < 2: \Delta_{peak} = 0.86 - 0.33 l/h \quad (2.27)$$

$$\text{For } l/h > 2: \Delta_{peak} = 0.15$$

The yield strength is taken as 2/3 the peak strength and the drift at yield is determined by dividing the yield load by the initial stiffness. The residual capacity is a combination of the residual friction resistance of the infill and the shear strength of column stirrups. The equation for residual strength, V_{res} is given as

$$V_{res} = A_v f_y n_s + P_w \mu_{res} \quad (2.28)$$

Where A_v is the total area of stirrups in one layer, f_y is the yield strength of stirrups, n_s is the number of stirrups crossing shear crack, P_w is the vertical load on infill and μ_{res} is the coefficient of sliding friction of damaged infill.

Chapter 3

Review of Available Experimental Studies

This chapter describes a series of experiments pertinent to the study presented here. Many experiments have been conducted on the performance of infilled frames, the four studies considered here have been selected due to the availability of on material properties and design details and the force-displacement relations. This includes the experiments by Mehrabi et al. (1994) which are used to validate the finite element method used in this study as well as the simplified method proposed in here. Tests by Leuchars and Scrivener (1979), Kakaletsis and Karayannis (2009), and Haider (1995) are included as the tests results from these experiments are used to validate the simplified method presented in Chapter 6.

There are many other experimental studies that are of importance to the study of infilled frames that have been left out of this discussion such as Al-Chaar (1998), Crisafulli (1997), Centeno (2004) and many others. This does not imply the studies considered in this chapter here offer more insight than those not discussed. Rather these studies have been included due to the availability and clarity of the results when testing single bay-single story unreinforced masonry infilled RC frames without openings. As the method is improved in future research to include cases with multiple stories or openings other studies become applicable and can be used to validate the expanded method. For the time being only the aforementioned studies are discussed below.

Leuchars and Scrivener 1979

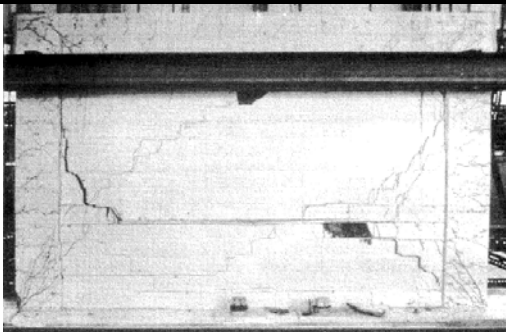
Three specimens were tested by Leuchars and Scrivener (1979) including a bare frame, an infilled frame with grouted masonry, and an infilled frame with reinforced,

grouted masonry. Of these three specimens the unreinforced infilled frame is of the most interest here as it most closely resembles the structures considered in this study.

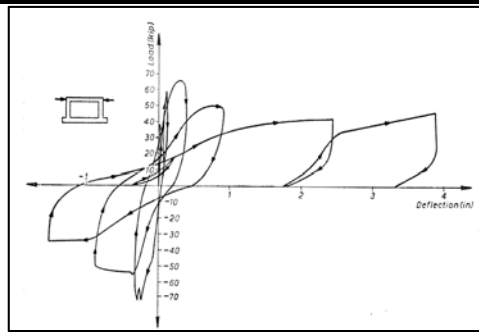
The force-vs-displacement curve given in Figure 3.1 is from Leuchars and Scrivener (1979) for the unreinforced infilled frame. The specimen underwent diagonal cracking and sliding in the infill, leading to major shear failures in the columns. This type of failure can be attributed to the rigid nature of the infill due to the grouted masonry. The panel first separated from the beam at a load of 38 kips, followed by diagonal cracking and sliding in the infill at 50 kips horizontal load. At 70 kips horizontal load the infill crack reached from corner to corner of the panel and causes a shear failure in the columns leading to a major drop of capacity.

Table 3.1. Properties of specimen tested by Leuchars and Scrivener (1979)

Specimen	Column dimensions (LxW) in	Infill dimensions (LxWxH) in	Total Stirrup area in ²	Stirrup spacing in	Column reinforcing ratio %	Vertical load Kips
Grouted Unreinforced infill	8 x 6	71 x 4.25 x 46	0.1	2	3.9	0



(a)



(b)

Figure 3.1 Test results from Leuchars and Scrivener (1979). (a) illustration of failure at 0.9" displacement and (b) force-vs-displacement behavior of specimen

Haider 1995

Four full scale, single story-single bay infilled frame specimens were tested by Haider (1995). The sequence of testing was such that the frames were first constructed and tested without the infill panel in place. The frames were tested up to 1% drift and then repaired, infilled with masonry, and tested again. Due to the initial damage to the RC frames three of the cases are have unusually low strength and stiffness. However the undamaged model A-1 had high shear reinforcing of the columns and a weak infill which led to a much higher stiffness and more ductile failure overall than the other specimens.

Table 3.2 Properties of specimens tested by Haider (1995)

Specimen	Column dimensions (LxW) in	Infill dimensions (LxWxH) in	Total Stirrup area in ²	Stirrup spacing in	Column reinforcing ratio %	Vertical load kips
A-1	10 x 10	89 x 3.5 x 86.5	0.22	5	1.76	0

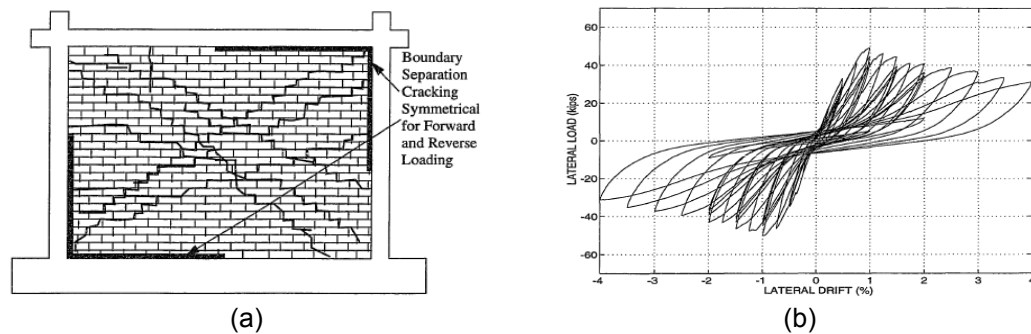


Figure 3.2 Test results for specimen A-1 from Haider (1995). (a) Crack pattern illustration and (b) force-vs-displacement behavior of specimen

Kakaletsis and Karayannis 2009

Ten 1/3 scale single story, single bay specimens were tested by Kakaletsis and Karayannis (2009) in a parametric study to determine the effects different openings on the behavior of infilled frames. Of these ten specimens, one was a bare frame, eight had an infill with an opening, and one specimen had a solid infill. The specimen with the solid

infill is the only relevant specimen to this study and will be the focus of the discussion for this experimental study. The properties of the infilled specimen are given in Table 3.3. The failure of this specimen included diagonal sliding in the infill and plastic hinges in the columns. The specimen has a weak infill with a frame designed to have ductile behavior. The force-displacement results and an illustration of the failure are provided in Figure 3.3.

Table 3.3 Properties of specimens tested by Kakaletsis and Karayannis (2009).

Specimen	Column dimensions (LxW) in	Infill dimensions (LxWxH) In	Total Stirrup area in ²	Stirrup spacing in	Column reinforcing ratio %	Vertical load Kips
Infilled specimen	5.85 x 5.85	46.8 x 2.3 x 31.2	0.022	1.5	0.88	0

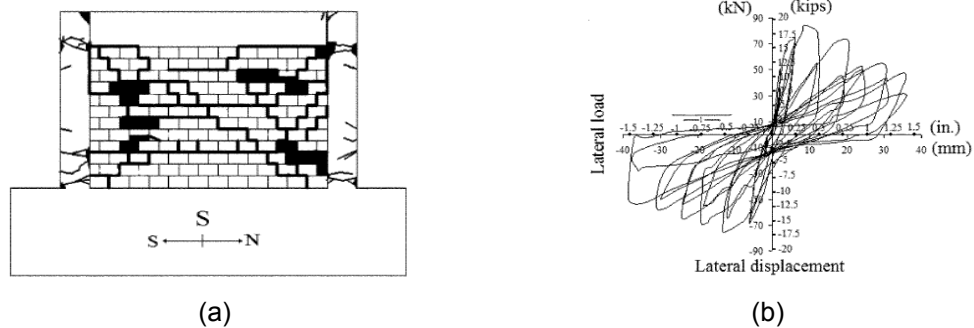


Figure 3.3 Test results from Kakaletsis and Karayannis (2009). (a) illustration of specimen failure and (b) force-vs-displacement behavior of specimen.

Mehrabi et al. 1994

Mehrabi et al. (1994) performed a well-documented and thorough experimental parametric study by testing the in-plane strength of 13 single story infilled frame structures at the University of Colorado at Boulder. The parametric study varied properties between the specimens including the specimen dimensions, vertical load, aspect ratio, loading type (cyclical or monotonic) as well as the number of bays. From this study 12 of the 13 specimens had a single bay and are discussed here. The properties of

the eleven infilled single bay specimens are given below in Tables 3.4 and 3.5. The odd numbered specimens in Table 3.4 had solid brick infills while the even numbered specimens in Table 3.5 had hollow brick infills. This difference in infill type was shown to make a considerable difference in the failure type for the specimens. The hollow brick cases often had flexural failures in the columns or delayed shear failures in the columns. On the other hand the solid brick cases typically all had major shear failures in the columns resulting in brittle behavior. The results of the specimens tested by Mehrabi et al. (1994) are presented in Figures 3.4 and 3.5. An example can be made with Figure (d) in both Figures 3.4 and 3.5. Specimen 8, which has a hollow infill, is shown in table 3.5 (d) and from the Figure the specimen's peak capacity is shown as 43 kips followed by a gradual load drop. Specimen 9 shown in Figure 3.4 (d) reuses the frame of Specimen 8 but instead has a solid brick infill. The addition of a solid infill increases the capacity from 43 kips in Specimen 8 to 65 kips in Specimen 9, and causes a more instantaneous load drop as seen in Figure 3.4 (d). The effect of aspect ratio was investigated by testing infills 84" and 116" long. The specimens with longer infill had generally more capacity than the shorter specimens. The effect of vertical load was investigated by changing the load from 66 kips in the base model to 99 kips in Specimen 12. The increased vertical load causes an increase in capacity for Specimen 12.

Table 3.4 Properties of solid brick specimens tested by Mehrabi et al. (1994)

Model #	f'_c psi	f'_m psi	Column dimensions (LxW) in	Infill dimensions (LxW) in	Infill height in	Total stirrup area in ²	Stirrup spacing in	Column reinforcing ratio %
3	4480	2200	7 x 7	84 x 3.625	56	0.10	2.5	3%
5	3030	2010	7 x 7	84 x 3.625	56	0.10	2.5	3%
7	4850	2000	8 x 8	84 x 3.625	56	0.10	1.5	4%
9	3900	1400	7 x 7	84 x 3.625	56	0.10	2.5	3%
11	3730	1660	7 x 7	116 x 3.625	56	0.10	2.5	3%

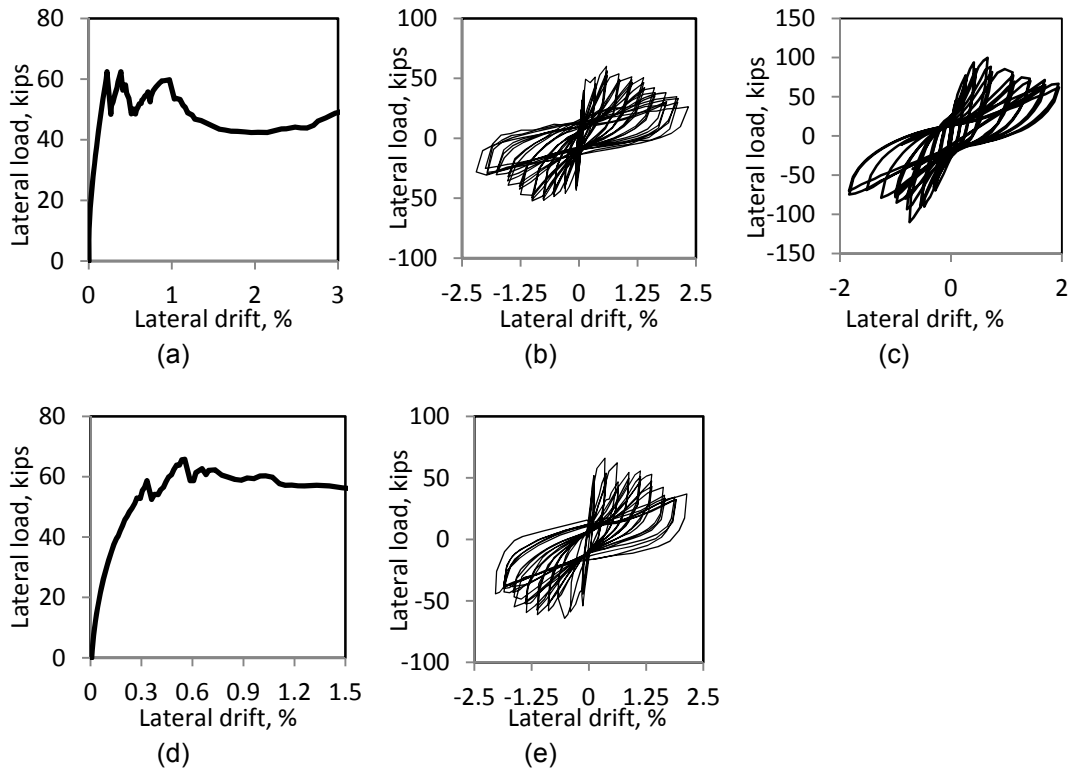


Figure 3.4 Force-vs-drift curves for Mehrabi et al. specimens with solid brick infill. (a) Specimen 3, (b) Specimen 5, (c) Specimen 7, (d) Specimen 9, (e) Specimen 11.

Table 3.5 Properties of hollow brick infilled specimens tested by Mehrabi et al. (1994)

Model #	f'_c psi	f'_m psi	Column dimensions (LxW) in	Infill dimensions (LxW) in	Infill height in	Total stirrup area in ²	Stirrup spacing in	Column reinforcing ratio %
2	4480	1400	7 x 7	84 x 1.25	56	0.10	2.5	3%
4	3890	1540	7 x 7	84 x 1.25	56	0.10	2.5	3%
6	3750	1500	8 x 8	84 x 1.25	56	0.10	1.5	4%
8	3900	1400	7 x 7	84 x 1.25	56	0.10	2.5	3%
10	3900	1540	7 x 7	116 x 1.25	56	0.10	2.5	3%
12	3900	1970	7 x 7	116 x 1.25	56	0.10	2.5	3%

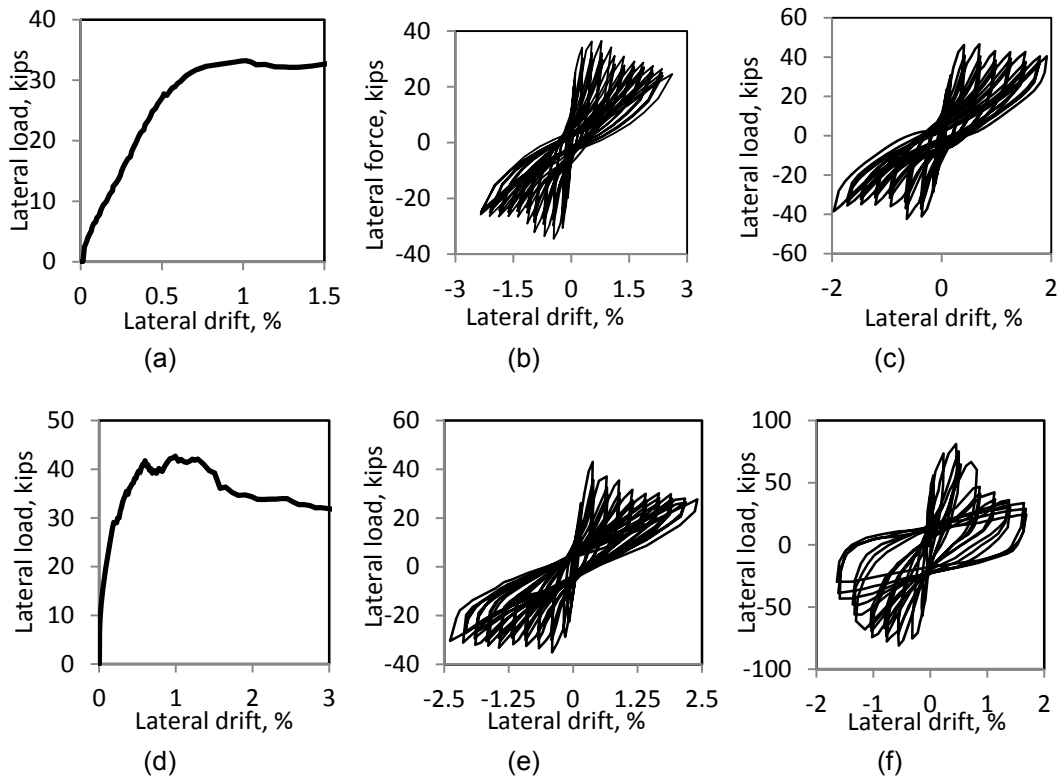


Figure 3.5 Force-vs-drift curves for Mehrabi et al. (1994) specimens with hollow brick infill. (a) *Specimen 2 initially damaged before testing, (b) Specimen 4, (c) Specimen 6, (d) Specimen 8, (e) Specimen 10, (f) Specimen 12

Blackard et al. 2009

Six large scale specimens were tested at the University of Colorado at Boulder in order to gain insight to the effect of openings and retrofit techniques on infilled frames. One of the six specimens had a solid infill while the other cases had various opening types or a repaired infill. The unretrofitted specimen with the solid frame, referred to as specimen CU1, served as the base model in both the experimental study as well as the parametric study used to establish the simplified method in Stavridis (2009). The specimen had a brittle failure due to the strong infill composed of two wythes of solid bricks and poor reinforcement detailing in the frame. The properties of specimen CU1 are

given in Table 3.6 below along with an illustration of the specimen design in Figure 3.5. The specimen design parameters are chosen to represent a 2/3 scale bay from a 3 story structure that would be tested in a study by Stavridis (2009). The force-vs-displacement relation for specimen CU1 when subjected to cyclical loading is shown in Figure 3.5.

Table 3.6 Properties of specimen CU1 from Blackard et al. (2009)

Specimen	Column dimensions (LxW) in	Infill dimensions (LxWxH) in	Total Stirrup area in ²	Stirrup spacing in	Column reinforcing ratio %	Vertical load Kips
Infilled specimen	11 x 11	130 x 7.2 x 73.5	0.15	11.5	1%	76

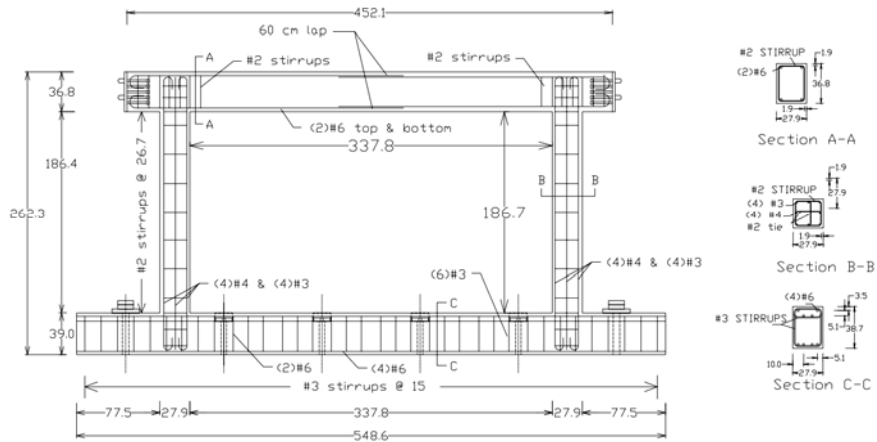


Figure 3.5 Design of RC frame for Specimen CU1 of Blackard et al. (2009) (units in cm)

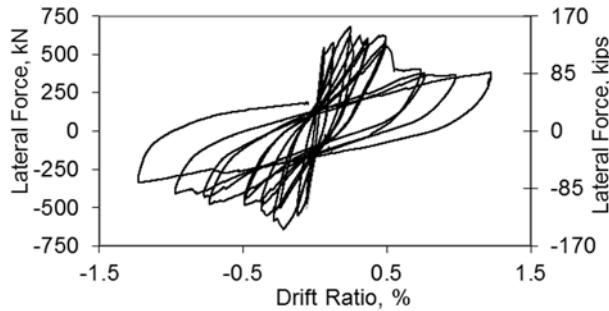


Figure 3.6 Force-vs-drift curve for specimen CU1 Blackard et al. (2009)

Chapter 4

Parametric Study

A parametric study was conducted to examine the influence of various parameters on the behavior of infilled frames. This chapter provides the material properties and geometry of the models considered, as well as the results of the parametric study. A finite element method described below was used to simulate the behavior of 59 models with varying properties undergoing monotonic lateral loading. The specimens were based on three baseline models referred to as CU1, CU1M8 and CU1S. Specimen CU1 is based on the specimen with the same name tested at the University of Colorado in a study on the influence of openings on infilled frames (Blackard 2009). The second set of models uses CU1M8 as a base model, which has the same frame properties as CU1 but has infill properties of two wythes of bricks as those used in Mehrabi et al. (1994) Specimen 8. The third and final set of models used CU1S as a base model which has the same frame and infill properties as CU1 but with column stirrup spacing equal to 1/4th of the spacing of that in CU1. The properties of the base models of the parametric study are given in Table 4.1.

Table 4.1 Properties of base models in parametric study

Base model	Infill type	Vertical load Kips	Infill aspect ratio (L/H)	Total Stirrup area in ²	Stirrup spacing in	Column reinforcing ratio %
CU1	Blackard et al. (2009)	76	1.77	0.15	11.5	1%
CU1M8	Mehrabi et al. (1994) Spec. 8	76	1.77	0.15	11.5	1%
CU1S	Blackard et al. (2009)	76	1.77	0.15	2.75	1%

Parametric Study Base Models

The models in the parametric study are all related by using the specimen CU1 from the study by Blackard et al. (2009), or a variation thereof, as a base model for all the specimen models. Due to the robust infill and the lightly reinforced frame, Specimen CU1 provides a good basis of a model that is expected to have brittle behavior controlled by the infill capacity. A second set of models have been created by replacing the CU1 infill with an infill matching the properties of specimen 8 from Mehrabi et al. (1994). This provides a base model with a weak infill and relatively ductile behavior. Finally, the original CU1 model is reused but with closer stirrup spacing in the frame. The last set of models has infills of comparable strength to the surrounding frame leading to a variety of failure patterns. With these three sets of models various failure patterns were observed. The naming scheme used for the cases in the parametric study have 'P1', 'P2' or 'P3' at the beginning of all cases indicating the initial baseline model used.

The first set of models is described in Stavridis (2009). The models are generally strong infill cases with brittle behavior. The infill of this specimen is composed of two wythes of solid clay brick. The frame is composed of columns that are 11" x 11" and have only 1% longitudinal reinforcement ratio and transverse stirrups spaced at 11.5". The first base model shows the characteristics of a strong infill-weak frame case as the peak, which occurs at 0.27% drift, is followed by a sudden load drop. The robust nature of the infill with such a weakly reinforced frame leads to the shear controlled brittle behavior. The finite element illustrations and force-vs-displacement results are given in Figure 4.3.

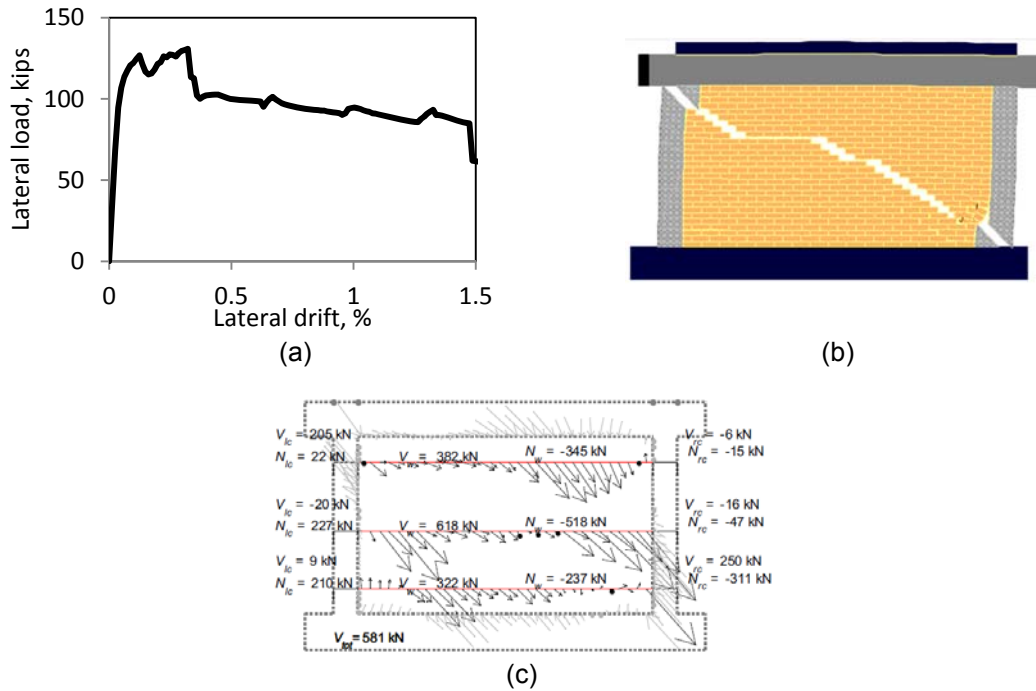


Figure 4.3 Specimen CU1, base model for first set of parametric study models. (a) Force-vs-drift curve, (b) Model at 1% drift and (c) Force distribution along three sections at point of peak strength.

The second set of models of the parametric study use the same frame properties as the first set of models, matching those of CU1. The infill of this set of models is considerably weaker, as it is modeled with the properties of the infill of specimen 8 tested by Mehrabi et al. (1994). Specimen 8 has an infill made of hollow clay bricks with a low modulus of elasticity. Unlike the brittle behavior of CU1, the weak infill specimen CU1M8 is much more ductile with a plateau at the peak followed by a small load drop to the residual strength plateau as shown in Figure 4.4. In this case the drift at peak occurs at 0.46% drift which is almost twice the drift of CU1 at peak. The comparison of CU1 and CU1M8 demonstrates the major impact of a rigid infill on the behavior of the structure. This case represents a flexural failure rather than a shear failure, as plastic hinges form in the frame prior to shear cracks. Furthermore, the hollow infill base model case has infill

crushing that develops at high drift that is not observed in the solid brick infill cases. The compressive struts in the infill that initiate crushing can be observed in the force illustration for CU1M8 shown in Figure 4.4 (c). The combination of sliding, cracking and crushing in the infill along with flexural failures in the frame is a common failure type for specimens with weak infills and frames with minimal flexural reinforcement.

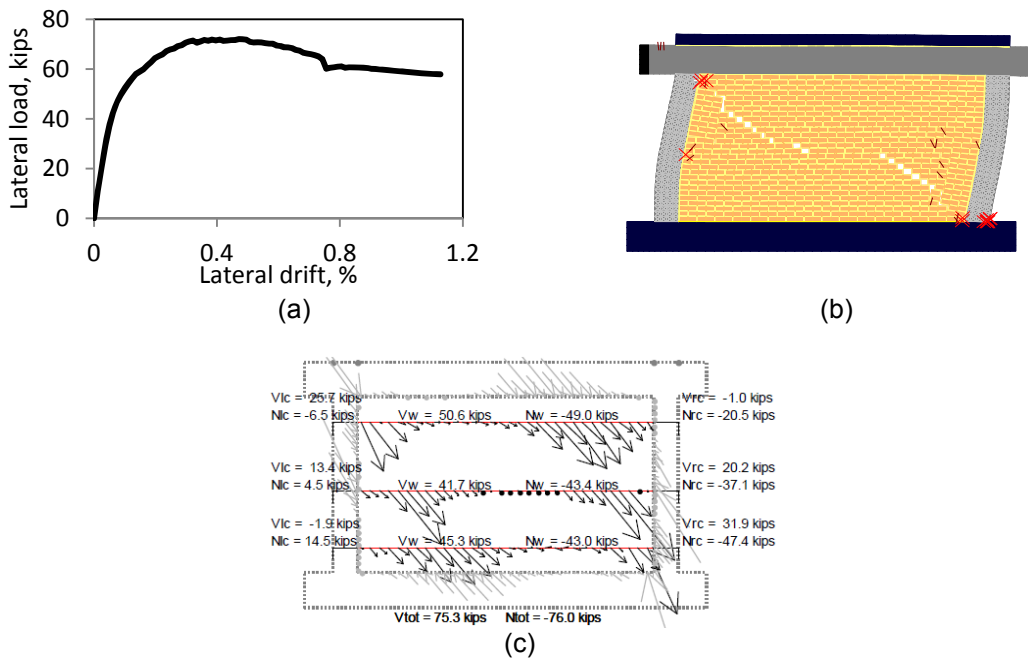


Figure 4.4 Specimen CU1M8, base model for second set of parametric study models. (a) Force-vs-drift curve, (b) Model at 1% drift and (c) Force distribution along three sections at point of peak strength.

The third set of models includes structures with infills that produce varying behavior. The third set of models use the CU1 infill and a modified CU1 frame. The CU1 frame has been modified for the base model of this set of cases to have stirrup spacing of 2.75" rather than the 11.5" stirrup spacing of CU1 thus significantly increasing the shear capacity of the frame to be close to that of the infill. As expected, various failure patterns were observed for the different cases considered. Figure 4.5 shows CU1S has a small

plateau at the peak strength which occurs at 0.30% drift. Despite the increased shear reinforcement the specimen has a major shear failure in the leeward column.

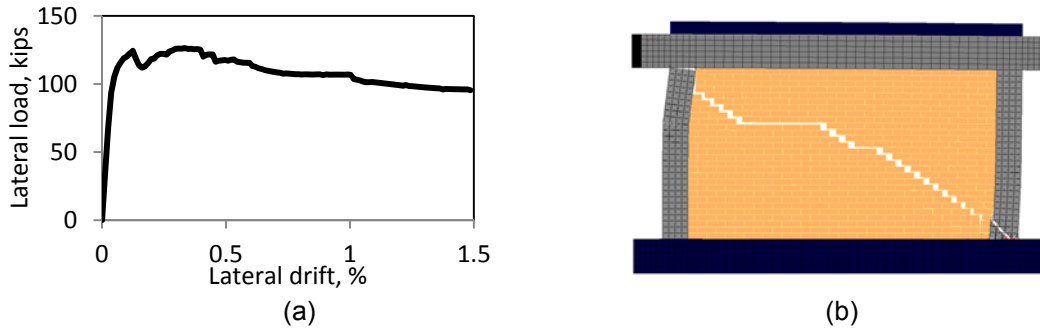


Figure 4.5 Specimen CU1S, base model for third set of parametric study models. (a) Force-vs-drift curve and (b) Model at 1% drift.

Parametric Study Models

Using the base models described in the previous section, 56 models were created with varying properties. In order to investigate the influence of each parameter independently only one parameter is changed between each model. The parameters changed between models include: vertical load, infill length, stirrup area, stirrup spacing, reinforcement ratio, and column size. The following letters indicate the variable being changed for the particular case: ‘F’, vertical load; ‘AR’, aspect ratio l/h ; ‘St’, area of stirrups; ‘D’, stirrup spacing; ‘Ro’, longitudinal steel area; ‘C’, column size. For example, model P1F40 is from the first set of models based on CU1 but has the vertical load changed to 40 kips.

Parametric Study Set 1

The properties of the first set of models is given in Table 4.2. Parameters varied in this set of models include infill length, stirrup area, stirrup spacing, reinforcement ratio and vertical load.

Table 4.2 Properties of first set of models in parametric study

	Specimen	Vertical load Kips	Infill aspect ratio (L/H)	Total Stirrup area in ²	Stirrup spacing in	Column reinforcing ratio %
Base model	CU1	76	1.77	0.15	11.5	1%
Vertical load	P1F0	0	1.77	0.15	11.5	1%
	P1F40	40	1.77	0.15	11.5	1%
	P1F80	80	1.77	0.15	11.5	1%
	P1F120	120	1.77	0.15	11.5	1%
	P1AR1	76	0.38	0.15	11.5	1%
Aspect ratio	P1AR2	76	0.90	0.15	11.5	1%
	P1AR3	76	1.39	0.15	11.5	1%
	P1AR4	76	2.15	0.15	11.5	1%
	P1AR5	76	2.72	0.15	11.5	1%
	P1AR6	76	3.10	0.15	11.5	1%
	Stirrup area	P1Stp5	76	1.77	0.07	11.5
P1St2		76	1.77	0.29	11.5	1%
P1St3		76	1.77	0.44	11.5	1%
P1St4		76	1.77	0.59	11.5	1%
Stirrup spacing		P1Dp5	76	1.77	0.15	5.75
	P1Dp25	76	1.77	0.15	2.875	1%
Column reinforcement ratio	P1Ro2	76	1.77	0.15	11.5	2%
	P1Ro3	76	1.77	0.15	11.5	3%
	P1Ro4	76	1.77	0.15	11.5	4%
	P1RoP5	76	1.77	0.15	11.5	0.5%

Parametric Study Set 2

The properties of the second set of models is given in Table 4.3. Parameters varied in this set of models include infill length, stirrup area, stirrup spacing, reinforcement ratio and vertical load.

Table 4.3 Properties of second set of models in parametric study

	Specimen	Vertical load kips	Infill aspect ratio (L/H) -	Total Stirrup area in ²	Stirrup spacing in	Column reinforcing ratio %
Base model	cu1m8	76	1.77	0.15	11.5	1%
Vertical load	P2f0	0	1.77	0.15	11.5	1%
	P2f40	40	1.77	0.15	11.5	1%
	P2f80	80	1.77	0.15	11.5	1%
	P2f120	120	1.77	0.15	11.5	1%
	P2AR1	76	0.38	0.15	11.5	1%
Aspect ratio	P2AR2	76	1.36	0.15	11.5	1%
	P2AR3	76	2.18	0.15	11.5	1%
	P2AR4	76	2.72	0.15	11.5	1%
	P2AR5	76	3.10	0.15	11.5	1%
	P2STp5	76	1.77	0.07	11.5	1%
Stirrup area	P2ST2	76	1.77	0.29	11.5	1%
	P2ST3	76	1.77	0.44	11.5	1%
	P2ST4	76	1.77	0.59	11.5	1%
	P2DP5	76	1.77	0.15	5.75	1%
Stirrup spacing	P2Dp25	76	1.77	0.15	2.875	1%
	P2Ro2	76	1.77	0.15	11.5	2%
Column reinforcement ratio	P2Ro3	76	1.77	0.15	11.5	3%
	P2Ro4	76	1.77	0.15	11.5	4%
	P2RoP5	76	1.77	0.15	11.5	0.5%

Parametric Study Set 3

The properties of the second set of models is given in Table 4.4. Parameters varied in this set of models include infill length, stirrup area, column width and vertical load.

Table 4.4 Properties of third set of models in parametric study

	Specimen	Vertical load kips	Infill aspect ratio (L/H) -	Total Stirrup area in ²	Column dimensions (LxW) in
Base model	CU1S	76	1.77	0.15	11 x 11
	P3F0	0	1.77	0.15	11 x 11
Vertical load	P3F40	40	1.77	0.15	11 x 11
	P3F80	80	1.77	0.15	11 x 11
	P3F120	120	1.77	0.15	11 x 11
	P3AR1	76	0.38	0.15	11 x 11
Aspect ratio	P3AR2	76	0.91	0.15	11 x 11
	P3AR3	76	1.39	0.15	11 x 11
	P3AR4	76	2.15	0.15	11 x 11
	P3AR5	76	2.72	0.15	11 x 11
	P3StP5	76	1.77	0.07	11 x 11
Stirrup area	P3St2	76	1.77	0.29	11 x 11
	P3St3	76	1.77	0.44	11 x 11
	P3St4	76	1.77	0.59	11 x 11
	P3C1	76	1.77	0.15	11 x 8
Column width	P3C2	76	1.77	0.15	11 x 12
	P3C3	76	1.77	0.15	11 x 16

Parametric Study Results

Effect of Vertical Load

The vertical load was changed in all three sets of models and was varied from 0 kips to 120 kips. The vertical load is distributed between the columns and infill proportionately to the axial stiffnesses of each element. The added vertical load increased the capacity of the specimens due to the increased friction strength which comes about from increased compressive stress in the infill. The first set of models in the

parametric study had such a strong infill that the specimens had a brittle failure for all values of vertical load. The weak infill of the second set models; however, with vertical load greater than 80 kips had an infill strong enough to initiate delayed shear failures in the columns. This behavior shows that the behavior of an infilled frame is not just dependent upon the specimen material properties alone, but instead the capacity of the individual elements. The final set of models had similar behavior to the second set of models in which the higher vertical caused a shift from ductile to brittle failure. While the vertical load is increased by 40 kips between each model, it is evident the peak strength increases by a fraction of the 40 kips increase. For example the increase in capacity is about 15 kips between each of the models of the third set with increased vertical load. As the force illustrations have shown, the struts in the infill typically form at a 45° implying the coefficient of friction is near one. Building on this assumption, the capacity would increase by equally to the vertical load were the vertical load not partially distributed to the columns.

It is evident in the force-vs-displacement graphs for the second set that as the vertical load is increased the behavior becomes more brittle. A closer look into model P2F40 indicates that the total infill capacity is only 39.7 kips while the column shear strength is 49.5 kips, therefore the infill lacks the strength to cause major shear failure in the column resulting in an overall ductile failure. This can be seen in the low shear forces in the columns in Figure 4.11. On the other hand, specimen P2F80 has combined cohesion and friction resistance of 46.0 kips due to the increased friction capacity which is now larger than the column shear capacity. The increased strength of the infill enables a higher transfer of force between columns and infill, ultimately resulting in major shear failure of the columns.

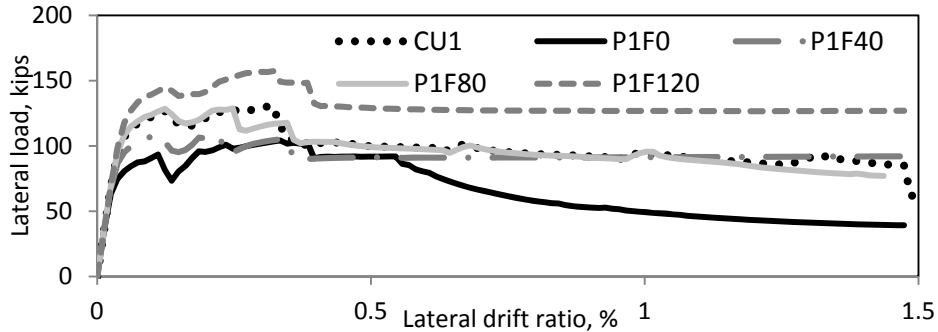


Figure 4.6 Parametric study results of first set models with different vertical loads.

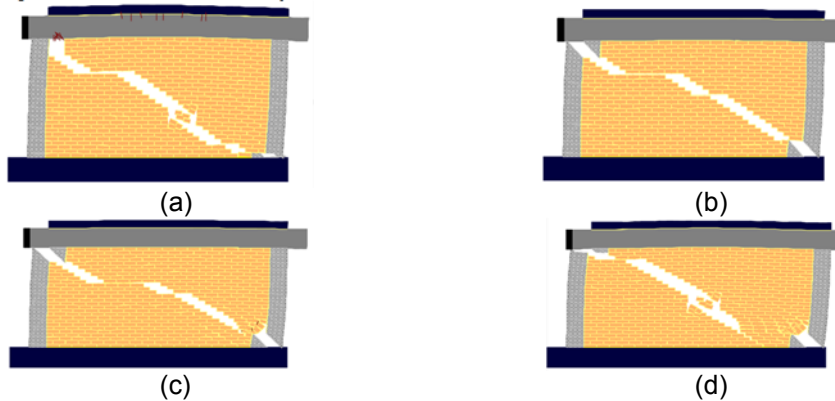


Figure 4.7 Cracking patterns at 1.0% drift for frames with different vertical load. (a) P1F0, (b) P1F40, (c) P1F80, (d) P1F120.

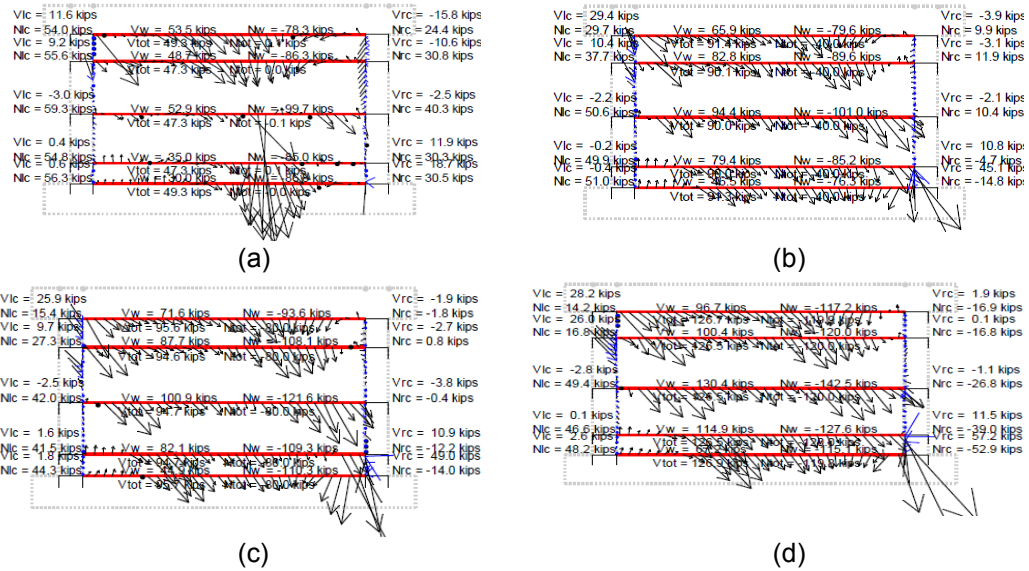


Figure 4.8 Force distribution along five cross sections at the instant of peak strength for cases of the first set with different vertical loads. (a) P1F0, (b) P1F40, (c) P1F80, (d) P1F120.

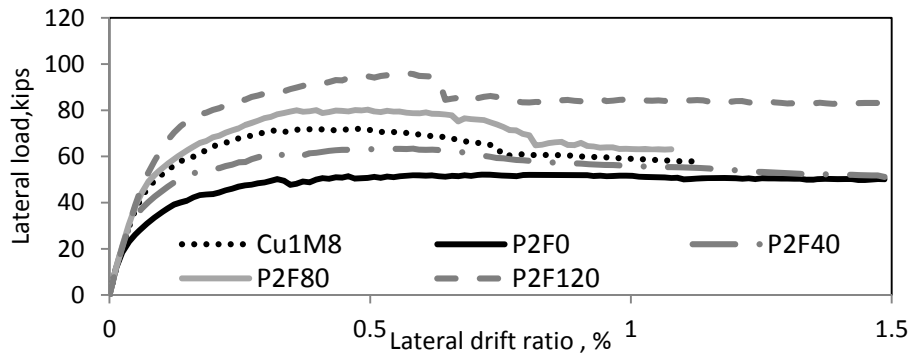


Figure 4.9 Parametric study results of second set models with different vertical loads

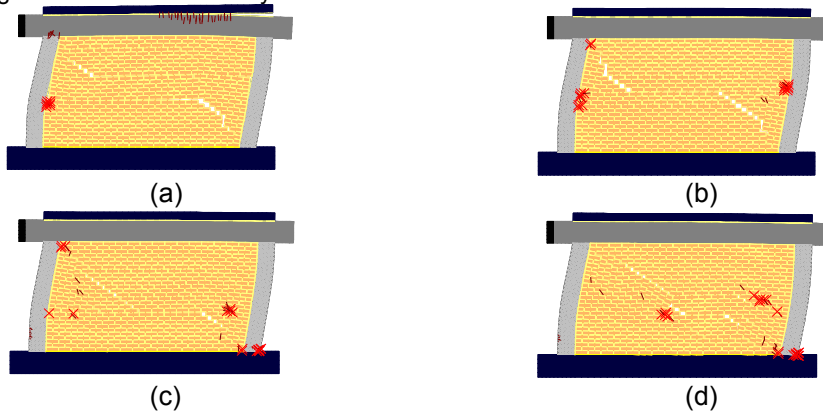


Figure 4.10 Cracking patterns at 1.0% drift for frames with different vertical load. (a) P2F0, (b) P2F40, (c) P2F80, (d) P2F120.

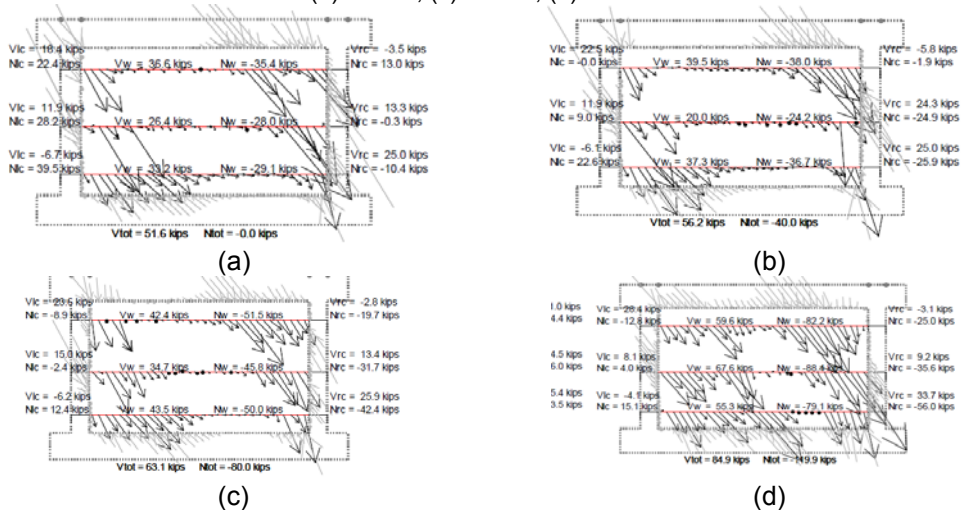


Figure 4.11 Force distribution along three cross sections at the instant of peak strength for cases of the second set with different vertical loads. (a) P2F0, (b) P2F40, (c) P2F80, (d) P2F120.

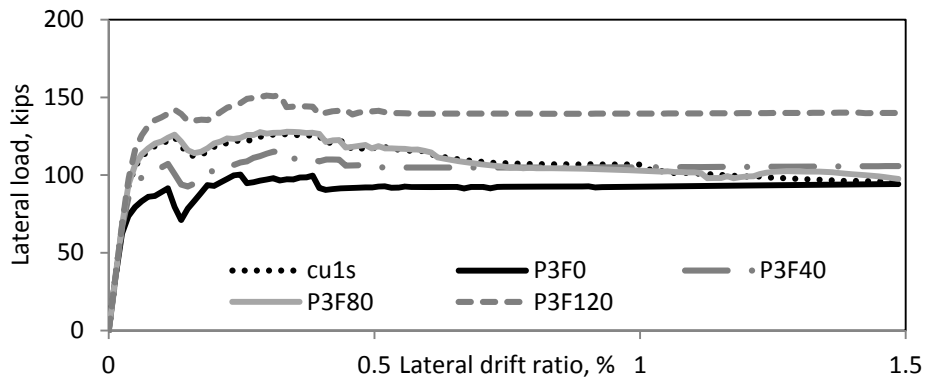


Figure 4.12 Parametric study results of third set models with different vertical load

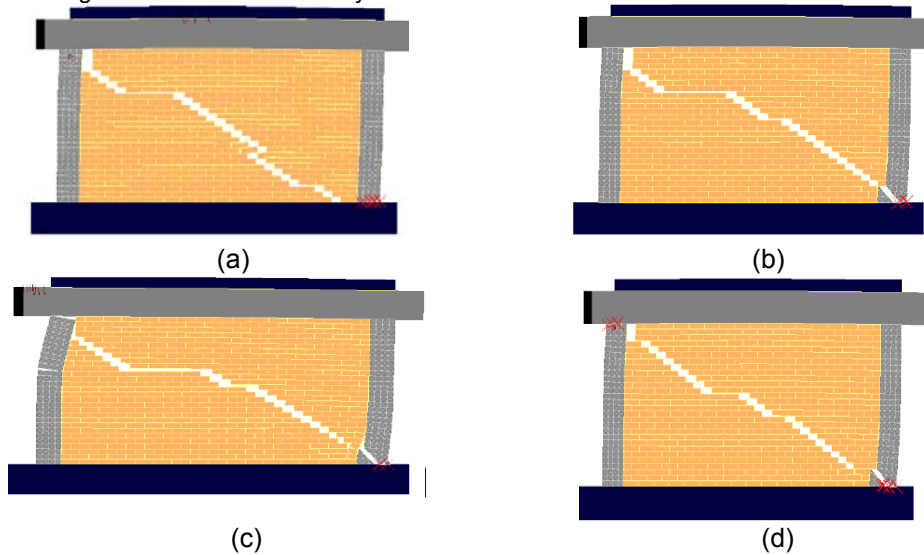


Figure 4.13 Cracking patterns at 1.0% drift for third set specimens with different vertical load.
 (a) P3F0, (b) P3F40, (c) P3F80, (d) P3F120.

Effect of Aspect Ratio

The term 'aspect ratio' is defined in this thesis as the infill length divided by the infill height, l/h , and was changed in all three sets of parametric study models. The base model had an infill aspect ratio of 1.77 which was changed by making models with aspect ratios ranging from 0.38 to 3.13 in increments of approximately 25% the base model aspect ratio. In all cases the aspect ratio was changed by varying the length of panel rather than the height. Increasing the infill length causes both the infill and columns to have increased capacity. The increase in infill capacity is partly attributed to the increase

in area of mortar that must be sheared before the masonry will begin to slide. Furthermore, a large percentage of the capacity is lost when diagonal sliding and cracking occurs resulting in a more drastic load drop after the peak strength in cases with longer infill lengths as seen in Figure 4.14. The longer distance between columns creates a larger moment arm to resist overturning, which leads to lower axial stresses in the columns. While the leeward column doesn't have a noticeable increase of capacity, the reduced tensile stress in the windward column allows much higher shear capacity. To the contrary, narrow specimens with low aspect ratios tend to have very high tensile stresses in the windward column making the column susceptible to major shear failures that develop at low drifts.

The specimens with aspect ratio of only 25% of the base model had infills too short to have enough shear strength to initiate a shear failure in the columns. In these cases the entire specimen deformed in a flexural manner similar to a cantilevered beam. These trends were observed in all three sets of models in the parametric study. While the low aspect ratio cases provide interesting insight to the flexural behavior of infilled frames, these cases are too narrow to simulate realistic structures. The results from the cases with varied aspect ratio are given in Figure 4.14 through 4.21. There is a similar trend in the first and second set of models where the model with lowest aspect ratio, P1AR1 or P2AR1, has very ductile behavior with a minimal load drop after the peak, while the model with highest l/h ratio, P1AR5 and P2AR5, have much higher strength and very brittle behavior.

Another trend noticed in the models with varied aspect ratio is the decrease of drift at peak load as the aspect ratio increases. This can be attributed to the increased stiffness of the structure due to the increased area of masonry. As shown in Figure 4.14 Specimen P1AR1 with aspect ratio of 0.91 has drift at peak of 0.6%, while specimen

P1AR5 has an aspect ratio of 3.13 and a drift at the peak load of only 0.14%. This decrease in drift where the peak occurs happens because of the different failure mechanisms of the two specimens which changes as the increased infill length makes the infill stronger than the columns.

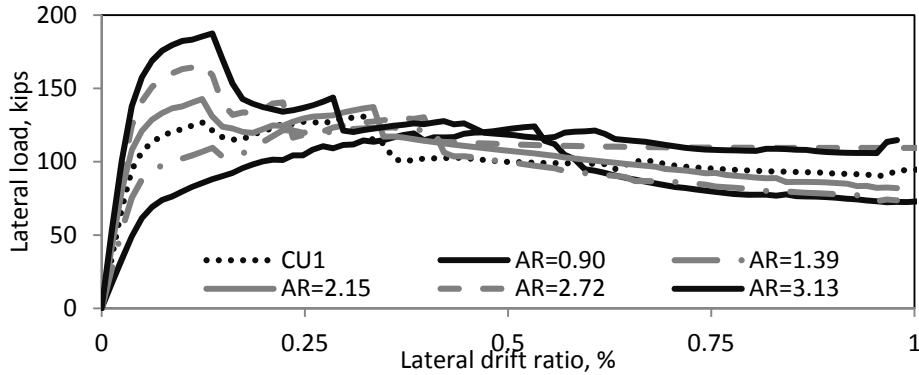


Figure 4.14 Parametric study results of first set models with different aspect ratios.

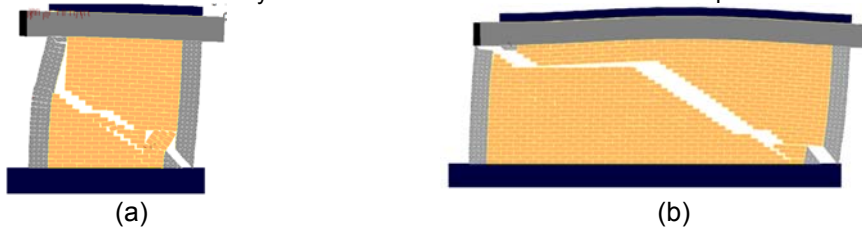


Figure 4.15 Cracking patterns at 1.0% drift for frames with different aspect ratio. (a) AR=0.9 (1/2 base AR) and (b) AR=2.15 (1 1/2 base AR).

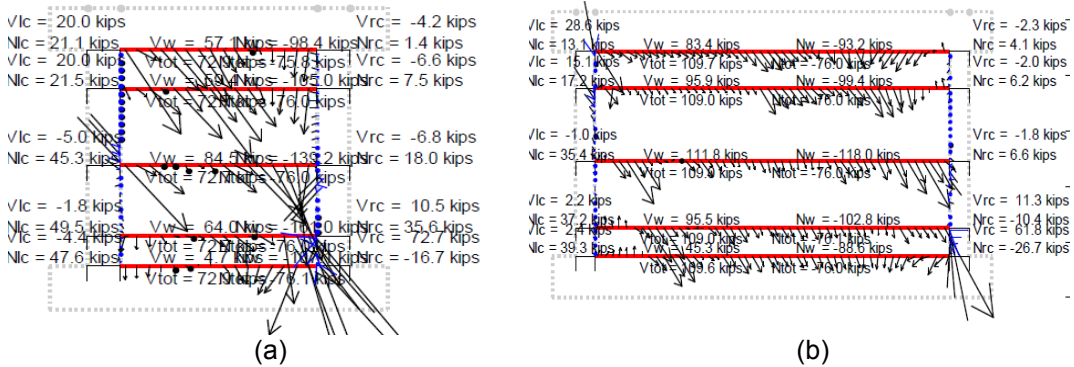


Figure 4.16 Force distribution along five cross sections at the instant of peak strength for cases of the first set with different aspect ratio. (a) AR=0.9 (1/2 base AR) and (b) AR=2.15 (1 1/2 base AR).

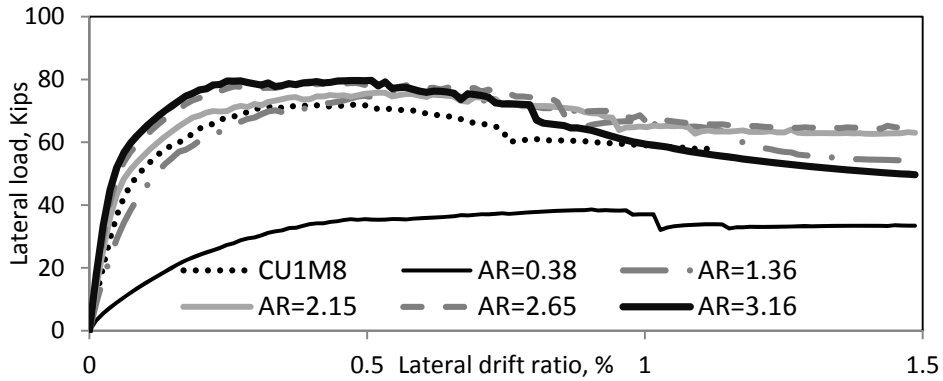


Figure 4.17 Parametric study results of second set models with different aspect ratio

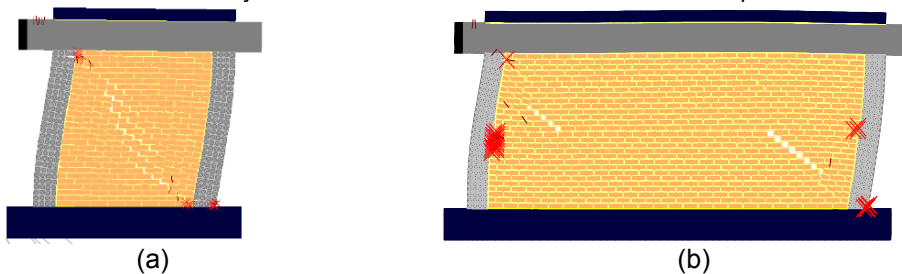


Figure 4.18 Cracking patterns at 1.0% drift for frames of second set with different aspect ratio. (a) AR=0.9 (1/2 base AR) and (b) AR=2.15 (1 1/2 base AR).

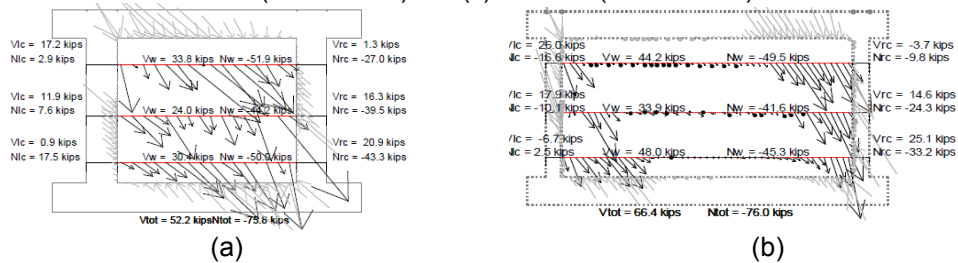


Figure 4.19 Force distribution along three cross sections at the instant of peak strength for cases of the second set with different aspect ratio. (a) AR=0.9 (1/2 base AR) and (b) AR=2.15 (1 1/2 base AR).

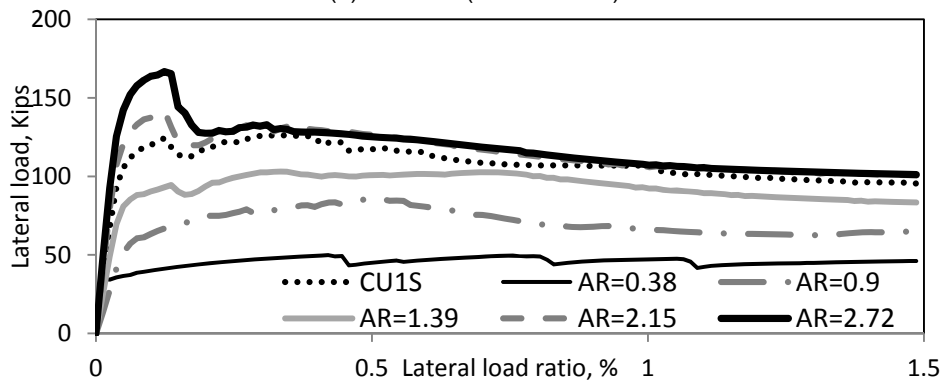


Figure 4.20 Parametric study results of third set specimens with different aspect ratio

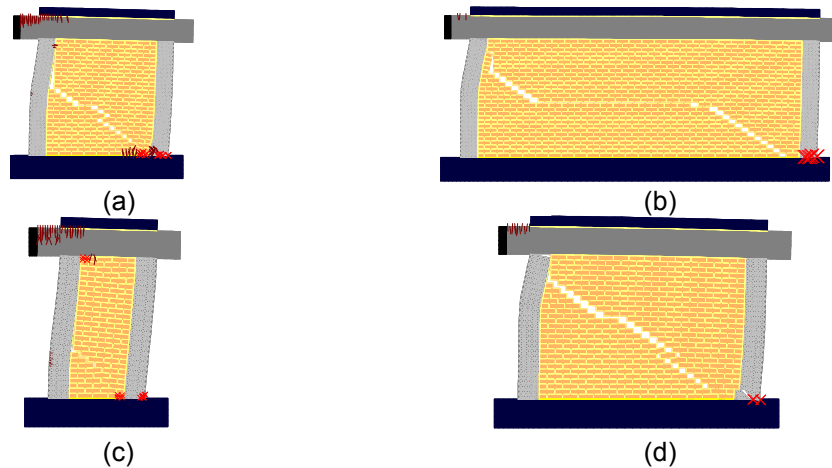


Figure 4.21 Cracking patterns at 1.0% drift for frames with different aspect ratio. (a) AR=0.91, (b) AR=2.72, (c) AR=0.38, (d) AR=1.39.

Effect of Shear Reinforcement

The amount of shear reinforcing in the columns was changed in all three sets of the parametric study. The amount of shear reinforcing was varied by differing the areas of stirrups as well as the stirrup spacing. The stirrup area is changed in percentages of the base model stirrup area of 0.15in^2 . The lower limit used in the columns is half of the base model, resulting in stirrup area of 0.07in^2 . The stirrup area is increased as 2, 3 or 4 times the base model area, resulting in stirrup areas of 0.29in^2 , 0.44in^2 , and 0.59in^2 . The stirrup spacing is only changed for the first two sets of models and is varied to be either $\frac{1}{2}$ or $\frac{1}{4}$ the base model stirrup spacing as columns are seldom found with shear reinforcement that has spacing larger than the column width. In all cases, the increase in shear reinforcement had little effect on the peak strength, but had a noticeable effect on the residual load capacity of the specimens and the ductility of the specimen. As the amount of shear reinforcement was increased, either by increased stirrup size or decreased stirrup spacing, the residual capacity increased.

The results of the specimens with varying shear reinforcement patterns are given in Figure 4.22 through 4.35. The difference in residual capacity is clear in the force-vs-drift curves for the three sets of models. The illustrations of the failure patterns show that the models with less stirrup area have major shear failures due to the inability to stop the shear failure from growing once started, while the models with higher stirrup area have a much more flexural failure. This is also true for decreased stirrup spacing. As shown in Figure 4.28, the decreased stirrup spacing minimizes the shear failure in the column. The cases from the second set have a weak infill and fail in flexure for both stirrups spacings. Because the models of the second set fail in flexure the added shear resistance discussed above is never seen resulting in the nearly identical behavior for P2DP5 and P2DP25 in Figure 4.33.

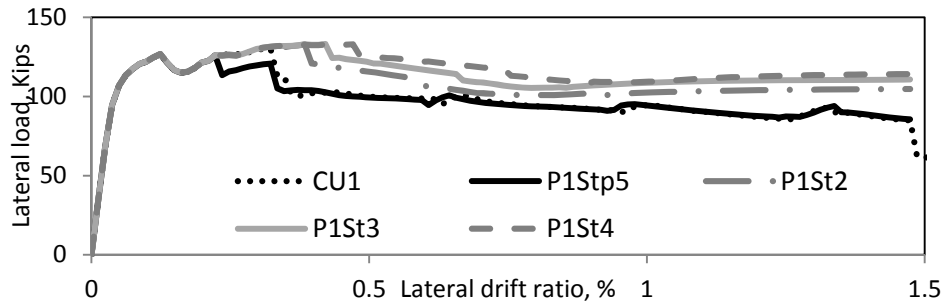


Figure 4.22 Parametric study results of first set specimens with different column transverse steel area

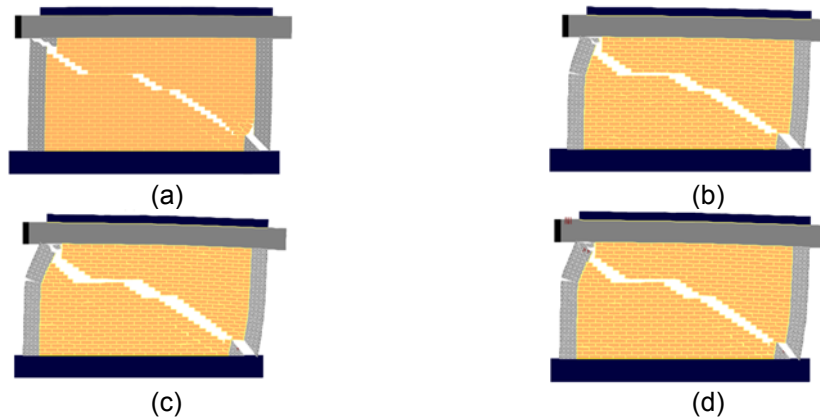


Figure 4.23 Cracking patterns at 1.0% drift for first set specimens with different transverse steel area. (a) P1St5, (b) P1ST2, (c) P1ST3, (d) P1ST4.

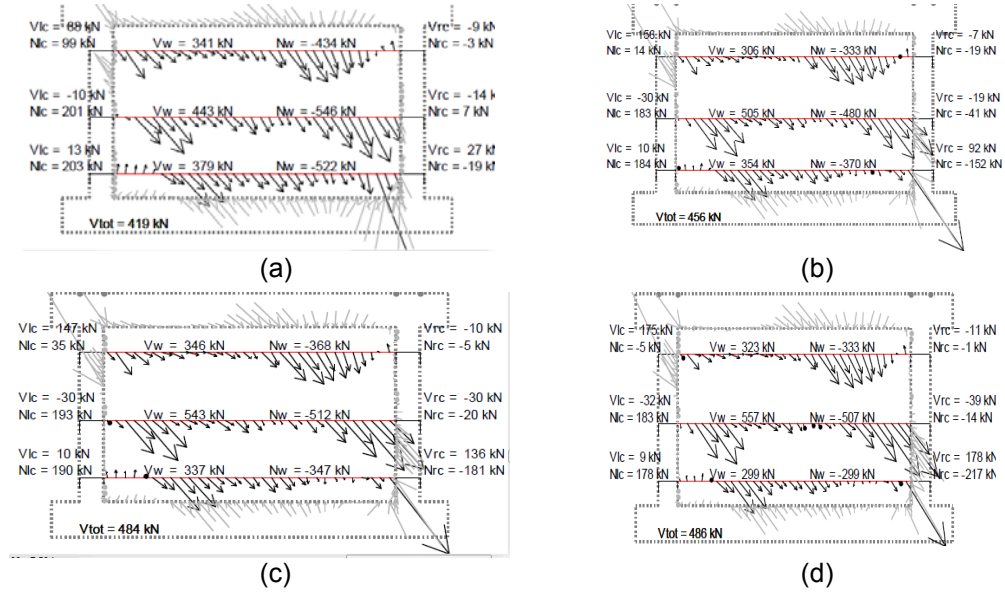


Figure 4.24 Force distribution along three cross sections at 1% drift for cases of the first set with different area of transverse steel. (a) P1Stp5, (b) P1ST2, (c) P1ST3, (d) P1ST4.

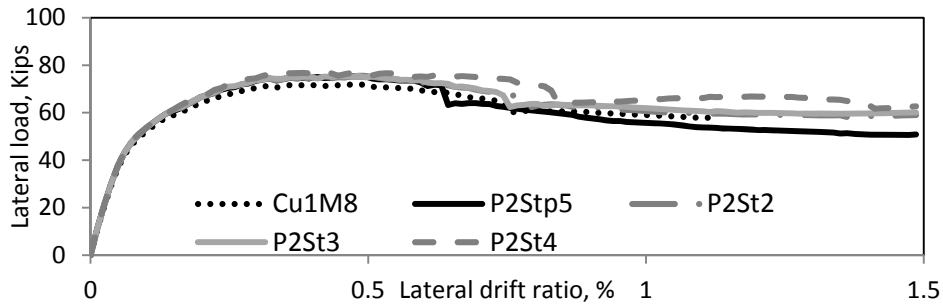


Figure 4.25 Parametric study results of second set specimens with different transverse steel area

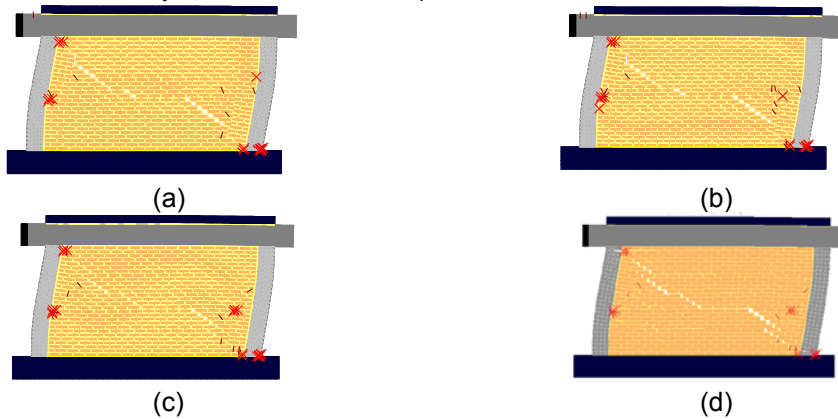


Figure 4.26 Cracking patterns at 1.0% drift for second set specimens with different transverse steel area. (a) P2Stp5, (b) P2ST2, (c) P2ST3, (d) P2ST4.

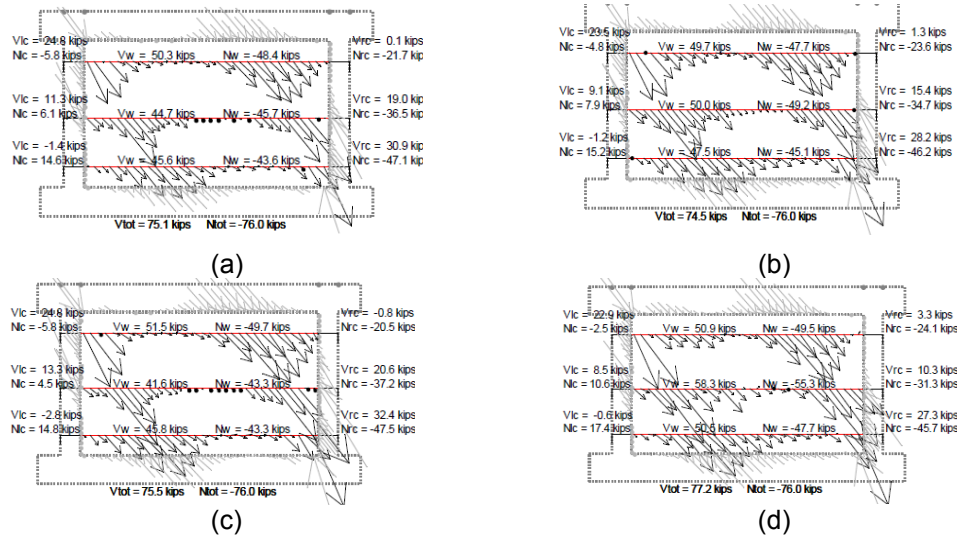


Figure 4.27 Force distribution along three cross sections at 1% drift for cases of the second set with different area of transverse steel. (a) P2Stp5, (b) P2ST2, (c) P2ST3, (d) P2ST4.

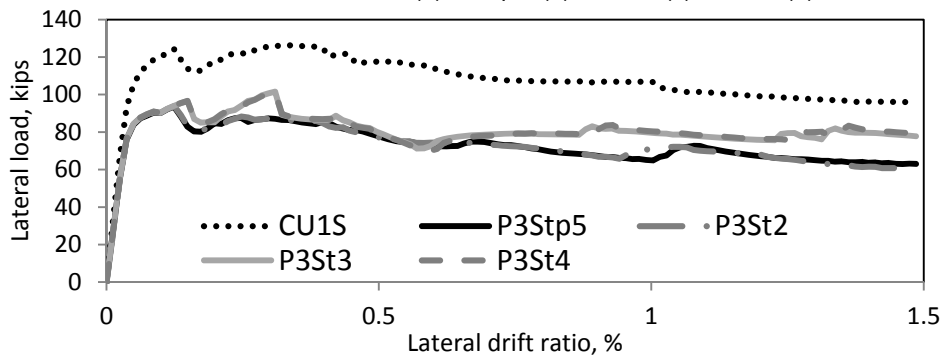


Figure 4.28 Parametric study results of third set specimens with different transverse steel area

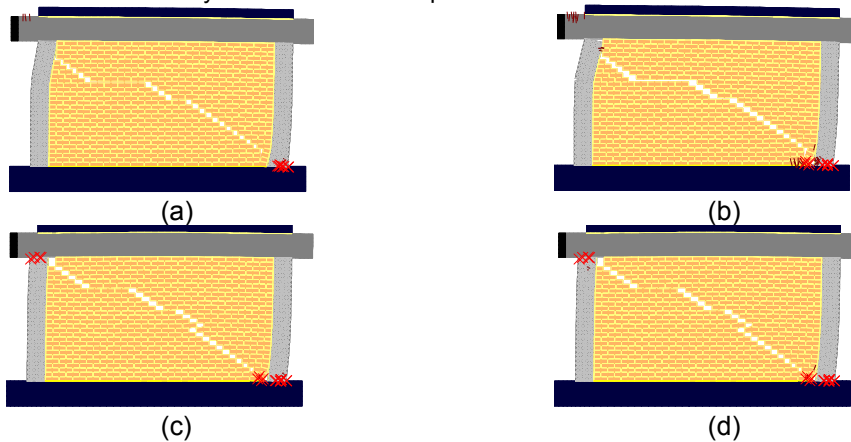


Figure 4.29 Cracking patterns at 1.0% drift for third set specimens with different transverse steel area. (a) P3Stp5, (b) P3ST2, (c) P3ST3, (d) P3ST4.

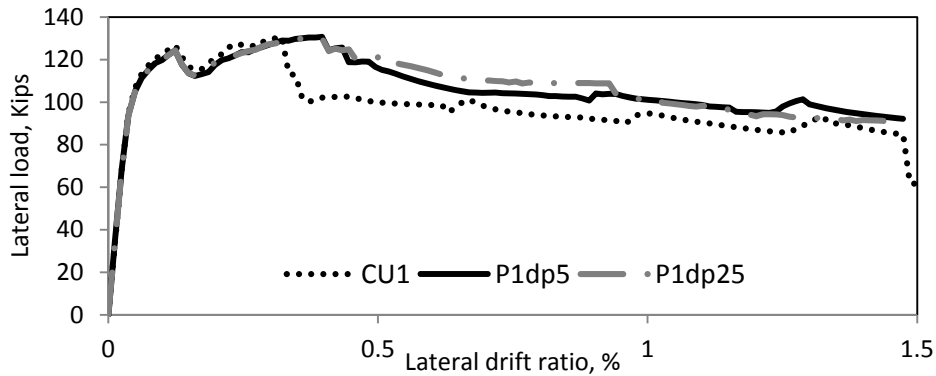


Figure 4.30 Parametric study results of first set specimens with different transverse steel spacing

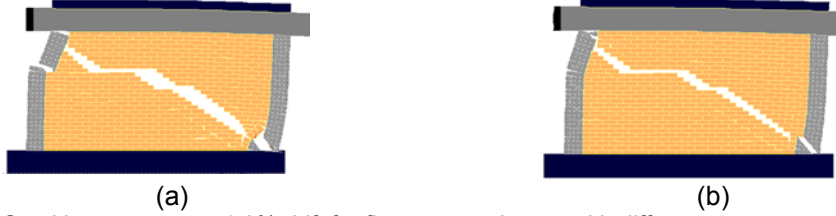


Figure 4.31 Cracking patterns at 1.0% drift for first set specimens with different transverse steel spacing. (a) P1Dp5 and (b) P1Dp25.

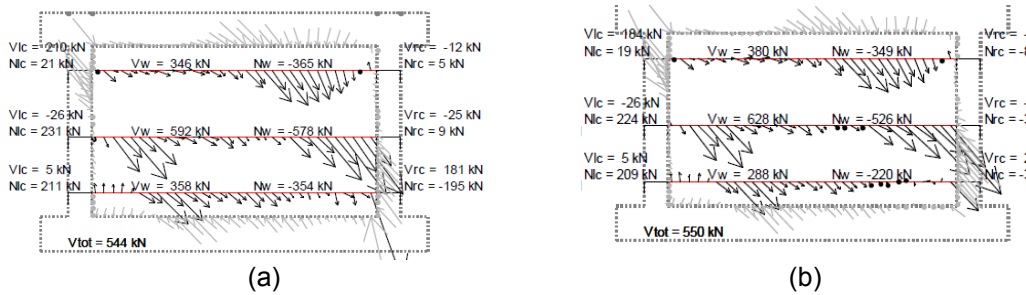


Figure 4.32 Force distribution along three cross sections at the instant of peak load for cases of the first set with different spacing of transverse steel. (a) P1Dp5 and (b) P1Dp25.

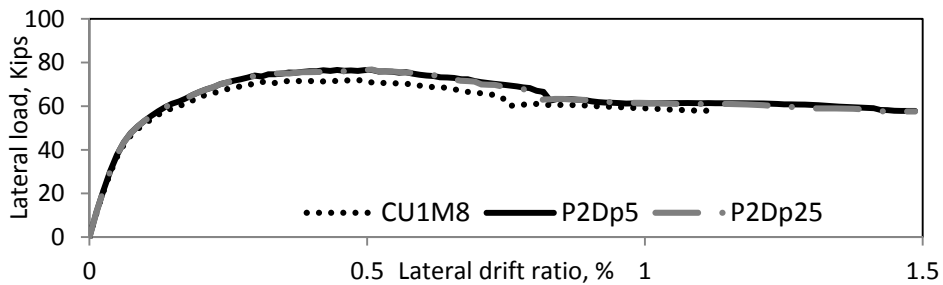


Figure 4.33 Parametric study results of second set specimens with different transverse steel spacing



Figure 4.34 Cracking patterns at 1.0% drift for second set specimens with different transverse steel spacing. (a) P2Dp5 and (b) P2Dp25.

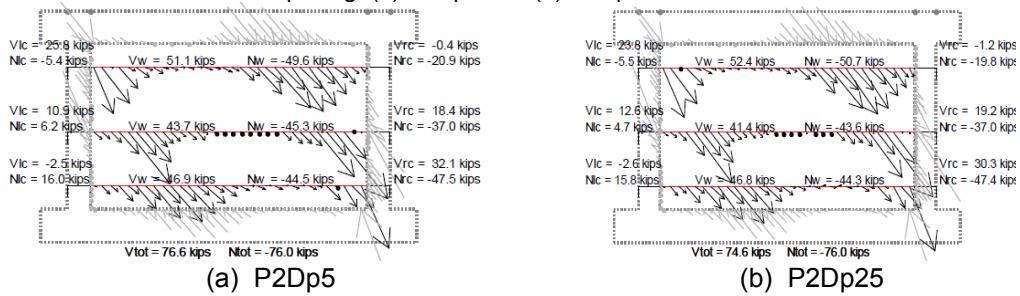


Figure 4.35 Force distribution along three cross sections at the instant of peak load for cases of the second set with different spacing of transverse steel

Effect of Longitudinal Reinforcement

The longitudinal reinforcement was changed in the first two sets of the parametric study. The base model longitudinal reinforcement ratio was set at 1%, and the reinforcement ratio was varied from 0.5% to 4% in the models discussed below. The amount of longitudinal reinforcement has little effect on the shear capacity of the frame, but does impact the flexural capacity. Therefore, frames with strong infills and low flexural reinforcement could fail in flexure before a shear failure occurs. In the frames with only 0.5% reinforcement ratio the lateral force to make plastic hinges in the column is only 1/4th the shear strength and thus a flexural failure is much more likely as shown in Figure 4.36 through 4.41. The columns with longitudinal reinforcement ratio of 4% require a much higher lateral force of 30 kips to create plastic hinges in the columns. This is considerably higher than the column shear strength. Similarly, frames with the reinforcement ratio of 2% and 3%, develop dominant shear failures seen in the failure illustrations of Figures 4.37 and 4.40. Although the addition of longitudinal reinforcement

may increase the plastic capacity of a frame, it does little in increasing the shear strength. Consequently the addition of longitudinal reinforcement without added shear reinforcement could cause a frame to have brittle failure.

Interestingly, in the case of increased flexural reinforcement for the second set models the column flexural strength is so high the weak infill creates shear failures in the column as the drift is increased. Similar to the strong infill case with flexural failures, the weak infill case with major shear failures was rare and only occurred in these three models throughout the study. The force-vs-drift curves for these models are given in Figure 4.39. As seen in the figure, the first model has a gradual load drop after a plateau at the peak strength, while the following cases have sudden failures directly after the peak strength. Because of the different failure patterns there is a noticeably higher peak strength in cases (b) through (d) than in case (a). The increased capacity can be attributed to the frame being strong enough to allow the infill to develop its full strength prior to excessive damage to the frame.

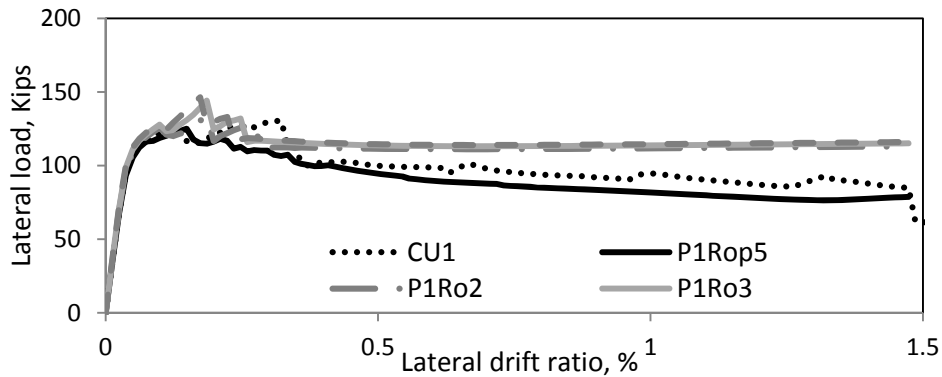


Figure 4.36 Parametric study results of first set specimens with different longitudinal steel area

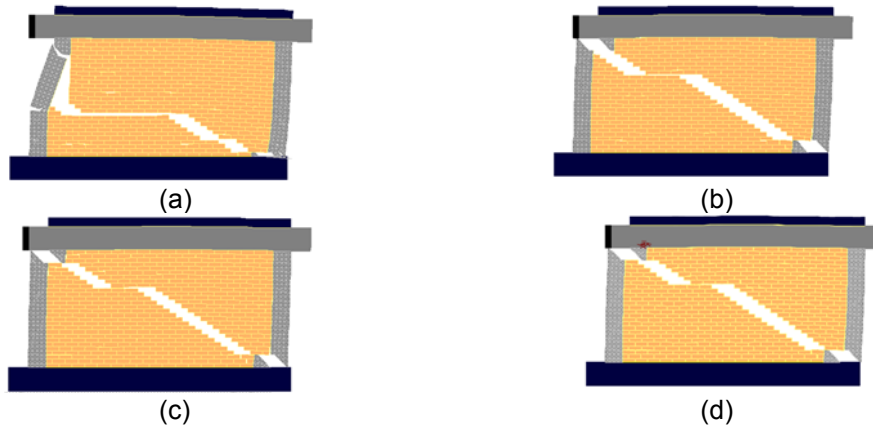


Figure 4.37 Cracking patterns at 1.0% drift for second set specimens with different longitudinal steel area. (a) P1ROp5, (b) P1RO2, (c) P1RO3, (d) P1RO4.

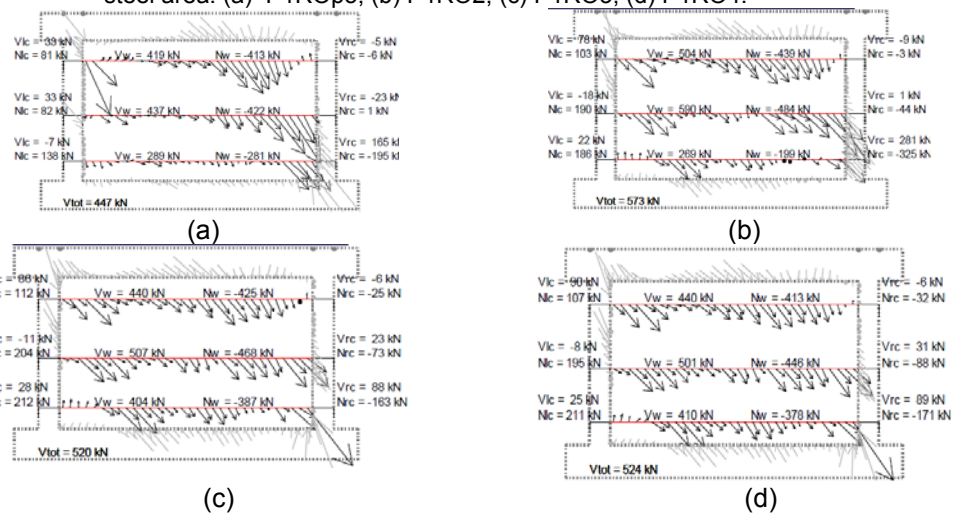


Figure 4.38 Force distribution along three cross sections at instant of peak load for cases of the first set with different area of longitudinal steel. (a) P1ROp5, (b) P1RO2, (c) P1RO3, (d) P1RO4.

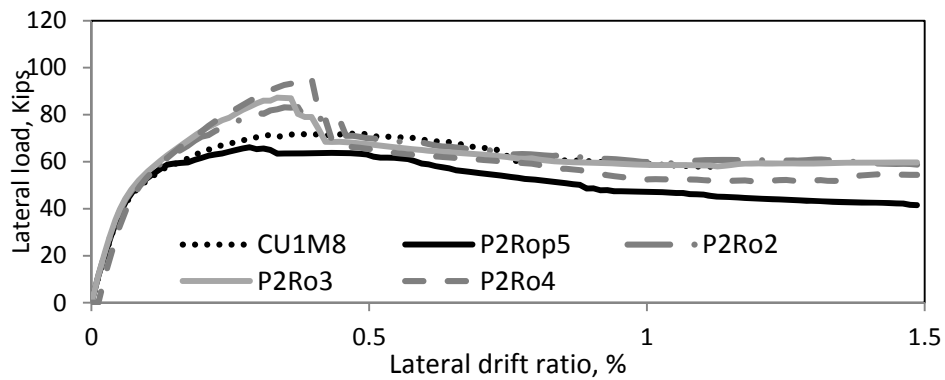


Figure 4.39 Parametric study results of second set specimens with different longitudinal steel area

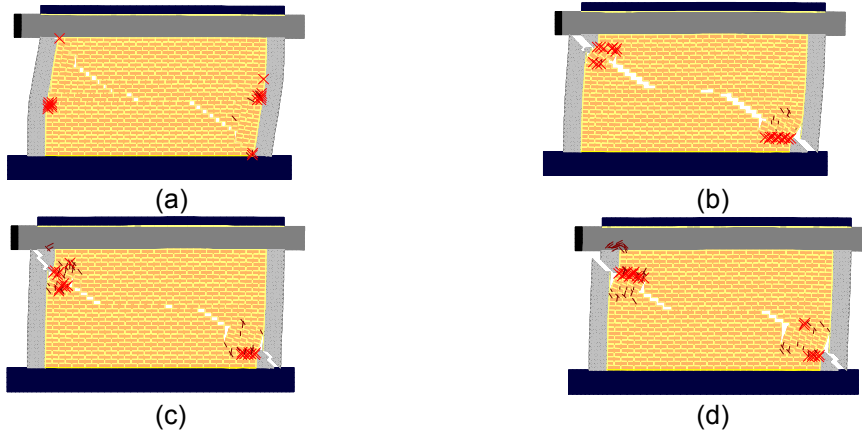


Figure 4.40 Cracking patterns at 1.0% drift for second set specimens with different longitudinal steel area. (a) P2ROp5, (b) P2RO2, (c) P2RO3, (d) P2RO4.

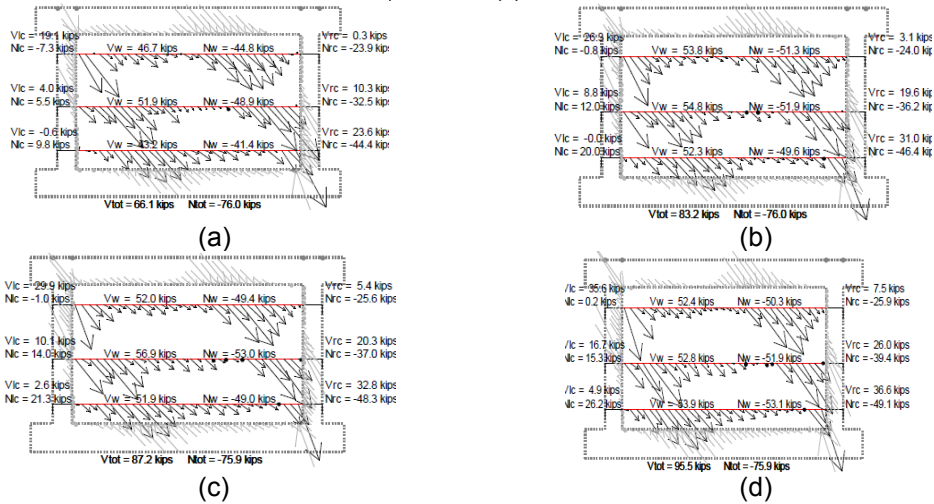


Figure 4.41 Force distribution along three cross sections at the instant of peak load for cases of the second set with different area of longitudinal steel. (a) P2ROp5, (b) P2RO2, (c) P2RO3, (d) P2RO4.

Effect of Column Width

The column width was only changed in the last set of models. The base model for this set had column dimensions of 11"x11" so the column width was modeled at 8", 12" and 16". The shear strength of the column is a function of both the width and length of the column and therefore to achieve a linear variation only the width has been changed. The width was varied rather than the length in order to influence the shear capacity more drastically than the flexural capacity. As expected, as the column width

increased the column capacity also increased, resulting in a minor increase in strength of the frame. The force-vs-displacement plots and failure patterns from the cases with varied column width are shown in Figures 4.42 and 4.43. An interesting observation is made from the failure illustrations in Figure 4.43. As the width of the column increases the frame begins to fail in flexure rather than shear. In model P3C1 the columns fail in shear due to the small column cross section and weak shear capacity of the column at 11.6 kips. However in model P3C3 the shear capacity has increased to 23.2 kips leading to a flexural failure in the model.

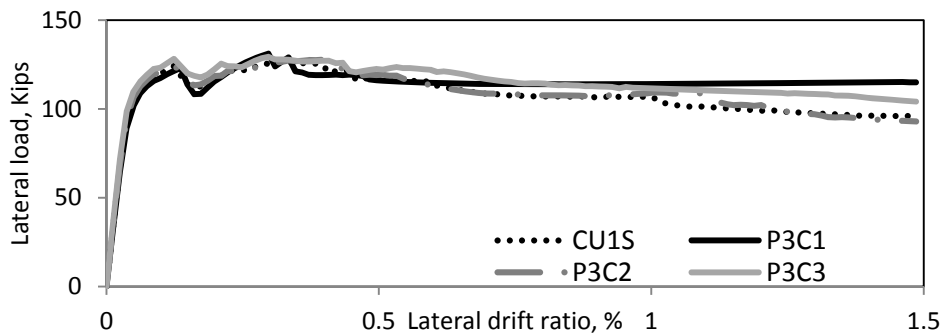


Figure 4.42 Parametric study results of third set specimens with different column width

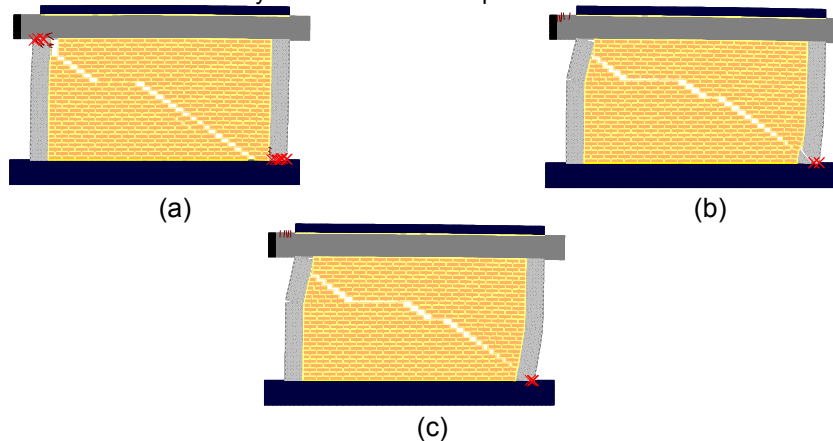


Figure 4.43 Cracking patterns at 1.0% drift for third set specimens with different column width. (a) P3C1, (b) P3C2 and (c) P3C3.

Chapter 5

Analysis of Parametric Study Results

The results of the parametric study and experimental cases were analyzed in order to identify trends at the critical stages of the infilled frames' failure. The analysis of failure patterns allowed the grouping of the models into a ductile or brittle category which could then be correlated with the material properties and design parameters. Afterwards attention was given to the lateral strength and associated drift with three characteristic points on the load-displacement curve, the apparent yield point, the peak load, and the point signifying the onset of residual load capacity.

Strong & Weak Definition

The most important outcome of the parametric study was the characterization of the failure behavior as brittle or ductile. The cases that exhibited brittle behavior typically had similar failure patterns which included sliding/diagonal cracking of the infill that led to major shear cracks in the columns. The cases with ductile behavior also had similar failure patterns of sliding in the infill with minor shear cracks or flexural failure of the columns as in cases with high shear reinforcement such as model P2St4. The models with ductile failures were generally composed of infills with minor contribution to the overall strength, which are therefore referred to as 'weak infill' models. The weak infill cases developed sliding and cracking in the infill followed by formation of plastic hinges in the columns. The weak infill cases can be divided once more into 'strong frame' or 'weak frame' cases. Cases with weak infills and weak frames will have shear failure in the column, while weak infill- strong frame are cases where enough shear strength exists in the columns to cause flexural failure of the columns first. The most common type of failure in weak infill cases is flexural failure thus weak infill- weak frame cases only occur in columns with higher flexural reinforcement.

Models with capacity dominated by the strength of the infill are referred to as 'strong infill' cases. As opposed to the weak infill cases, the strong infill cases generally had brittle failures. Strong infill cases will have sliding and cracking in the infill initially followed by a major shear failure in the column. The strong infill cases can be further divided into 'strong frame' or 'weak frame' depending on the frame strength. If the frame has enough shear strength to enforce crushing of the infill before ultimately failing in flexure the frame is labeled as a strong infill- strong frame case. This condition requires a higher shear capacity of the reinforcement alone and does not occur in many of the models of the study. The most common failure pattern of the strong infill cases is the early shear failure of the columns with these cases classified as strong infill- weak frame. This led to the labeling of all infilled frames with one of four descriptions: weak infill-weak frame, weak infill-strong frame, strong infill- strong frame, strong infill-weak frame.

The specimen properties from the parametric study were correlated with the various failure patterns in order to determine a quantifiable indicator of a frame's behavior. The first goal was to determine a ratio of masonry strength to frame strength that could consistently indicate if a certain infill were strong or weak. The ratio V_m / V_n , where V_m is the infill strength given by Equation 5.1 and V_n is the frame strength given by Equation 5.2, is greater than one when the infill is stronger than the frame, and less than one when the infill is weaker than the frame. The method for determining if the frame is strong or weak utilizes a ratio of the frame flexural capacity to the frame shear capacity. The frame can be defined as weak or strong if the ratio V_p/V_n , where V_p is the plastic strength of the columns given by Equation 5.4 and V_n is the shear strength of the columns given by Equation 5.2. In models with strong infills the ratio V_p/V_n is greater than 0.75 if the frame will undergo shear failure at or near the peak drift. If the ratio is less than 0.75 the frame will develop a shear failure in the column prior to the peak strength being

achieved. In cases with weak infills the ratio V_p/V_n is greater than 0.2 when the frame is controlled by shear failure and less than 0.2 when a flexural failure is expected. Based on these ratios the behavior of an infilled frame can be predicted as described in the following section. The classification system is illustrated in Table 5.1.

Table 5.1 Classification of infilled frames

$V_m/V_n > 1$ $V_p/V_n > 0.75$	Strong infill weak frame	$V_m/V_n < 1$ $V_p/V_n > 0.2$	Weak infill weak frame
$V_m/V_n > 1$ $V_p/V_n < 0.75$	Strong infill strong frame	$V_m/V_n < 1$ $V_p/V_n < 0.2$	Weak infill strong frame

$$V_m = P_w \mu + A_w C \quad (5.1)$$

$$V_n = V_c + A_v f_y n_s \quad (5.2)$$

$$V_c = 2\sqrt{f'_c} b d \quad (5.3)$$

$$V_p = \frac{M_{p,top} + M_{p,bot}}{h} \quad (5.4)$$

$$M_p = A_s (1.25 f_y) (d - d') \quad (5.5)$$

Where V_m is the horizontal sliding strength of the infill, P_w is the vertical load applied to the infill, μ is the coefficient of sliding friction, A_w is the cross sectional area of the infill, and C is the cohesive strength of the mortar joints. V_n is the shear strength of a single column in the frame, V_c is the shear strength of concrete, A_v is the total area of one layer of shear reinforcement, f_y is the yield strength of the stirrups and n_s is the number of stirrups crossing a shear crack. The expected shear crack is assumed to develop at a 45 degree angle with the horizontal axis, therefore it can be assumed that the number of stirrups within d (where d is the depth of the column) from the top of column is to be used

as n_s in Equation 5.2. V_c is the shear strength of concrete, f'_c is the compressive strength of concrete, b is the width of the column. V_p is the shear to cause plastic hinges in column, M_p is the plastic moment capacity of column as defined by FEMA 306, h is the panel height, A_s is the area of longitudinal reinforcement in tension, and d' is the effective depth to the longitudinal reinforcement in compression zone of the column.

Strong Infill- Weak Frame Cases

The strong infill cases with weak frames had major shear failures along with sliding and cracking in the infill as shown in Figure 5.1.

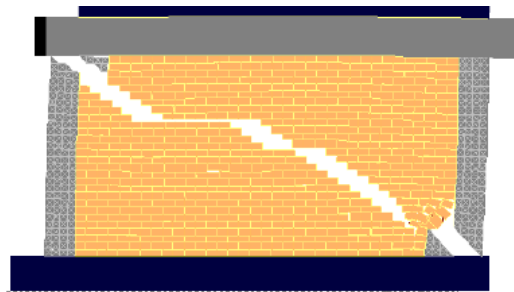


Figure 5.1 Typical failure pattern of Strong infill- weak frame specimens

The columns of these cases typically had failed in shear prior to the model reaching its peak strength. Because of the early column failure the peak capacity is entirely dominated by the shear strength of the infill, V_m , as given by Equation 5.1 which uses the addition of the infill cohesion and infill friction to estimate the sliding capacity of the infill. Once the strong infill- weak frame models reached the residual load plateau, only the friction remaining in the infill and the column shear stirrups provided capacity. The residual strength of these cases is estimated as the sum of the residual sliding friction in the infill and the shear capacity provided by the column shear reinforcement as shown in Equation 5.6.

$$V_{res} = A_v f_y n_s + P_w \mu_{res} \quad (5.6)$$

Where V_{res} is the residual load capacity of an infilled frame, A_v is the total area of stirrups in one layer, n_s is the number of stirrups crossing the column shear crack, P_w is the vertical load on the infill, μ_{res} is the coefficient of residual sliding friction of the damaged infill.

Strong Infill- Strong Frame Cases

The strong infill- strong frame cases had increased flexural reinforcement allowing the frame to act more ductile and resist shear failure until the infill had reached its peak strength. The failure of Strong infill- strong frame cases resembles that shown in Figure 5.2.

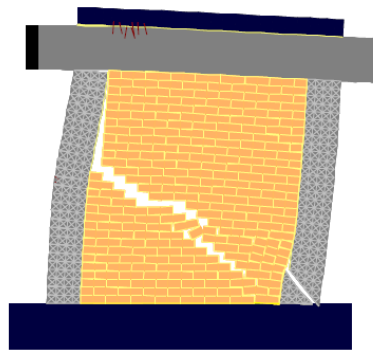


Figure 5.2 Typical failure pattern of Strong infill- strong frame specimens

Because the column shear failures occur at the peak strength the capacity of the columns is added to the capacity of infill as found in Equation 5.7.

$$V_{max} = (V_{c1} + V_{c2}) + P_w \mu + A_w C \quad (5.7)$$

Where V_{c1} and V_{c2} are the shear capacity of the windward and leeward columns respectively, as given by Equation 5.3. Because the windward column is typically under high tensile stress it is suggested to use $V_{c1} = 0$. The failure pattern of the strong infill- strong frame cases is the same as the strong infill- weak frame cases once the residual load has been reached, thus Equation 5.6 is suggested for use in the strong infill- strong frame cases.

Weak Infill- Weak Frame Cases

The weak infill- weak frame cases represent infilled frames with high frame flexural reinforcement that prevented the formation of plastic hinges in the frame. Due to the high flexural strength of the frame the weak infill- weak frame cases have a similar failure to the strong- infill strong frame with the addition of infill crushing as shown in Figure 5.3.

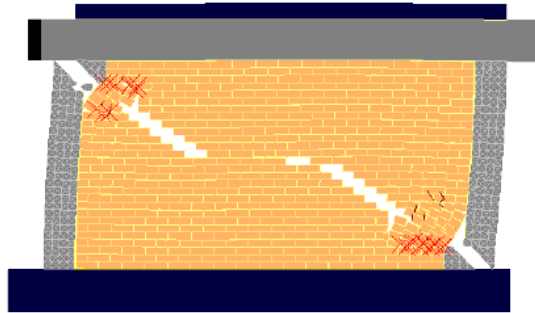


Figure 5.3 Typical failure pattern of weak infill- weak frame specimens

The infill crushing occurs after the peak load and therefore has no effect on the peak capacity. The peak strength of the weak infill- weak frame cases is estimated by Equation 5.7. The residual capacity is again given by Equation 5.6 as the shear and sliding failure have left only the friction and shear reinforcement to provide capacity. Although the failure pattern is similar to the strong infill- strong frame cases, the weak infill crushing results in a much more ductile failure overall producing an entirely force-vs-displacement relation.

Weak Infill- Strong Frame Cases

The weak infill- strong frame cases represent infilled frames where plastic hinges are expected in the columns rather than shear failures. This is the most common type of failure for weak infill cases with frames that have average flexural reinforcement. Along with the frame flexural failures, the diagonal sliding, cracking and crushing failures are all

present in the masonry in weak infill- strong frame cases with the failure pattern shown in Figure 5.4.

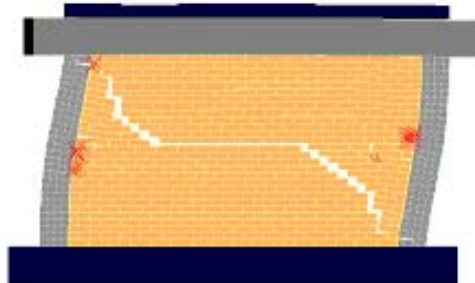


Figure 5.4 Typical failure pattern of weak infill- strong frame specimens

The columns in the weak infill- strong frame will typically have a plastic hinge failure near the top and bottom of each column and possibly a minor shear failure in each column which forms prior to the plastic hinges. Because these cases are the most ductile of the four classifications major infill cracking is expected meaning the cohesion of the mortar is overcome before the peak strength is reached. Equation 5.8 provides the estimated peak capacity for weak infill- strong frame cases.

$$V_{max} = (V_{c1} + V_{c2}) + P_w\mu + 2V_p \quad (5.8)$$

The failure pattern at the residual stage of weak infill- strong frame cases had pronounced flexural failures in the columns as well as the shear failures in the columns and sliding/ cracking of the infill that was observed in the other types of infilled frames. The addition of the flexural failure provided increased residual capacity for weak infill- strong frame cases. At high drifts the longitudinal reinforcement resists further rotation at the plastic hinge, which in turn adds to the capacity provided by the transverse reinforcement and infill friction. The residual capacity of weak infill- strong frame cases is estimated with Equation 5.9.

$$V_{res} = A_v f_y n_s + P_w \mu_{res} + 2V_p \quad (5.9)$$

The breakdown of models as weak or strong is shown graphically in Figure 5.5 through 5.7 with strong infill specimens shown in black and weak infill cases in grey.

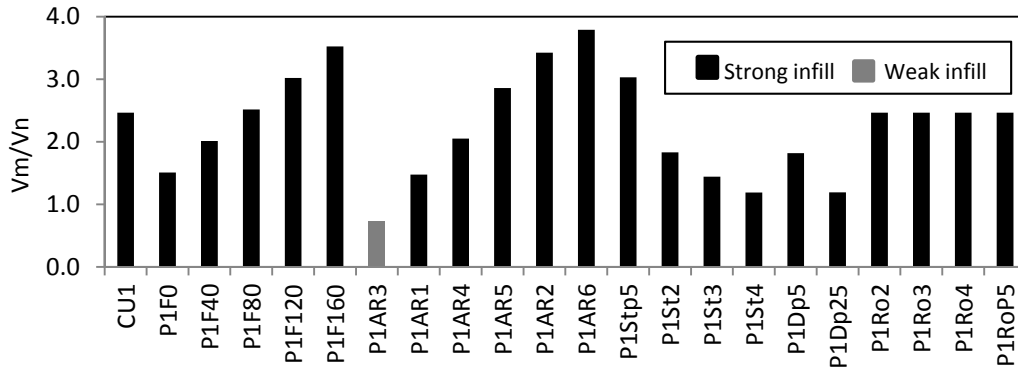


Figure 5.5 Ratio of V_m/V_n for the first set of models in parametric study

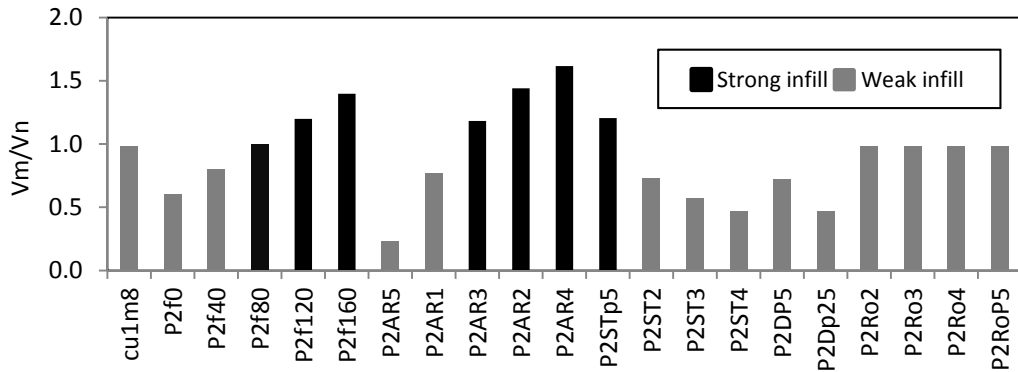


Figure 5.6 Ratio of V_m/V_n for the second set of models in parametric study

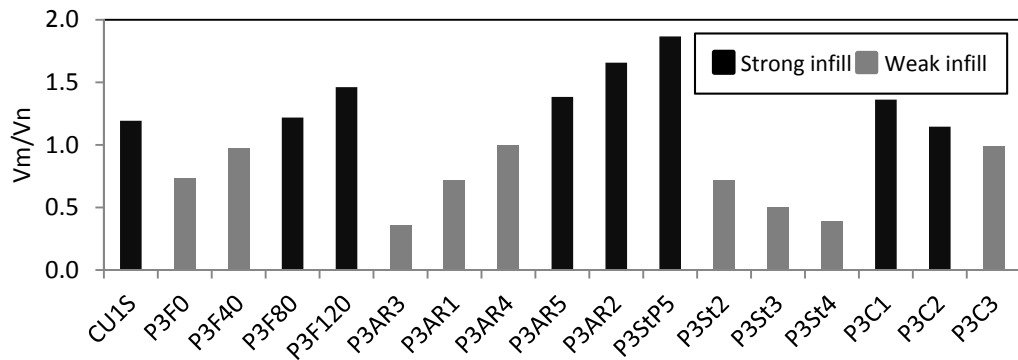


Figure 5.7 Ratio of V_m/V_n for the third set of models in parametric study

Chapter 6

Simplified Method Overview

The analysis of the parametric study models and experimental models discussed in the previous chapters was used to develop a series of steps for predicting the failure pattern and estimating the force-vs-displacement relation of an infilled frame. The proposed simplified method aims to estimate the force and drift at three characteristic points to develop a backbone curve similar to that recommended in ASCE 41-06 (ASCE 2006) for any single-bay, single-story masonry infilled RC frame. While many methods for analysis have been proposed, as discussed Chapter 2, many of the methods were very limited in scope and only were only validated with a limited number of specimens that developed the same failure pattern. The result was a series of proposed methods that emphasized the observed failure while giving little or no attention to other common failure types. The aim of the simplified method in this report is to expand the guidelines proposed by Stavridis (2009) for frames with strong infills and generalize the method to include ductile, weak infill cases. The goal is to provide guidance as to which failure is most likely for a given specimen, and the accompanying capacity associated with the predicted failure.

Initial Stiffness

The initial stiffness, K_i , can be calculated as a combination of the flexural stiffness of the composite section and shear stiffness of the infill as shown in Equation 6.1. The flexural stiffness of the composite section, K_f , is determined with the equation for a cantilevered wall as shown in Equation 6.2. The equation is applicable for a composite section by substituting the equivalent moment of inertia of a homogenous section, I_e , for

the moment of inertia used in the equation. The shear stiffness, K_s , is found with Equation 6.3.

$$K_i = \frac{1}{\frac{1}{K_f} + \frac{1}{K_s}} \quad (6.1)$$

$$K_f = \frac{3E_c I_e}{h^3} \quad (6.2)$$

$$K_s = \frac{A_w G_w}{h_w} \quad (6.3)$$

Where E_c is the modulus of elasticity of concrete, h is the height of the specimen from top of foundation to beam mid-height, A_w is the cross sectional area of infill, G_w is the shear modulus of elasticity for the infill and h_w is the height of infill.

Apparent Yield Point

The yield point on the curve indicates the point at which the infilled frame begins to act non-linearly. This point indicates the development of nonlinearities in the frame and infill such as the beginning of cracking in the columns and sliding in the infill. The drift at this point is not directly given by an equation, but it can be estimated with the initial stiffness and yield load known. Based on the experimental and analytical results, it was found that the force at the yield point, V_y , is typically 60-80% of the peak load, V_{max} . Based on this observation an equation was proposed by Stavridis (2009) for estimating the yield strength. This equation has been adopted here as shown below in equation 6.4.

$$V_y = \frac{2}{3} V_{max} \quad (6.4)$$

Point at Peak Load

The method proposed by Stavridis (2009) describes a relation between the drift at peak and the aspect ratio of the infill. The recommendations by Stavridis (2009) apply for frames with a strong infill based on the models with changed aspect ratio in set one of the parametric study. This relation was further elaborated upon with the parametric study presented here and different equations were developed for strong and weak infills. The equations for the points at peak and residual strength are provided at the end of the

section in Table 6.1. As expected the weak infills generally had a higher drift at the peak load for a given aspect ratio compared to the strong cases. This is reflected in Equation 6.5 and Equation 6.6. It was noted that as the infill gets longer, the behavior becomes more brittle leading to the decreasing trend observed in the Figure 6.1 and 6.2.

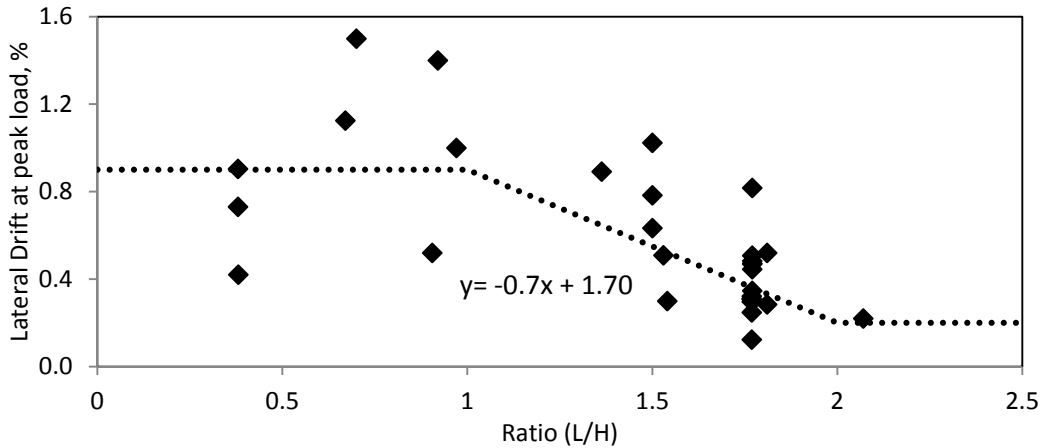


Figure 6.1 Lateral drift at peak load vs aspect ratio of infill for weak infill specimens

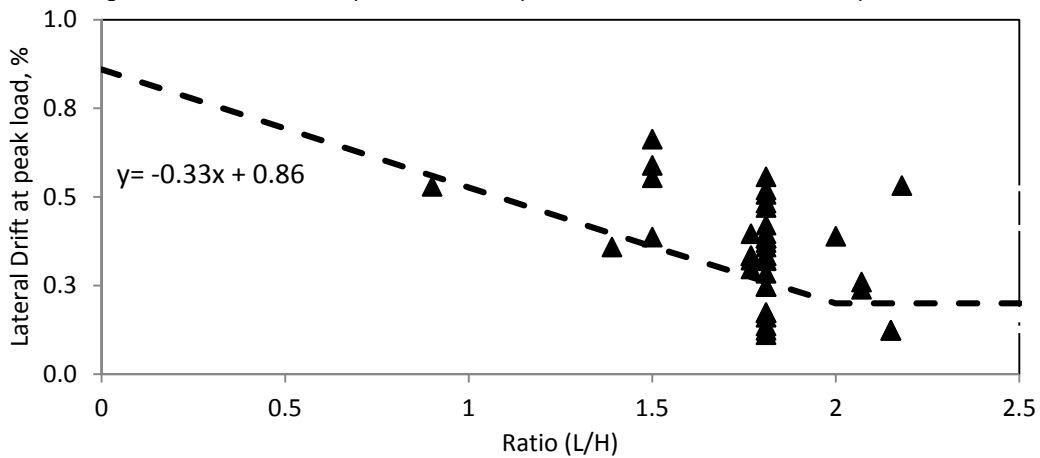


Figure 6.2 Lateral drift at peak load vs aspect ratio of infill for strong infill specimens

Estimating the peak strength is more complicated than finding the drift at the peak capacity, as the capacity is dependent on the mechanisms causing the ultimate failure as discussed in Chapter 5. The simplified equations presented here consider the various possible failure mechanisms such as cracking and sliding of the infill, shear

failure of the columns and flexural failure of the columns. The cracking and sliding of the infill is resisted by the cohesion of the mortar joints and the frictional resistance between the rows of bricks. The lower of the column's flexural and shear capacity governs the capacity provided to the system by the columns.

The equations for peak strength in Table 6.1 provide the steps to calculate the peak strength of an infilled frame based on the types of failures described in Chapter 5. Equation 6.7 applies to strong infill- strong frame cases and includes the contribution of the column shear strength to the capacity as the shear failure is not expected early on with lower V_p/V_n ratio. Equation 6.8 applies to strong infill- weak frame cases and only considers the contributions from friction and cohesion as a shear failure is expected prior to the peak strength being reached and the capacity is governed entirely by the infill. Equation 6.9 applies to weak infill- weak frame cases and thus includes the shear capacity of the columns. Weak infill- weak frame cases typically have such low shear reinforcement or high flexural reinforcement that the columns fail in shear. This has led to the inclusion of the column shear strength in Equation 6.9. Equation 6.10 applies to weak infill- strong frame and includes both the flexural and shear failure of the column as both failures are likely for this type of infilled frame. The peak is usually reached at high drift for weak infill- strong frame cases by which point the cohesion in the mortar has been surpassed. Because of this the cohesive strength of the infill is not included in the capacity for weak infill- strong frame cases.

The term P_w appears in all of equations 6.7 through 6.10 and represents the vertical load carried by the infill. The vertical load from the upper floors is distributed between the RC columns and the infill. However the distribution changes during loading due to the redistribution of load paths as failures occur in the structural elements. The vertical load on the infill is constantly changing as shown in Chapter 4 and it cannot be

easily estimated. The vertical load on the infill can be approximated by one of two methods. In the first approach the total vertical load can be distributed to the infill and columns based on the axial stiffnesses of the infill and RC columns assuming a perfect bond between the beam and infill. The second method is applicable to cases with little or no vertical load, such as single story structures or structures where the infill is not bonded well with the frame. In these cases as the infilled frame undergoes horizontal loading a portion of the masonry infill dilates vertically and compressive stresses build between the bounding frame and the infill. Figure 6.3 shows the results from a test conducted by Mehrabi et al. (1994) in which the horizontal displacement of an infilled frame is displayed on the x-axis and the vertical displacement shown on the y-axis. In order to quantify the vertical load applied to the infill from the bounding frame the vertical strain of the infill is used to estimate with the vertical confining stress applied by the frame.

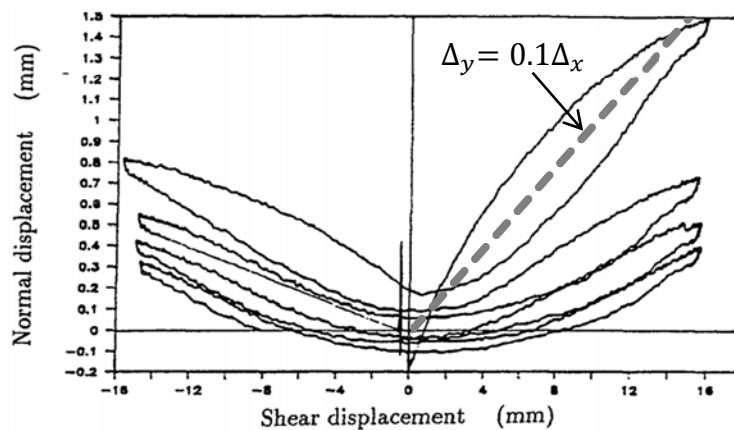


Figure 6.3 Shear displace-normal displacement relation results from Mehrabi et al. (1994)

From the figure the linear relation $\Delta_y = 0.1\Delta_x$ is assumed where Δ_y is the vertical shear dilatation and Δ_x is the horizontal displacement due to the applied lateral load. Furthermore, a majority of cases were observed to reach the residual strength plateau around 1.0% drift on average. From this the Equation 6.11 below is derived. The vertical displacement as calculated in Equation 6.11 can be substituted into the equation for axial

deformation as shown in Equation 6.12 to find the load caused in the frame from the expanding infill. It is assumed that the tensile strength of the frame is provided by the longitudinal reinforcement of the columns alone resulting in the use of A_s in Equation 6.12.

$$\Delta_{y,res} = f(\Delta_x) \approx 0.1\Delta_x \quad (6.11)$$

$$P_y = \frac{\Delta_{y,res} E_s A_s}{h_c} \quad (6.12)$$

$$P_w \approx \frac{0.1\Delta_x A_s E_s}{h_c} \quad (6.13)$$

Where P_w is the vertical load applied to infill from the bounding frame, A_s is the area of longitudinal steel in frame columns and E_s is the elastic modulus of steel in RC columns.

Equation 6.13 can be used directly to estimate the vertical load from frame confinement depending on the lateral displacement. For further simplification a lateral drift of 1% is assumed to represent the onset of the residual load plateau and was used in Equation 6.13 for the analysis of all models. The vertical load applied to the infill at the point of peak capacity is estimated by using the drift provided by Equation 6.5 or 6.6 in Equation 6.13. As mentioned before, the second procedure for calculating the vertical load is predominantly applicable to cases with minimal vertical load, as the effect of shear dilation decreases as the vertical stress is increased as described by Mehrabi et al. (1994). The maximum between the applied vertical load as distributed according to vertical stiffness and the load from the bounding frame as discussed above is to ultimately be used in equations 6.7-6.10.

Point at Onset of Residual Load

The drift at which the load capacity reaches its residual load capacity was also analyzed. As shown in Figure 5.6 through 5.8 the drift at the onset of the residual capacity is generally 40-80% higher than the drift at peak load, depending on how ductile

the structure is. Based on results of the study, the following equations based on the drift at peak discussed above are presented in Table 6.1.

The lines shown on Figure 5.6, 5.7 and 5.8 represent the cutoffs prescribed in Equations 5.10 and 5.11. The average residual drift of weak infill specimens is generally higher than that of a strong infill and is approximated by the dashed horizontal line on Figure 6.4, 6.5 and 6.6. The residual drift for strong infill cases is slightly lower on average than the weak infill cases and is approximated by the solid horizontal line on Figure 6.4, 6.5 and 6.6. The absolute values of the drift at peak load are shown alongside of the values for the drift at the onset of residual load for the parametric study models in Figures 6.7 through 6.9.

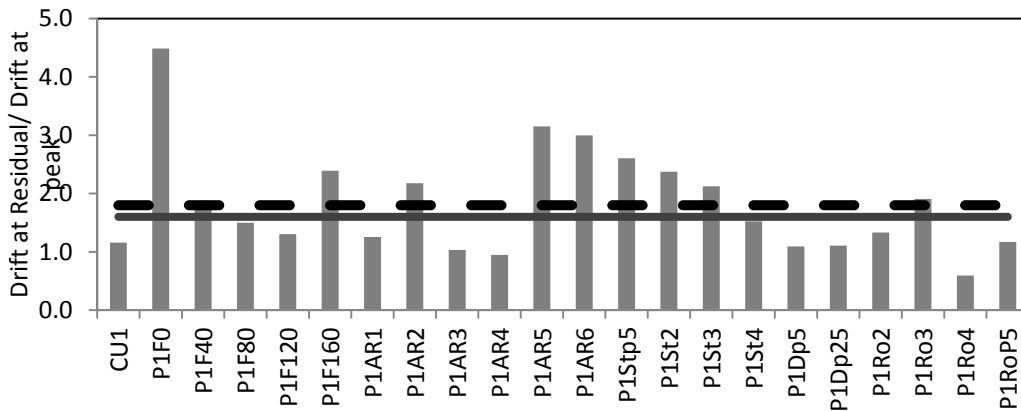


Figure 6.4 Drift at residual load/ drift at peak for first set of models

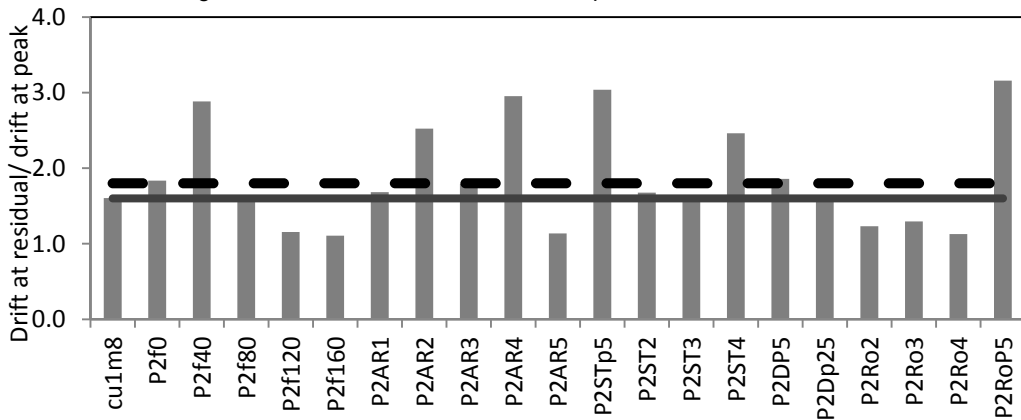


Figure 6.5 Drift at residual load/ drift at peak for second set of models

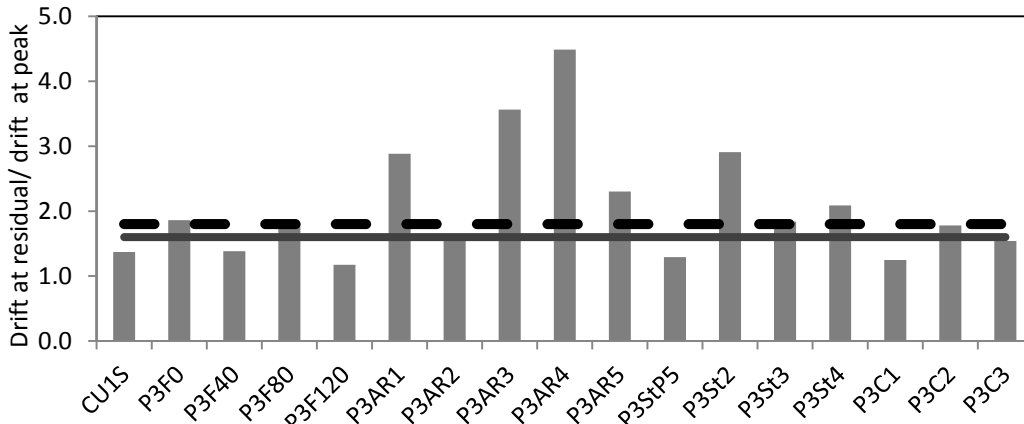


Figure 6.6 Drift at residual load/ drift at peak for third set of models

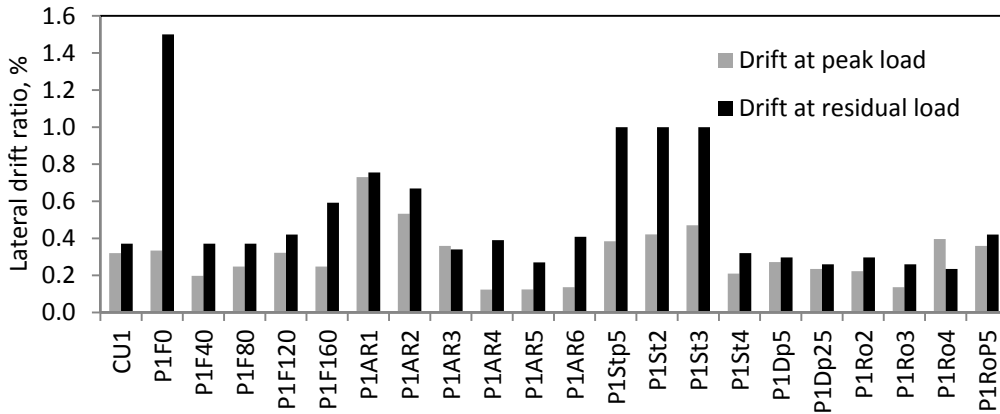


Figure 6.7 Drift at peak and residual load for first set of models

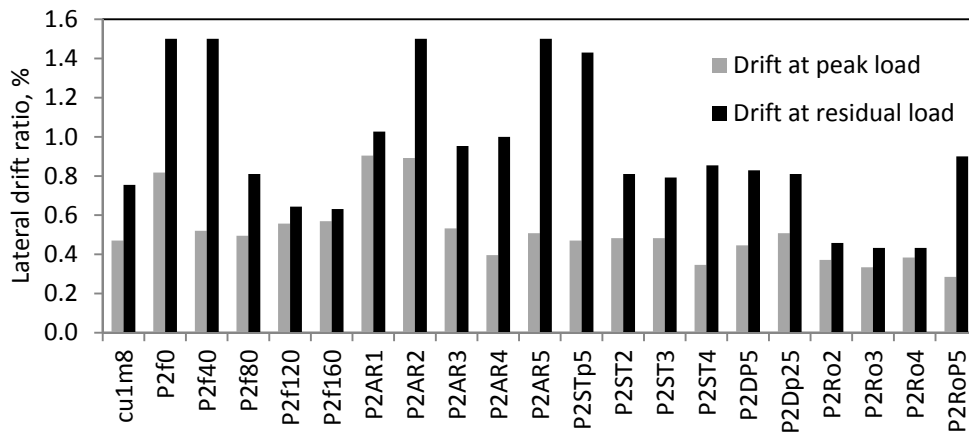


Figure 6.8 Drift at peak and residual load for second set of models

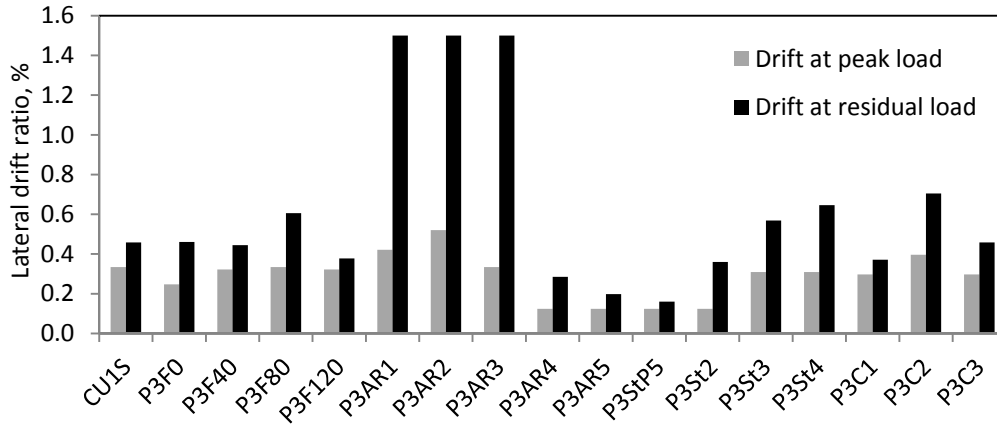


Figure 6.9 Drift at residual load for third set of models

Equation 6.16 or 6.17 can be used to estimate the residual load capacity remaining in an infilled frame. In the calculation of the residual strength, one should consider that the infill undergoes substantial sliding and cracking prior to reaching its residual strength; therefore the coefficient of sliding friction of the infill, μ_{res} , can be considered to be 0.7 or lower. The vertical load applied to the infill at the residual stage is different from that used at the peak load point due to the redistribution of forces. Rather, the load applied to the infill is estimated as the maximum between the total externally applied vertical load, and the vertical load calculated in Equation 6.13 due to frame confinement. The entire external vertical load is applied at the residual capacity stage because the columns are assumed to carry none of the vertical load due to damage. In cases in which the residual capacity is calculated as higher than the peak strength, Equations 6.16 and 6.17 are limited to be equal to the capacity at peak.

Table 6.1 Equations of simplified method for peak and residual load points

	Strong infill- Strong frame	Strong infill- Weak frame	Weak infill- Weak frame	Weak infill- Strong frame
Drift at peak load	For $l/h < 2$: $\Delta_{peak} = 0.86 - 0.33 l/h$ (6.5) For $l/h > 2$: $\Delta_{peak} = 0.15$		For $l/h < 1$: $\Delta_{peak} = 0.9$ For $1 < l/h < 2$: $\Delta_{peak} = 1.6 - 0.7 l/h$ (6.6) For $l/h > 2$: $\Delta_{peak} = 0.15$	
Peak strength	$V_{max} = V_{c1} + V_{c2} + P_w \mu + A_w C$ (6.7)	$V_{max} = P_w \mu + A_w C$ (6.8)	$V_{max} = V_{c1} + V_{c2} + P_w \mu + A_w C$ (6.9)	$V_{max} = V_{c1} + V_{c2} + P_w \mu + 2V_p$ (6.10)
Drift at onset of residual capacity	$\Delta_{res} = 1.6 \Delta_{peak}$ (6.14)		$\Delta_{res} = 1.8 \Delta_{peak}$ (6.15)	
Residual capacity	$V_{res} = A_v f_y n_s + P_w \mu_{res} \leq V_{max}$ (6.16)			$V_{res} = A_v f_y n_s + P_w \mu_{res} + 2V_p \leq V_{max}$ (6.17)

Where V_{max} is the peak capacity of infilled frame, A_w is the area of the infill, C is the cohesive bond strength of infill, V_c is the shear strength of each column as in Equation 5.3, and P_w is the vertical load on infill, V_{res} is the residual load capacity of an infilled frame, A_v is the total area of stirrups in one layer, n_s is the number of stirrups crossing shear crack, P_w is the vertical load on the infill, μ_{res} is the coefficient of residual sliding friction of the damaged infill and V_p is the shear to cause plastic hinges in both columns as in Equation 5.4.

Chapter 7

Validation of the Proposed Method

The simplified analytical method described in Chapter 6 has been validated with the results of the parametric study as well as the specimens from the tests discussed in Chapter 3 to evaluate the accuracy of the method. The method is considered successful in cases where the capacity at yield, peak and residual is equal to or slightly less than the corresponding capacity in the tested specimens or the FEM models. Another goal of the simplified method is to ensure the drift is matched or slightly less at the yield, peak and residual points.

Validation with Results from Mehrabi et al. (1994)

The results from the tests by Mehrabi et al. (1994) have been used to check the accuracy of the simplified method. These results are shown in Table 7.1. The specimen classifications are provided here but an in depth description of the specimen failures is given by Mehrabi et al (1994).

Table 7.1 Results from Mehrabi et al. (1994)

Specimen	V_m (kips)	V_n (kips)	V_p (kips)	V_c (kips)	V_p/V_n	V_m/V_n	Infill type	Frame type
spec 2	17.2	37.9	7.3	6.6	0.2	0.4	weak	weak
spec 3	62.3	37.9	7.3	6.6	0.2	1.4	strong	weak
spec 4	23.1	37.5	7.3	6.1	0.2	0.5	weak	weak
spec 5	64.4	36.7	7.3	5.4	0.2	1.5	strong	weak
spec 6	18.2	60.1	17.7	7.8	0.3	0.3	weak	strong
spec 7	59.8	50.7	18.2	8.9	0.4	1.0	strong	weak
spec 8	24.3	37.5	7.3	6.1	0.2	0.6	weak	weak
spec 9	63.8	37.5	7.3	6.1	0.2	1.5	strong	weak
spec 10	26.4	37.5	7.3	6.1	0.2	0.6	weak	weak
spec 11	79.5	37.3	14.6	6.0	0.4	1.8	strong	weak
spec 12	46.3	37.5	14.6	6.1	0.4	1.1	strong	weak

Weak Infill Cases

Specimens 2, 4, 6, 8 and 10 all had hollow bricks and were generally weak infill specimens with ductile failures. Specimen 2 was damaged prior to testing resulting in the low stiffness and force-vs-drift behavior hence it can be ignored. Specimen 4 is a weak infill- strong frame case, and the calculated peak strength is within 4% of the peak strength of the specimen. Specimen 6 is also loaded cyclically similar to Specimen 4, but has increased column size and column reinforcement. Due to the weak infill- weak frame condition Specimen 6 has higher peak strength than predicted. Specimen 8 is a weak infill-weak frame case and the behavior is captured with the simplified method as shown in Table 7.2. The calculated peak strength of Specimen 8 is within 12% of the experimental peak strength and the calculated residual strength is within 16% of the test results. Specimen 10 was loaded cyclically and had a larger aspect ratio than the first 9 specimens in this test. The calculated peak strength of Specimen 10 is within 10% of the experimental results. The cyclic force-vs-drift plot of Specimen 10 is shown with the results of the simplified method in Table 7.2.

Strong Infill Cases

Specimens 3,5,7,9,11 and 12 had solid-brick in the infills resulting in generally brittle failures for the specimens. Specimen 3 is a strong infill- weak frame case and is well matched by the simplified method with the calculated peak strength within 1% of the experimental peak strength as shown in Table 7.2. Specimen 5 is a case with a strong infill-strong frame due to the higher material strengths of the specimen. Specimen 7 is another strong infill- strong frame case. The peak strength calculated with the simplified method is within 1% of the peak strength in the positive loading direction and within 8% of the peak strength in the negative loading direction. Specimen 9 has a strong infill and a weak frame and thus major shear failures occur. The calculated peak strength of

Specimen 9 is within 4% of the experimental results and the residual strength is within 10% of the experimental residual load plateau also as shown in Table 7.2. The initial stiffness of Specimen 9 is overestimated because the frame had existing damage prior to testing. Specimens 11 and 12 both are strong infill-strong frame cases due to the increased aspect ratio of the specimens and solid brick infill. The only cases overestimated at the specimens analyzed from Mehrabi et al. (1994) are Specimens 5, 11 and 12. For all other cases the simplified method is within a 15% underestimate of the peak strength and within 25% of the residual strength.

Table 7.2 Comparison of simplified method results with Mehrabi et al. (1994)

Specimen	Force-vs-drift relation
3	
4	

Table 7.2—Continued

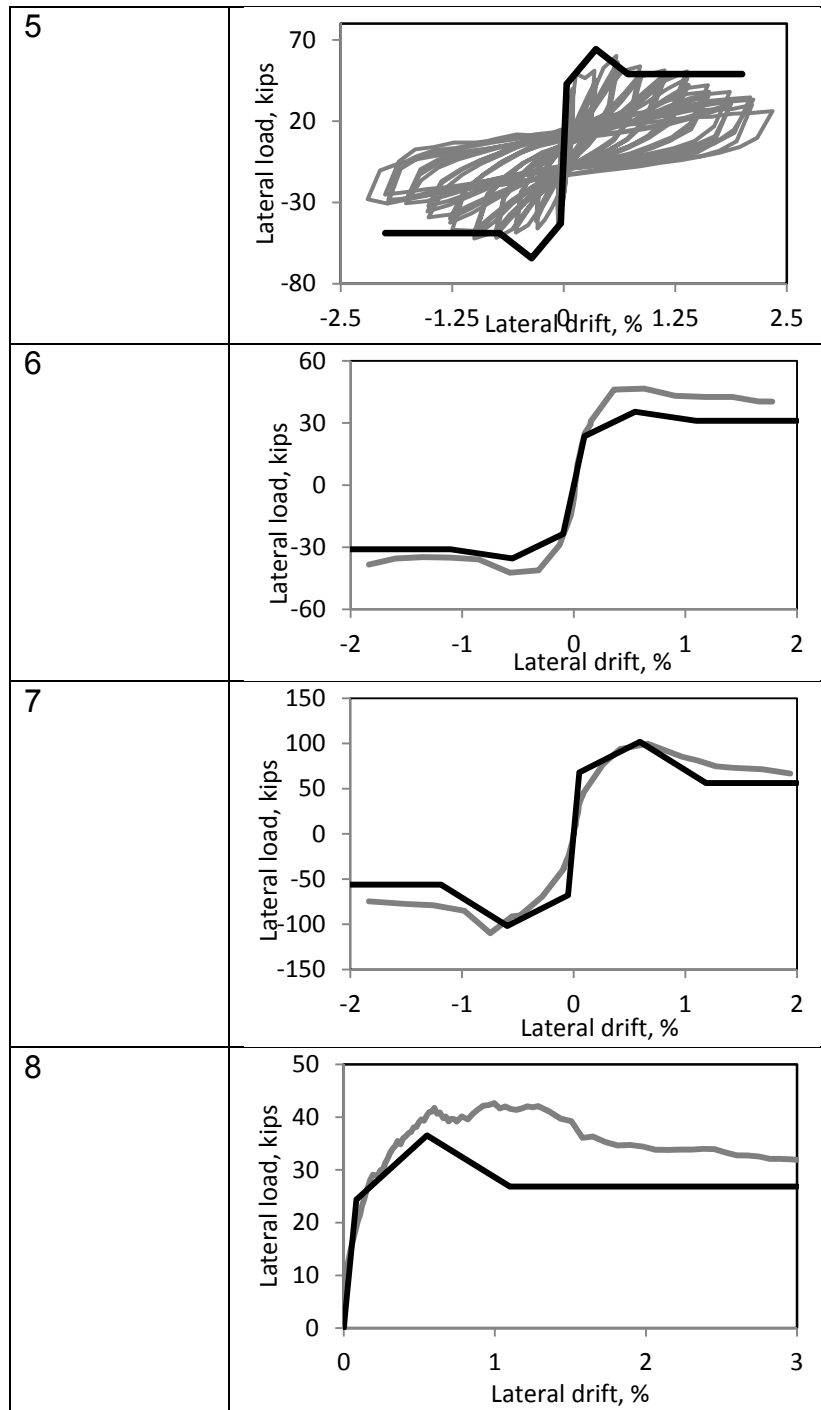
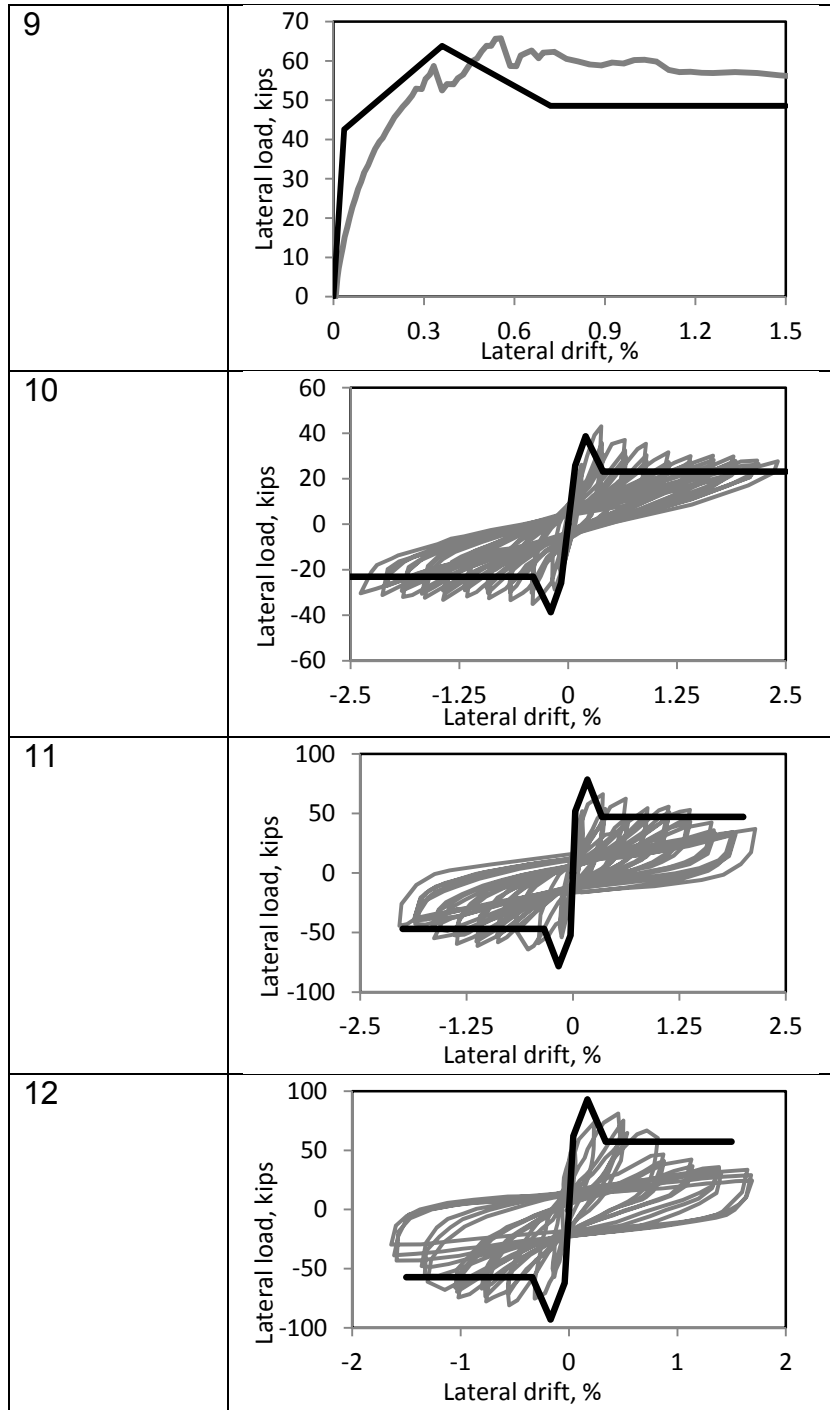


Table 7.2—Continued



Comparison of Simplified Method with Other Experiments

The case study results from the experimental studies is given in Table 7.3 below.

Table 7.4 shows experimental results for the force-vs-drift relations from the tests described in Chapter 4 along with the simplified method results. As seen in the figure, the simplified method captures the characteristic points from the test results.

Leuchars and Scrivener 1979

The test by Leuchars and Scrivener (1979) involved a strong infill-weak frame specimen due to the grouted infill. As Seen in Table 7.4 the simplified method is within 5% of the peak and residual strength in both loading directions.

Haider 1995

The specimen tested by Haider (1995) was not subjected to a vertical load. Hence the confining load from the bounding frame is used to calculate the strength at the peak and residual points. The specimen has a weak infill and a ductile failure as indicated by the smooth load drop after the peak strength had been reached. The force-vs-displacement of the Kakaletsis and Karayannis 2009

The force-vs-displacement results from Kakaletsis et al. (2009) are shown in Table 7.4. The simplified method backbone curve is within 20% of the peak and 5% of the residual load in both loading directions.

Table 7.3 Results from selected experimental studies

Test	V_m (kips)	V_n (kips)	V_p (kips)	V_c (kips)	V_p/V_n	V_m/V_n	Infill type	Frame type
Leuchars et al.	57.3	27.8	15.2	5.7	0.56	2.06	strong	weak
Haider	14.2	46.7	16.8	14.1	0.36	0.3	weak	strong
Kakaletsis et al.	24.5	21.3	18.6	10.2	0.87	1.15	strong	strong

Table 7.4 Comparison of simplified method results from selected experiments

Test	Force-vs-drift relation
Leuchars et al. (1979)	
Haider (1995)	
Kakaletsis et al. (2009)	

Comparison of Simplified Method with Analytical Models

Models with Vertical Load Changed

The vertical load was varied in all three sets of models as the vertical load has a direct influence on the failure type and infill strength. Table 7.5 below shows the results from the parametric study models with vertical load changed. The results are discussed in the following sections.

Table 7.5 Results from parametric study of cases with different vertical load

Model	V_m (kips)	V_n (kips)	V_p (kips)	V_c (kips)	V_p/V_n	V_m/V_n	Infill type	Frame type
P1F0	74.9	33.6	9.5	16.0	0.3	1.5	strong	weak
P1F40	99.8	33.6	9.5	16.0	0.3	2.0	strong	weak
P1F80	124.8	33.6	9.5	16.0	0.3	2.5	strong	weak
P1F120	149.7	33.6	9.5	16.0	0.3	3.0	strong	weak
P1F160	174.7	33.6	9.5	16.0	0.3	3.5	strong	weak
P2f0	29.9	33.6	9.5	16.0	0.3	0.6	weak	strong
P2f40	39.7	33.6	9.5	16.0	0.3	0.8	weak	strong
P2f80	49.6	33.6	9.5	16.0	0.3	1.0	strong	weak
P2f120	59.4	33.6	9.5	16.0	0.3	1.2	strong	weak
P2f160	69.3	33.6	9.5	16.0	0.3	1.4	strong	weak
P3F0	74.9	86.5	9.5	16.0	0.11	0.7	weak	strong
P3F40	99.8	86.5	9.5	16.0	0.11	1.0	weak	strong
P3F80	124.8	86.5	9.5	16.0	0.11	1.2	strong	weak
P3F120	149.7	86.5	9.5	16.0	0.11	1.5	strong	weak

First Set of Models in Parametric Study

The first models in the parametric study were analyzed in Stavridis (2009) and have been included here because they served as the starting point to the parametric study. In general these were all strong infill specimens even in the case of the frame with zero vertical load. As shown in Table 7.6 the simplified method captures the behavior of these specimens.

Table 7.6 Comparison of simplified method results from cases with varied vertical load

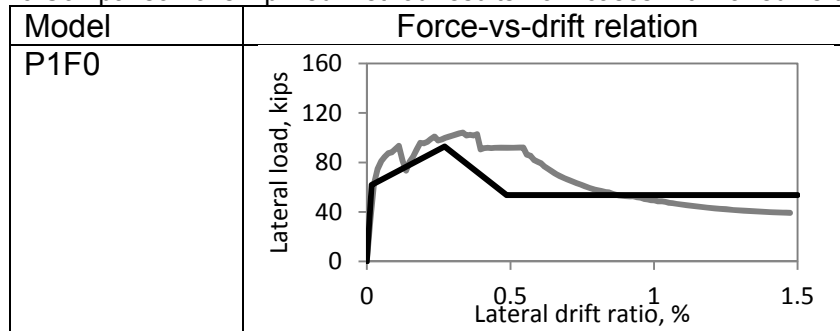
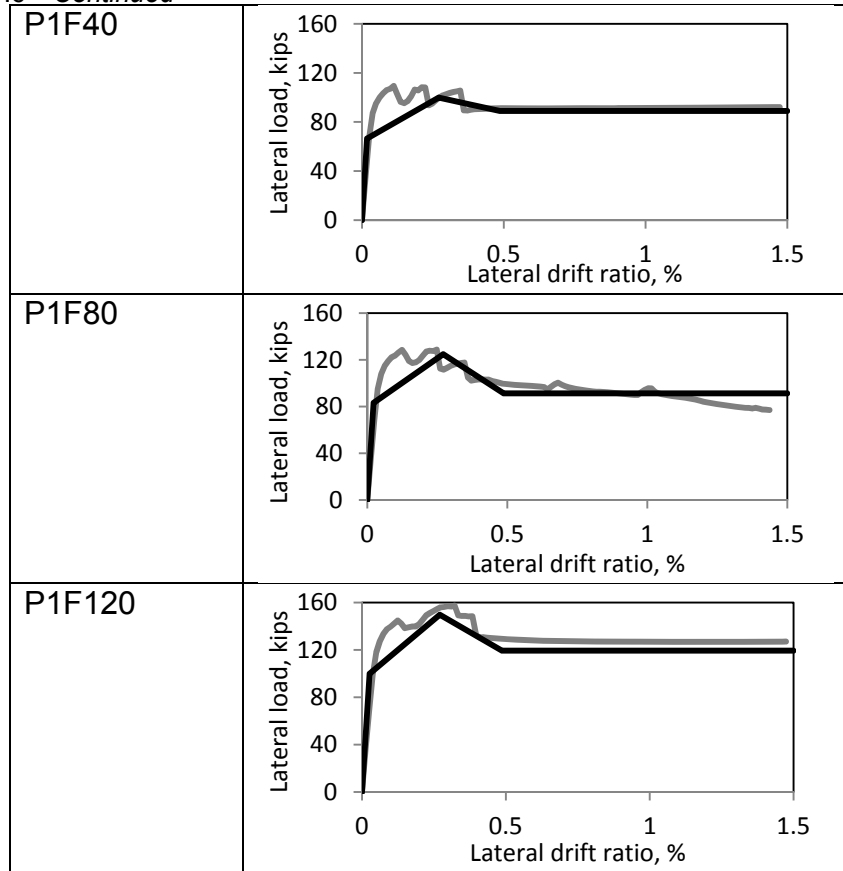


Table 7.6—Continued



The models shown in Table 7.6 have increasing peak capacity as the vertical load increases. The increase of capacity is attributed to the increased friction resistance in the infill. In the case of zero vertical load the resistance of the infill comes entirely from cohesive bond strength which is calculated as 74.9 kips and the friction caused by the compression from the bounding frame. The combination of cohesive strength and frictional resistance is enough to allow the compressive strut in the infill to develop and cause shear failures in the columns which only have shear capacity of 49.5 kips. The cases of set one have such strong infills relative to the surrounding frames that even when there is no vertical load the infill has enough capacity to initiate shear failures in the columns.

Second Set of Models in Parametric Study

The cases in this set had a generally weak infill compared with the set one models leading to flexural behavior at low vertical loads, and shear behavior at high vertical load. The results of the second set of models with varied vertical load are shown in Table 7.7. The models with 0 or 40 kip vertical load had values of V_m/V_n of 0.6 and 0.8 respectively, indicating the infill is weaker than the frame. The specimens with 80 or 120 kips vertical load have V_m/V_n of 1.08 and 1.2 respectively which indicates the specimens have a stronger infill than the frame resulting in shear failures in the columns. This behavior is shown by the graphs in Table 7.7 where (a) and (b) have a minimal load drop and ductile behavior, while (c) and (d) have a considerable load drop and much more brittle behavior.

Table 7.7 Comparison of simplified method results from cases with varied vertical load

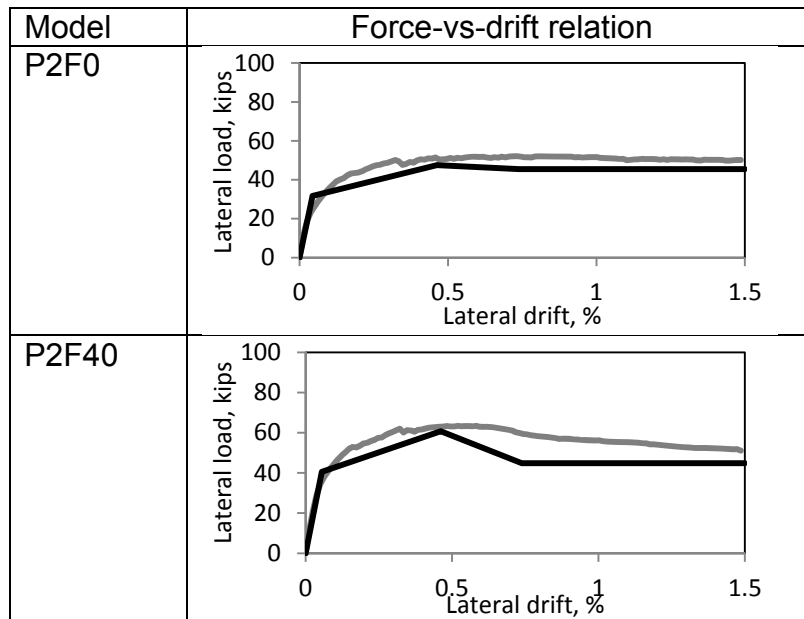
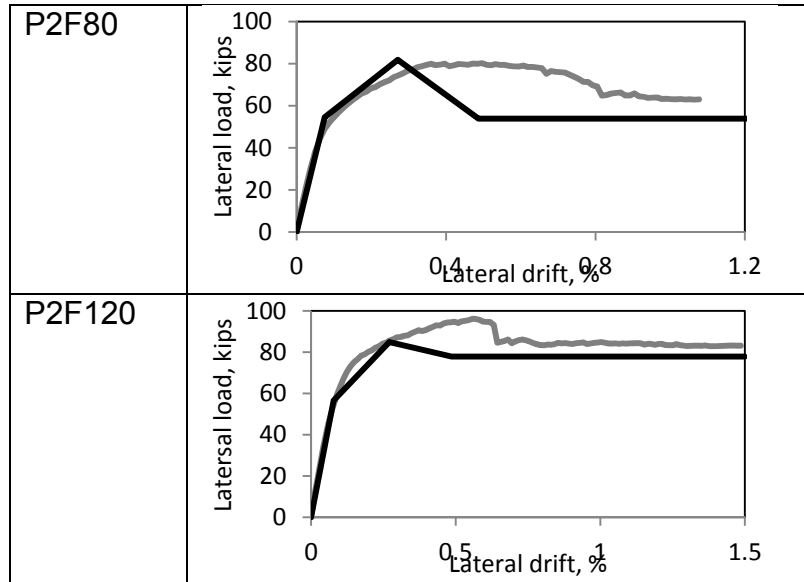


Table 7.7—Continued



Third Set of Models in Parametric Study

The third set cases have comparable infill and frame strength, therefore the increase of vertical load causes a shift from ductile to brittle behavior as in the second set of models. The behavior from the third set of models with varied vertical load is shown in Table 7.8. The simplified method accurately captures the increased capacity associated with increased vertical load.

Table 7.8 Comparison of simplified method results from cases with varied vertical load

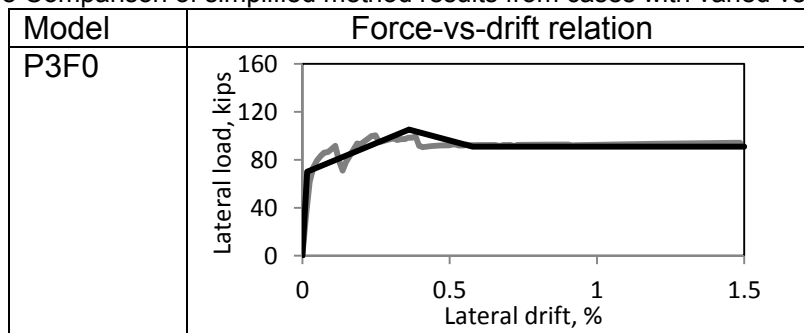
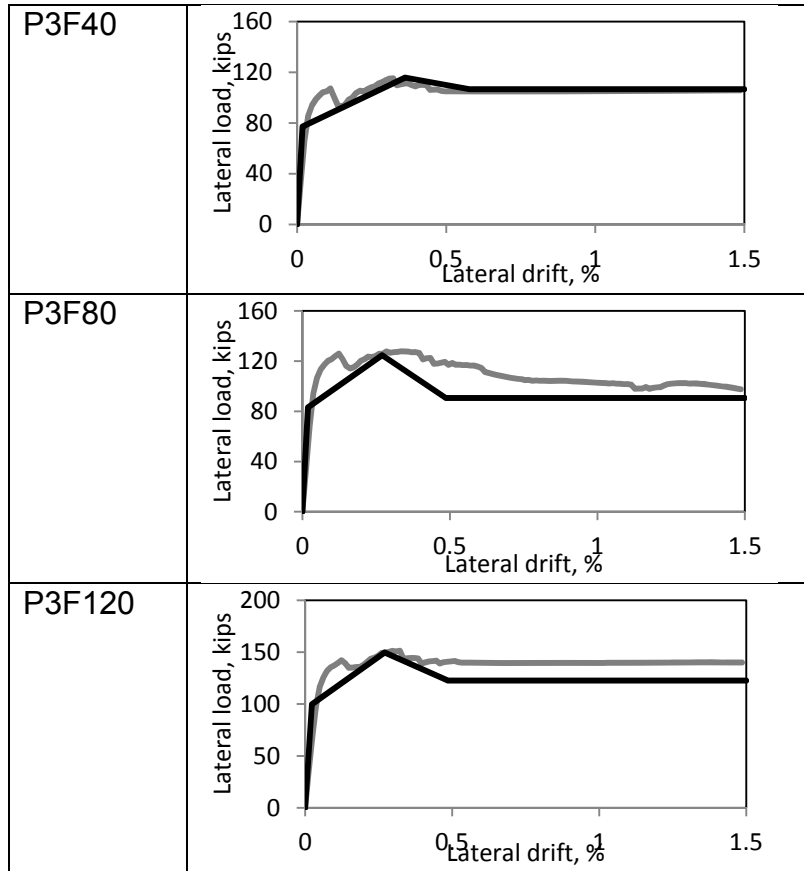


Table 7.8—Continued



Models with Aspect Ratio Changed

The choice in aspect ratios is made to produce a wide range of points in the correlation of peak drift and aspect ratio. Therefore, the models with the lower bound of aspect ratio are rather unrealistic for use in an actual structure, but provide insight about the drift at peak load for specimens with low aspect ratio. The results for the cases with varied aspect ratio are given in table 7.9.

Table 7.9 Results from parametric study of cases with different aspect ratio

Model	V_m (kips)	V_n (kips)	V_p (kips)	V_c (kips)	V_p/V_n	V_m/V_n	Infill type	Frame type
P1AR1	36.1	33.6	9.5	16.0	0.3	0.7	weak	strong
P1AR2	73.2	33.6	9.5	16.0	0.3	1.5	strong	weak
P1AR3	101.7	33.6	9.5	16.0	0.3	2.1	strong	weak

Table 7.9—Continued

P1AR4	141.8	33.6	9.5	16.0	0.3	2.9	strong	weak
P1AR5	169.8	33.6	9.5	16.0	0.3	3.4	strong	weak
P1AR6	187.9	33.6	9.5	16.0	0.3	3.8	strong	weak
P2AR1	11.4	33.6	9.5	16.0	0.3	0.2	weak	strong
P2AR2	38.3	33.6	9.5	16.0	0.3	0.8	weak	strong
P2AR3	58.6	33.6	9.5	16.0	0.3	1.2	strong	weak
P2AR4	71.4	33.6	9.5	16.0	0.3	1.4	strong	weak
P2AR5	80.1	33.6	9.5	16.0	0.3	1.6	strong	weak
P3AR1	36.1	86.5	9.5	16.0	0.6	0.4	weak	strong
P3AR2	73.2	86.5	9.5	16.0	0.6	0.7	weak	strong
P3AR3	101.7	86.5	9.5	16.0	0.6	1.0	weak	strong
P3AR4	141.8	86.5	9.5	16.0	0.6	1.4	strong	weak
P3AR5	169.8	86.5	9.5	16.0	0.6	1.7	strong	weak

First Set of Models in Parametric Study

As shown in Table 7.10 the frame strength increases and ductility decreases as the infill gets longer for the first set of specimens. In all cases a brittle behavior is observed. Similar to the cases with different vertical load, the infill is so robust the specimens with different aspect ratio tend to all have shear controlled behavior. The simplified method matches the behavior well for the cases with realistic geometry but the simplified method underestimates the strength in the cases with very low panel length. The underestimation from the simplified method is attributed to the calculation of infill capacity which is highly dependent on infill area. In the cases with very low infill length the infill capacity is predicted low; however, the low aspect ratio of the structure causes it to act as a composite cantilevered beam which has higher strength than predicted by the simplified method. This type of failure is no of concern because it is very rare and only seen in cases with very low aspect ratio which doesn't occur often in buildings.

Table 7.10 Comparison of simplified method results from cases with varied aspect ratio

Model	Force-vs-drift relation
P1 AR2=0.91	
P1 AR3=1.39	
P1 AR4=2.15	
P1 AR5=2.72	
P1 AR6=3.13	

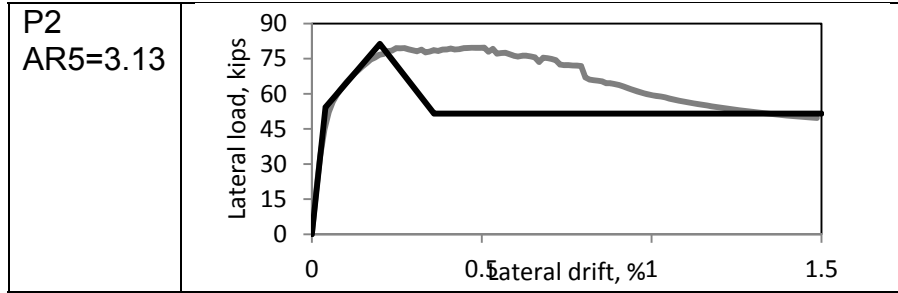
Second set of Models in Parametric Study

The second set of models had varying behaviors from ductile to brittle as with the vertical load cases. The case with aspect ratio of 3.16 shown in Table 7.11 has a sudden load drop after the peak indicating brittle behavior while the case with aspect ratio of 1.36 shown in Table 7.11 has a minimal load drop after the peak. The shift in behavior is due to the infill becoming strong enough to initiate shear failures in the columns. The structures shown in (a) and (b) have low enough infill length that the compressive struts are unable to create shear failures in the columns and the model fails in flexure.

Table 7.11 Comparison of simplified method results from cases with varied Aspect ratio

Model	Force-vs-drift relation
P2 AR2=1.39	
P2 AR3=2.15	
P2 AR4=2.72	

Table 7.11—Continued



Third Set of Models in Parametric Study

The third set of models vary in behavior, from the ductile failure of the low aspect ratio cases to the brittle behavior of the high aspect ratio cases. Similar to the first two sets of models, the models of the third set have major shear cracks in the cases with long infill panels such as that in Table 7.12. The transition from ductile to brittle behavior is apparent when comparing the model with aspect ratio of 0.91 to the model with aspect ratio of 2.72 in Table 7.12.

Table 7.12 Comparison of simplified method results from cases with varied Aspect ratio

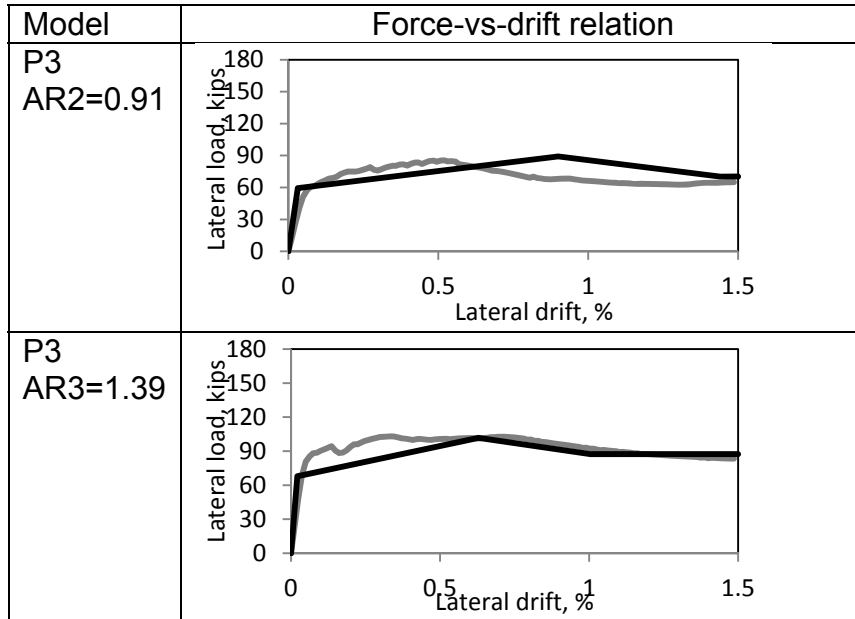
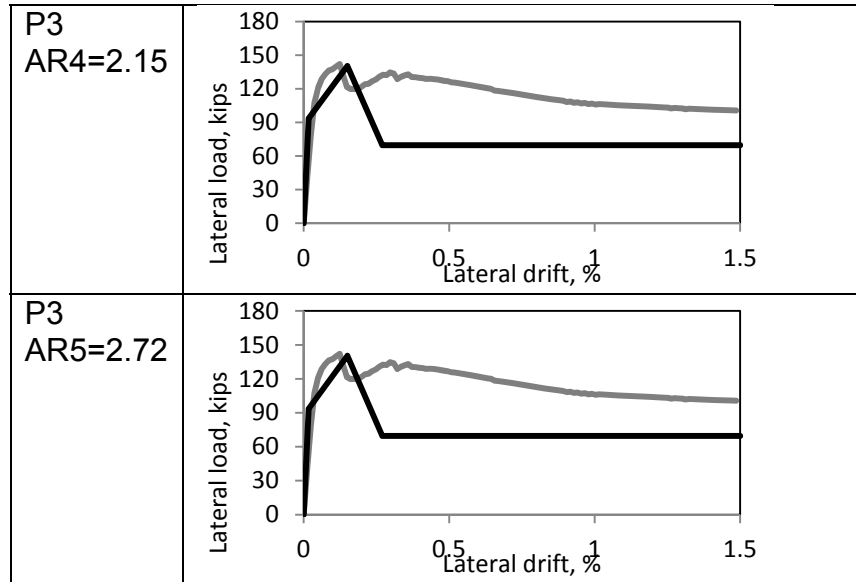


Table 7.12—Continued



Models with Stirrup Area Changed

The stirrup area is changed in all three sets of models from a value of 0.07 in² to 0.59 in². As mentioned previously, increasing the transverse steel in a column increases the residual capacity of the frame and can occasionally alter the failure type of the structure. In the three sets of models the behavior was observed to transition from shear controlled to flexural controlled failures as the shear reinforcement was increased as shown below in Table 7.13.

Table 7.13 Results from parametric study of cases with different transverse steel area

Model	V_m (kips)	V_n (kips)	V_p (kips)	V_c (kips)	V_p/V_n	V_m/V_n	Infill type	Frame type
P1Stp5	122.3	24.4	9.5	16.0	0.4	3.0	strong	weak
P1St2	122.3	50.8	9.5	16.0	0.2	1.8	strong	weak
P1St3	122.3	68.8	9.5	16.0	0.1	1.4	strong	weak
P1St4	122.3	86.8	9.5	16.0	0.1	1.2	strong	weak
P2STp5	48.6	24.4	9.5	16.0	0.4	1.2	strong	weak
P2ST2	48.6	50.8	9.5	16.0	0.2	0.7	weak	weak
P2ST3	48.6	68.8	9.5	16.0	0.1	0.6	weak	weak
P2ST4	48.6	86.8	9.5	16.0	0.1	0.5	weak	weak
P3StP5	122.3	49.6	9.5	16.0	0.6	1.9	strong	weak

Table 7.13—Continued

P3St2	122.3	155.2	9.5	16.0	0.6	0.7	weak	strong
P3St3	122.3	227.2	9.5	16.0	0.6	0.5	weak	strong
P3St4	122.3	299.2	9.5	16.0	0.6	0.4	weak	strong
P1Dp5	122.2	51.2	9.5	16.0	0.1	1.8	strong	weak
P1Dp25	122.2	86.5	9.5	16.0	0.1	1.1	strong	weak
P2DP5	48.6	51.2	9.5	16.0	0.2	0.7	weak	weak
P2Dp25	48.6	86.5	9.5	16.0	0.1	0.5	weak	weak

First Set of Models in Parametric Study

The peak load of the specimens with increased stirrup area does not change much between models. Rather the increased shear reinforcement prevents a shear crack at the from developing and provides additional capacity once the column has failed in shear. Table 7.14 shows the post-peak strength increases as the area of transverse steel is increased, and this is matched by the simplified method results. The model in (a) is controlled by shear failure and thus the residual strength is limited to the sum of the stirrup yield strength and the residual frictional capacity in the infill. The other three cases that have increased stirrup area qualify for flexural cases at the residual point due to the ratio of shear strength to flexural strength.

Table 7.14 Comparison of simplified method results from cases with varied area of steel

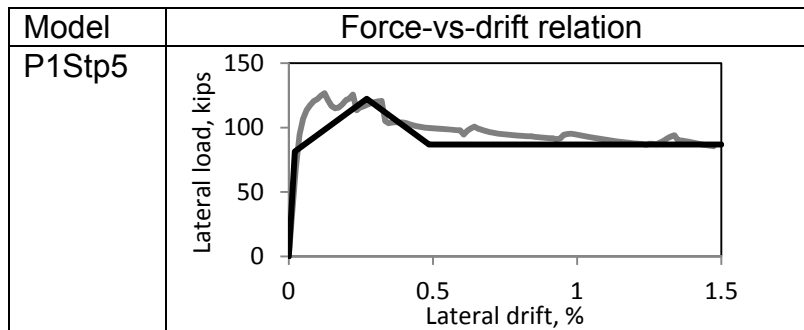
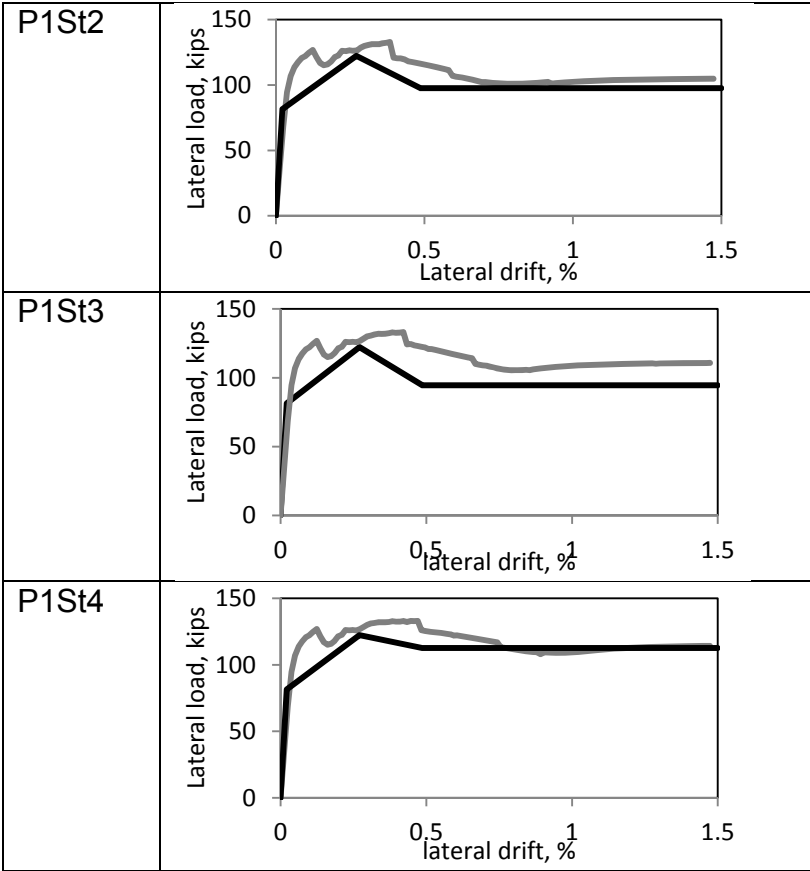


Table 7.14—Continued



Second Set of Models in Parametric Study

The strength of the infill compared to that of the frame are so close that varying the transverse reinforcement in the frame to a low value allows the infill to act in strong infill-weak frame manner. This is observed in Table 7.15 of the four cases only the case with the minimum area of stirrups has a substantial load drop after the peak. The opposite behavior is observed for the case with maximum shear reinforcement as the frame is strong enough in that case to withstand the forces of the infill and avoid shear failure.

Table 7.15 Comparison of simplified method results from cases with varied area of steel

Model	Force-vs-drift relation
P2Stp5	
P2St2	
P2St3	
P2St4	

Third Set of Models in Parametric Study

While the first two models shown in Table 7.16 have considerable load drop after the peak strength, the cases with even more stirrup area have a smaller load drop after

the peak. The peak strength and residual load capacity are well matched by the simplified method results.

Table 7.16 Comparison of simplified method results from cases with varied area of steel

Model	Force-vs-drift relation
P3Stp5	
P3St2	
P3St3	
P3St4	

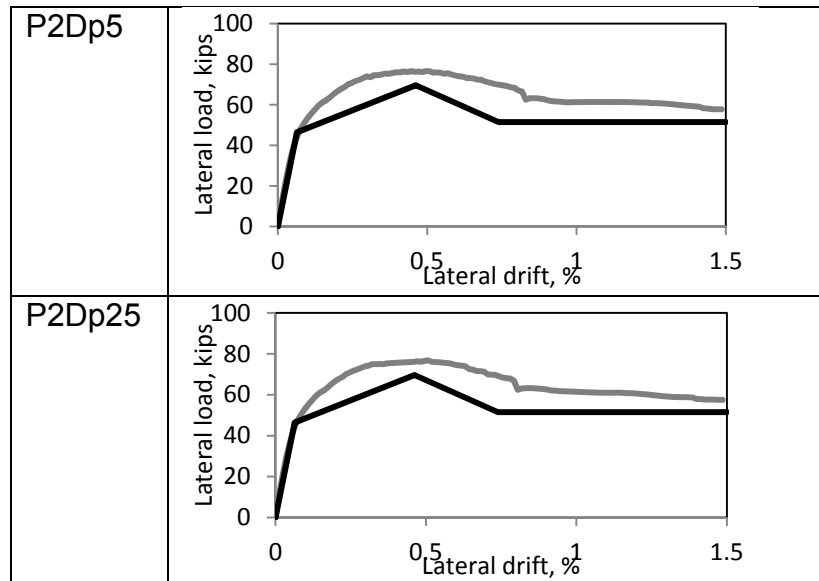
Models with Stirrup Spacing Changed

The stirrup spacing was changed in the first two sets of models only, as the third set of models were set to have single stirrup spacing for all cases. In general the simplified method matches the strength and drift of these cases well. The first and second set models are shown in Table 7.17 which shows the simplified method captures the behavior the analytical model results. The simplified method does well to capture the peak and residual strength of the specimens. Rather than calculating the residual capacity based on shear, a combination of plastic moment capacity and shear capacity are used to find the residual strength. This combination is only used in weak infill cases with where flexural failures are more likely due to low infill shear strength.

Table 7.17 Comparison of simplified method results from cases with varied steel spacing

Model	Force-vs-drift relation
P1Dp5	
P1Dp25	

Table 7.17—Continued



Models with Longitudinal Steel Area Changed

The longitudinal reinforcement of the columns was varied in the first two sets of models. The amount of longitudinal reinforcement had little impact on the strength of most first set models as the failure of a majority of frames is dependent on shear behavior rather than flexural behavior. The second set behavior was also not affected by increasing the flexural steel other than in the case of the minimum flexural steel, where a dominant flexural failure occurs. The results from the cases with varied longitudinal steel area are given in Table 7.18.

Table 7.18 Results from parametric study of cases with different longitudinal steel area

Model	V_m (kips)	V_n (kips)	V_p (kips)	V_c (kips)	V_p/V_n	V_m/V_n	Infill type	Frame type
P1RoP5	122.3	33.6	4.9	16.0	0.1	2.5	strong	weak
P1Ro2	122.3	33.6	18.2	16.0	0.5	2.5	strong	weak
P1Ro3	122.3	33.6	25.5	16.0	0.8	2.5	strong	strong
P1Ro4	122.3	33.6	33.6	16.0	1.0	2.5	strong	strong
P2RoP5	48.6	33.6	4.9	16.0	0.1	1.0	weak	weak
P2Ro2	48.6	33.6	18.2	16.0	0.5	1.0	weak	strong
P2Ro3	48.6	33.6	25.5	16.0	0.8	1.0	weak	strong
P2Ro4	48.6	33.6	33.6	16.0	1.0	1.0	weak	strong

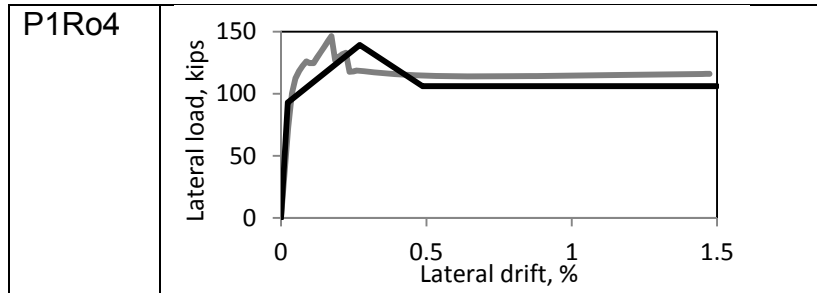
First Set of Models in Parametric Study

As shown in Table 7.19 the behavior of the models doesn't change much between cases other than in the first case which has the minimum longitudinal steel area. In this case the windward column undergoes a major flexural failure with hinges near the top and mid-height of the column. It is evident that when the shear required to initiate plastic hinges in the column is less than the shear strength of the column, a flexural failure will occur as in the case of 0.5% reinforcement ratio. The simplified method works well to match the strength of the analytical models.

Table 7.19 Comparison of simplified method results from cases with varied longitudinal steel area

Model	Force-vs-drift relation
P1Ro5	
P2Ro2	
P1Ro3	

Table 7.19—Continued



Second Set of Models in Parametric Study

The second set of models with varied longitudinal steel had a similar behavior to the first set of models. The behavior becomes more brittle with higher longitudinal steel, as the increased flexural reinforcement forces allows the shear failure in the column. The force-vs-displacement results for the models of the second set are given in Table 7.20. As seen in the table the models with the higher reinforcement ratio have a more drastic load drop than the cases with lower reinforcement.

Table 7.20 Comparison of simplified method results from cases with varied longitudinal steel area

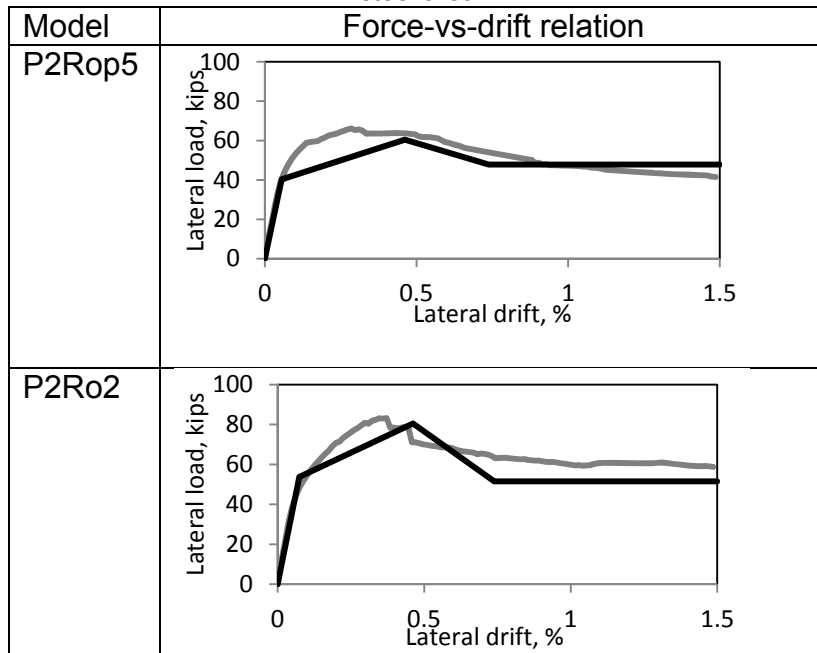
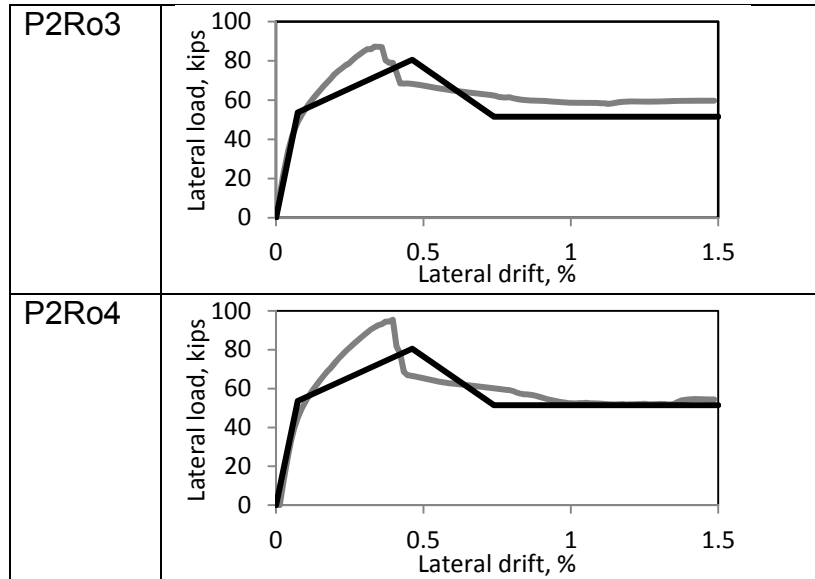


Table 7.20—Continued



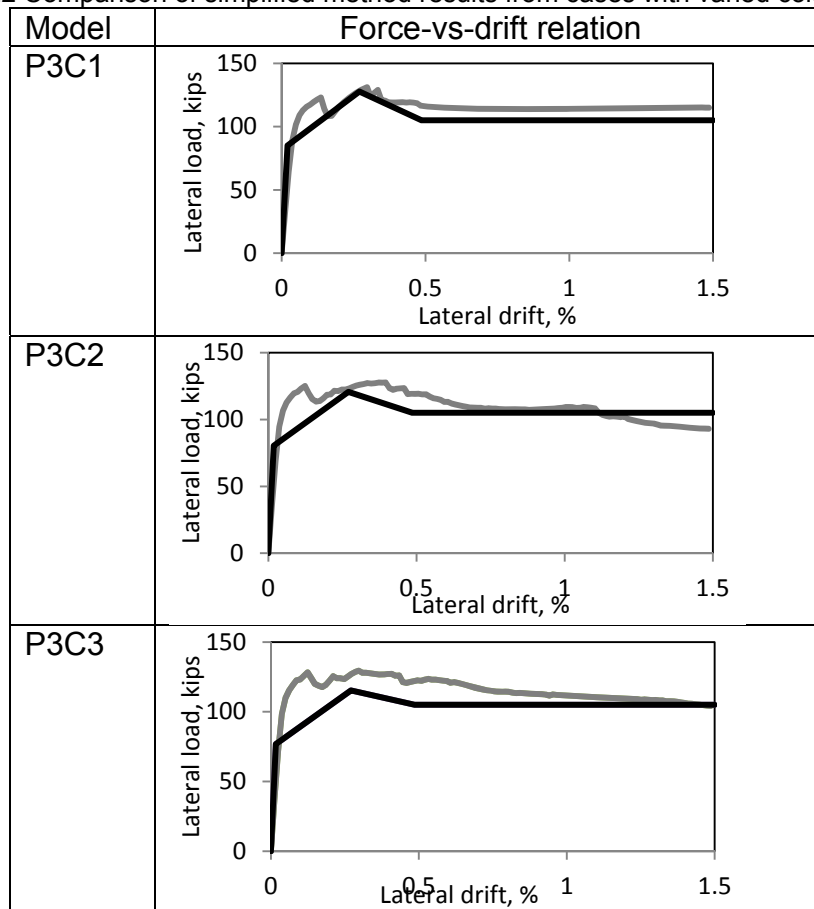
Models with Column Width Changed

The column dimensions are only changed in the final set of models. The results from the models with varied column width are given in Table 7.21 and Table 7.22. The sudden load drop in case P3C1 is due to the shear failure in the column. Cases P3C2 and P3C3 both have a flexural failure in the windward column and shear failure in the leeward column. The flexural failure is what allows the gradual load drop of cases P3C2 and P3C3. The simplified method captures the peak strength and drift for the cases and underestimates the residual capacity.

Table 7.21 Results from parametric study of cases with different column width

Model	V_m (kips)	V_n (kips)	V_p (kips)	V_c (kips)	V_p/V_n	V_m/V_n	Infill type	Frame type
P3C1	127.7	82.2	6.5	11.6	0.6	1.4	strong	weak
P3C2	120.7	88.0	10.6	17.4	0.6	1.1	strong	weak
P3C3	115.4	93.8	12.5	23.2	0.5	1.0	weak	strong

Table 7.22 Comparison of simplified method results from cases with varied column width



Comparison with Other Methods from Literature

To further validate the simplified method proposed in Chapter 6 the results of the method have been compared with the results from various other recognized simplified methods including FEMA 306 (1999), Stafford-Smith & Coull (1991), Rosenbluth (1980), and Galanti et al. (1998). Figure 7.1 shows how the results obtained with the equations from the proposed method of this thesis and the aforementioned studies when used to calculate the peak capacity of the infilled frames used in the study from Mehrabi et al. (1994) and the parametric study models. The peak strength is used to compare methods

as it is the focus of many of these studies and provisions for the drift or residual capacity are not given.

As seen in Figure 7.1 through 7.4 the simplified method is a very close match to the experimental or analytical result in all cases while the other illustrated methods tend to be major underestimates of the experimental or analytical result. For the cases shown, the other methods are far too conservative to have an applicable use. Furthermore, the other methods considered include equivalent strut methods and limit state methods, yet neither yields accurate results for these cases.

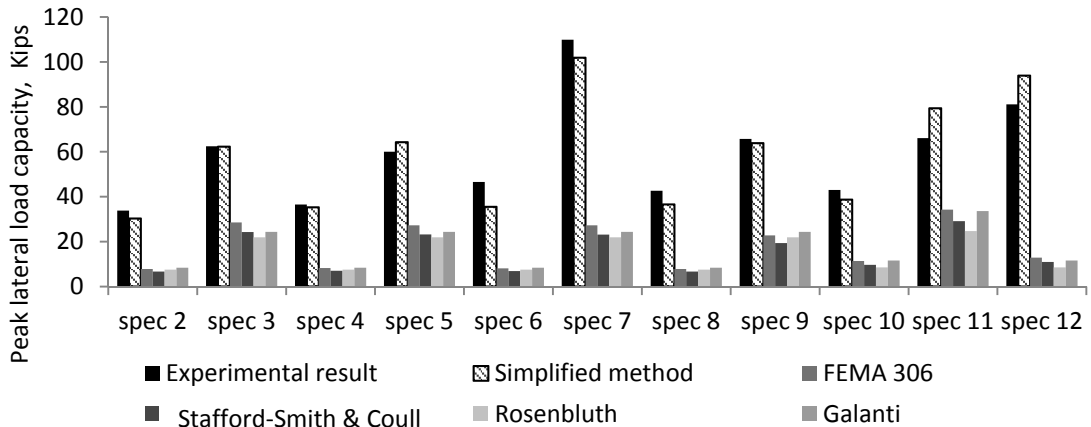


Figure 7.1 Comparison of simplified method with other methods from literature

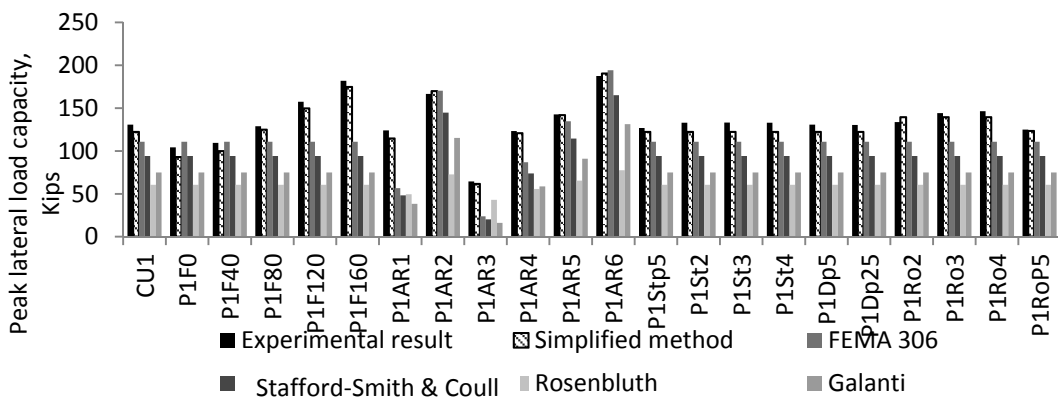


Figure 7.2 Comparison of simplified method with other methods from literature with models from set 1

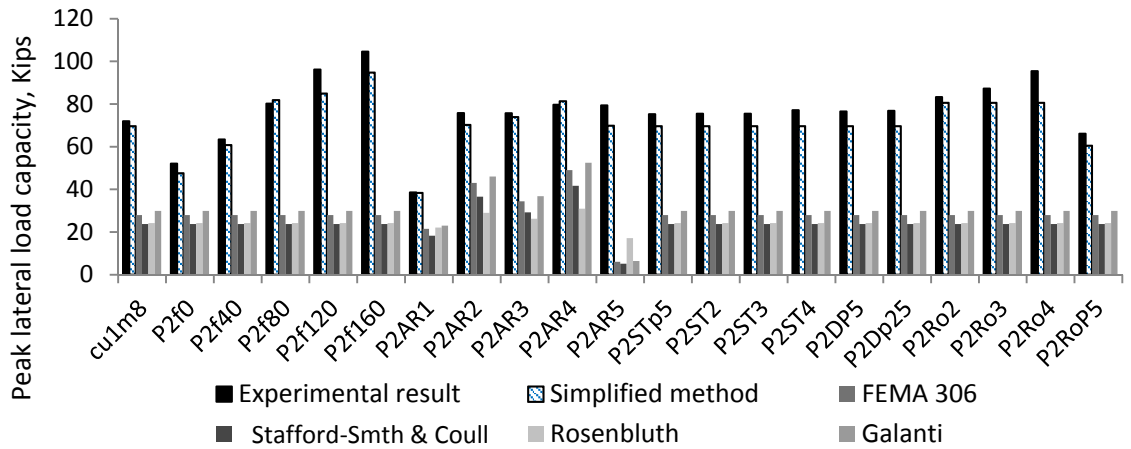


Figure 7.3 Comparison of simplified method with other methods from literature with models from set 2

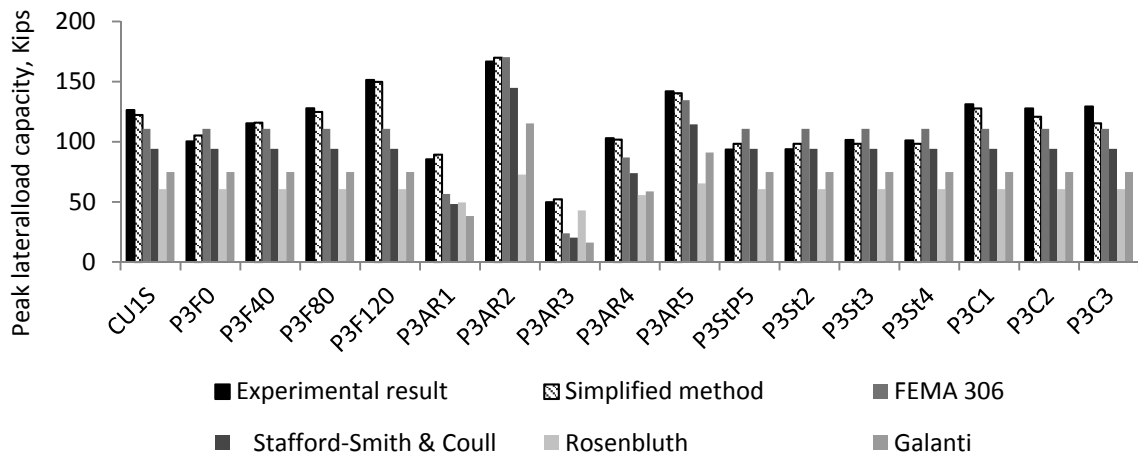


Figure 7.4 Comparison of simplified method with other methods from literature with models from set 3

Chapter 8

Summary

This thesis describes methods for the analysis of masonry infilled frames. Following the introduction, the methods described by previous researchers including the equivalent strut methods, limit state methods and finite element methods were reviewed. The experiments of Mehrabi et al. (1994), Leuchars et al. (1979), Kakaletsis et al. (2009), and Haider (1995) were presented next to introduce the properties and behavior of tested specimens. These tests showed the brittle or ductile nature of infilled frames and gave insight to the ideology of the parametric study carried out later. In order to conduct a parametric study a finite element modeling scheme is used as described by Stavridis and Shing (2010) in Chapter 4. The finite element method is described briefly in order to discuss the constitutive models, the validation of the method with specimens from Mehrabi et al. (1994).

With the described finite element method, 59 models were analyzed in order to observe the influence of various parameters on the behavior of the infilled frame. Trends observed in the results of the parametric study include the type of failure as it relates to the specimen properties, the drift at peak capacity and the drift at the residual load. Based on these trends a simplified method is proposed that will capture the behavior of infilled frames whether strong or weak. This simplified method provides guidance to obtain the strength and drift at yield, peak and the onset of residual capacity. With these points known a backbone curve of the force-vs-drift behavior can be generated for any infilled frame. Finally, the simplified method has been validated with 13 experimental specimens from the studies described in Chapter 3 as well as the 59 analytical parametric study models. The simplified method is shown to be accurate by a vast majority of the specimens and is therefore considered useful on a wide scale.

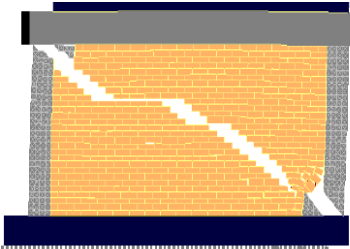
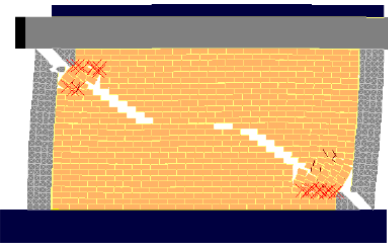
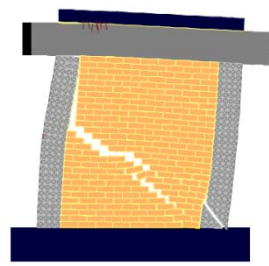

Conclusions

The analysis carried out in this study yielded many important conclusions. Beginning with the previously proposed analytical methods it was clear there was no agreed upon method for the determination the behavior of an infilled frame. The equivalent strut methods fell short in that they were based upon the limit state of infill crushing in most cases, however this study has shown the infill is not always expected to have crushing. The methods considering other limit states such as column shear failure or flexural failure have been developed independently and the shortcoming of these methods is often in the validation or the application of the limit state procedures. Often times the limit state methods are validated for only a few tested cases and thus cannot accurately capture the behavior of a wide range of specimen properties. Furthermore, many limit state methods apply to specific failure patterns but a recommendation to predict the exact failure method is not typically given. Unlike other structural systems where all limit states are equally possible and the lowest capacity governs the design, infilled frames may or may not fail based on the weakest limit state. Rather, the behavior of infilled frames depends upon both the relative strength of the frame and infill as well as the individual limit state capacities of the unique elements. To provide a means of predicting the failure patterns and behavior of an infilled frame a parametric study was conducted here. The parametric study investigated the effect of design parameters and specimen geometry and provided many useful observations.

The most impactful of the observations from the parametric study is the failure of a masonry infilled concrete frame can be classified into one of four groups including weak infill- weak frame, weak infill- strong frame, strong infill- strong frame and strong infill- weak frame. The strong infill cases are brittle and have capacity governed by the infill, while the weak infill cases are generally more ductile and have capacity governed by the

frame either in shear or flexure. Table 8.1 below shows the breakdown of groupings and examples of the typical failure pattern for each.

Table 8.1 Failure patterns of each class of infilled frames

 <p>Strong infill weak frame</p>	 <p>Weak infill weak frame</p>
 <p>Strong infill Strong frame</p>	 <p>Weak infill strong frame</p>

Many observations about the behavior of infilled frames were made from the results of the parametric study. Each parameter that was varied yielded insight as to the influence the variable has in the structural behavior.

Vertical load- As the vertical load is increased the peak and residual capacity of the infill increase due to the increased friction resistance. This increase in strength can cause a shift in failure mechanisms, for example as the infill gains capacity it can become strong enough to force shear failures in the columns. This effect on the failure mechanism ultimately impacts the deflection of the specimen, as a brittle failure

specimen will have minimal deflection prior to failure, while a ductile specimen will have higher drift at the peak and onset of residual load.

Aspect ratio- As the aspect ratio (*infill length/infill height*) is increased by making the panel longer the strength and stiffness of the structure is affected. The increased area of a longer infill increased the bond area, which leads to increased strength in the infill. Furthermore, the increased length between columns reduces the tensile stress in the windward column, making it stronger in shear. It may be expected that larger walls will have more strength, but the correlation between the drift at the peak strength and aspect ratio required the results of all the models to uncover. As the aspect ratio increases the structure becomes stiffer overall, which decreases the drift of which the peak load occurs. This observation is different for cases with strong or weak infills, as a strong infill will likely have a brittle failure which occurs at lower drift than a ductile failure.

Transverse reinforcement- As the shear reinforcement in the columns is increased the models gain higher residual load capacity and are more ductile overall. This is because increasing the shear reinforcement, either by increasing the stirrup area or decreasing the spacing, prevents the development of major shear cracks and helps maintain a residual strength at high drifts.

Longitudinal reinforcement- As the flexural reinforcement of the column is increased the likelihood of a flexural failure diminishes. The increased reinforcement allows for higher moment capacity in the columns before the formation of plastic hinges. As the infill needs room to deflect, this leads to a shear failure in the column resulting in a brittle failure. Other than affecting the type of failure mechanism which can carry many implications as the strength is directly related to the failure type, the longitudinal

reinforcement doesn't appear to have a direct influence on the strength or stiffness of an infilled frame.

Column width- As the column width increased the shear capacity of the columns increased. This increase of shear strength could not be fully utilized though; as the column width grew the columns became stronger in shear than flexure, resulting in flexural failures of the columns.

The results of the finite element analysis show the highly nonlinear behavior of an infilled frame can be captured. The simplified method described in this report serves this purpose of accurately capturing the behavior of a wide array of infilled frames with no requirement for specialized software. The simplified method, which incorporates the observations mentioned above, has been validated for cases with various failure types, geometry and loading conditions ensuring its applicability for many possible scenarios. The method considers the strength of an infilled frame as a combination of the shear/siding strength of the infill with the shear or flexural strength of the frame. Furthermore, the drift of the infilled frame is determined at the yield point by use of a suggested initial stiffness equation, and found at the peak through a correlation with the infill aspect ratio.

The methods described in this thesis can be used to evaluate the behavior of an infilled frame with small computational effort. This solves the challenging problem of analyzing infilled frames without complicated finite element methods. Furthermore, this gives a reliable method for evaluating the strength of structures with infilled frames to aid in the decision to retrofit or reinforce structures that may be vulnerable to ground motion.

Recommended Future Research

The next steps in elaborating on the simplified method proposed here is to include the effect of openings and multiple bays on an infilled frame. This would allow the

analysis of RC frame buildings in which the entire perimeter is infilled with masonry infills which are very common worldwide. With a method developed that is accurate for multiple bay walls with openings, an entire building could quickly be assessed for vulnerability to seismic loading.

References

- ASCE/SEI 41-06. (2006). "Seismic Rehabilitation of existing buildings." ASCE, New York.
- Barua, H. K., & Mallick, S. K. (1977). Behaviour of mortar infilled steel frames under lateral load. *Building and Environment*, 12(4), 263-272.
- Blackard, B., K. Willam, and S. Mettupulayam (2009). "Experimental observations of masonry infilled RC frames with openings." ACI Special Publication SP-265, American Concrete Institute, Farmington Hills, MI.
- Decanini, L. and Fantin, G. (1986). "Modelos simplificados de la mamposteria incuida en porticos, caracteristicas de rigides y Resistencia lateral en estado limite," (in Spanish), *Journadas Argentinas de Ingeniria Estructural*, Buenos Aires, Argentina
- Durrani, A. J., & Luo, Y. H. (1994). Seismic retrofit of flat-slab buildings with masonry infills. In *Technical Report* (pp. 1-8). National Center for Earthquake Engineering Research.
- EERI (2000). "1999 Kocaeli, Turkey earthquake reconnaissance report." *Earthquake Spectra*, Vol. 16, Issue S1.
- Federal Emergency Management Agency (FEMA). (1999). "Evaluation of Earthquake Damaged Concrete and Masonry Wall Buildings – Basic Procedures Manual," FEMA-306, Applied Technology Council (ATC-43 Project), Redwood City CA.
- Fiorato, A., Sozen, M., Gamble, W.(1970). "An Investigation of the Interaction of Reinforced Concrete Frames with Masonry Filler Walls". University of Illinois Urbana Dept. of Civil Engineering
- Flanagan, R. D., & Bennett, R. M. (2001). In-plane analysis of masonry infill materials. *Practice Periodical on Structural Design and Construction*, 6(4), 176-182.
- Galanti, F. M. B., Scarpas, A., & Vrouwenvelder, A. C. W. M. (1998). Calibration of a capacity design procedure for infilled reinforced concrete frames. In *Proc., 11th European conference on Earthquake Engineering*.

Haider, S. (1995). In-plane cyclic response of reinforced concrete frames with unreinforced masonry infills (Doctoral dissertation, Masters Thesis, Rice University. <http://hdl.handle.net/1911/13956>).

Holmes, M. (1961). "Steel Frames with Brickwork and Concrete Infilling," *Proceedings of the Institution of Civil Engineers*, 19, 473-478.

Kakaletsis, D. and Karayannis, C. (2009). "Experimental Investigation of Infilled Reinforced Concrete Frames with Openings," *ACI Structural Journal*, 106, No. 2, 132-141.

Leuchars, J. and Scrivener, J. (1976). "Masonry Infill Panels Subjected to Cyclic In-Plane Loading," *Bulletin of the New Zealand National Society for Earthquake Engineering*, 9, No. 2, 122-131.

Liau, T.C. (1984). "An Approximate Method of Analysis for Infilled Frames With or Without Openings," *Building Science*, 7, 233-238.

Lotfi, H., Shing, P.B. (1991) "An appraisal of smeared crack models for masonry shear wall analysis". Department of Civil, Environmental, and Architectural Engineering, University of Colorado, Boulder, CO

Mainstone, R. (1971). "On the Stiffnesses and Strengths of Infilled Frames," *Proceedings of the Institution of Civil Engineers*, Supplement IV, 57-90.

Mehrabi, A.B., Shing, P.B., Schuller, M. and Noland, J. (1994). "Performance of masonry-infilled R/C frames under in-plane lateral loads." Rep. CU/SR-94-6, Dept. of Civ., Envir., and Arch. Engrg., Univ. of Colorado, Boulder CO.

Mehrabi, A.B. and P. B. Shing (1997). "Finite element modeling of masonry-infilled RC frames." *J. Struct. Eng., ASCE*, Vol. 123(5), 604-613.

Paulay, T and M.J.N. Priestley (1992) *Seismic Design of Reinforced Concrete and Masonry Buildings*, John Wiley & Sons, Inc, Hoboken, New Jersey, pp 768.

Polyakov, S. V. (1956). Masonry in framed buildings. Gosudarstvennoe izdatel'stvo Literaturny postroitel'stvu i arkhitekture. Translated from Russian by G.L.Cairns.

Rosenblueth, E. (1980). Design of Earthquake Resistant Structures. Pentech Press.

Shing P.B. and B. Spencer (1999). "Modeling of Shear Behavior of RC Bridge Structures." Proc. of the US-Japan Seminar on Post-Peak Behavior of RC Structures Subjected to Seismic Loads – Recent Advances and Challenges of Analysis and Design, NSF-JSPS-JCI, Tokyo, Japan, 315-333.

Stafford-Smith, B. and Carter, C. (1969). "A Method for the Analysis of Infilled Frames," Proceedings of the Institution of Civil Engineers, 44, 31-48.

Stafford-Smith, B. and Coull, A. (1991) "Ch. 8 Infilled-frame structures," Tall building structures: analysis and design, 168-183.

Stavridis, A. (2009). "Analytical and Experimental Study of Seismic Performance of Reinforced Concrete Frames Infilled with Masonry Walls," Ph.D. Dissertation, University of California at San Diego, La Jolla CA.

Stavridis, A. and Shing, P.B. (2010). "Finite Element Modeling of Nonlinear Behavior of Masonry-Infilled RC Frames," Journal of Structural Engineering, 136, No.3, 285-296.

Wood, R.H. (1978). Plasticity, Composite Action and Collapse Design of Unreinforced Shear Wall Panels in Frames," Proceedings of the Institution of Civil Engineers, Part 2, 65, 381-411.

Biographical Information

Austin Reese earned his B.S. in civil engineering at The University of Texas at Austin before coming to The University of Texas at Arlington to pursue a graduate degree in civil engineering with structural emphasis. While at UT- Arlington, Austin focused on the research of masonry infilled reinforced concrete frames. Austin plans to pursue professional licensure as a structural engineer and now works as a structural consultant with a company in Ft. Worth, Texas helping in the design of senior living facilities.